GAS BREAKTHROUGH IN COMPACTED AVONLEA BENTONITE

BY

HAROLD B. HUME

A Thesis
Submitted to the Faculty of Graduate Studies
in Partial Fulfillment of the Requirements
for the Degree of

MASTER OF SCIENCE

Department of Soil Science
University of Manitoba
Winnipeg, Manitoba

©February, 1999

National Library of Canada
Acquisitions and Bibliographic Services
395 Wellington Street
Ottawa ON K1A 0N4
Canada

Bibliothèque nationale du Canada
Acquisitions et services bibliographiques
395, rue Wellington
Ottawa ON K1A 0N4
Canada

Your file Votre référence

Our file Notre référence

The author has granted a non-exclusive licence allowing the National Library of Canada to reproduce, loan, distribute or sell copies of this thesis in microform, paper or electronic formats.

The author retains ownership of the copyright in this thesis. Neither the thesis nor substantial extracts from it may be printed or otherwise reproduced without the author's permission.

L'auteur a accordé une licence non exclusive permettant à la Bibliothèque nationale du Canada de reproduire, prêter, distribuer ou vendre des copies de cette thèse sous la forme de microfiche/film, de reproduction sur papier ou sur format électronique.

L'auteur conserve la propriété du droit d'auteur qui protège cette thèse. Ni la thèse ni des extraits substantiels de celle-ci ne doivent être imprimés ou autrement reproduits sans son autorisation.

0-612-35063-0

Canada

THE UNIVERSITY OF MANITOBA

FACULTY OF GRADUATE STUDIES

*****

COPYRIGHT PERMISSION PAGE

GAS BREAKTHROUGH IN COMPACTED AVONLEA BENTONITE

BY

HAROLD B. HUME

A Thesis/Practicum submitted to the Faculty of Graduate Studies of The University of Manitoba in partial fulfillment of the requirements of the degree of

MASTER OF SCIENCE

HAROLD B. HUME ©1999

Permission has been granted to the Library of The University of Manitoba to lend or sell copies of this thesis/practicum, to the National Library of Canada to microfilm this thesis and to lend or sell copies of the film, and to Dissertations Abstracts International to publish an abstract of this thesis/practicum.

The author reserves other publication rights, and neither this thesis/practicum nor extensive extracts from it may be printed or otherwise reproduced without the author's written permission.

ABSTRACT

Hume, Harold B. M.Sc., The University of Manitoba, February, 1999. Gas Breakthrough in Compacted Avonlea Bentonite. Major Professors: Jim Graham, Malcolm N. Gray and Dennis W. Oscarson.

Several processes may generate gas in the proposed Canadian nuclear fuel waste disposal vault. The consequences of gas formation depend, in part, on whether gas remains in the vault or escapes. Since a bentonite-based buffer is one of the proposed vault sealing materials, an understanding of gas migration through clay is important.

Using specially-designed systems and five-minute pressure increments, the pressures required to pass gas through compacted Avonlea bentonite specimens (the gas-breakthrough pressures) were studied. Tests were conducted on saturated and unsaturated plugs with dry densities (ρ_c) between 0.6 and 1.5 Mg/m^3, using pressure increments of 0.2 MPa (low-pressure apparatus) and 1.0 MPa (high-pressure apparatus). The breakthrough pressure (p_b) of unsaturated specimens was measured with the low-pressure apparatus; p_b increased with increasing degree of saturation (S_r), provided that S_r was greater than about 80%. In specimens with a high degree of saturation, only inconsistent breakthrough was obtained at $\rho_c > 0.60$ Mg/m^3 before the 50 MPa limit of the equipment was reached. The agreement between results from saturated clay and

predictions made using models based on a capillary-pressure theory of gas breakthrough is poor.

Tests were also conducted on saturated specimens at constant pressure (p_c = 0.3 to 19.8 MPa), between ρ_c = 0.8 and 1.4 Mg/m^3, and the time to breakthrough (t_b) was measured. Breakthrough occurred in all of these tests, but often after a much longer time than the duration of the increasing-pressure tests. This shows that a model based on capillarity alone is insufficient to describe gas breakthrough. At 1.00 Mg/m^3 and p_c = 0.3 to 2.8 MPa, an inverse linear relationship exists between t_b and p_c. Models of the breakthrough process that assume a hydraulic-conductivity mechanism also suggest that t_b and p_c should be inversely related. Furthermore, excellent agreement was obtained between one of the models (the Kozeny-Carman time model) and the experimental data. The constant-pressure results do not exclude a lower limit to the pressure at which breakthrough is obtained, imposed by capillary-pressure theory, but t_b is likely determined by the time required for water to flow from the plug and thus create a passage for gas. Furthermore, if a lower limit to breakthrough exists, it is lower than measured in the increasing-pressure tests and much lower than predicted by some of the pressure models.

ACKNOWLEDGMENTS

I would like to thank the members of my supervisory committee:

Dr. Jim Graham for insightful guidance and the generous provision of lab space;

Dr. Malcolm Gray for technical advice and wise counsel;

Dr. Dennis Oscarson for technical guidance, encouragement and long-time friendship; and,

Dr. Tee Boon Goh for encouragement and assistance with the university community.

In addition, I am particularly grateful to Ms. Krista Gelmich Halayko for demonstrating the operation of the gas-breakthrough equipment and for her collaboration during the period of our studies, and to Dr. Jong-Won Choi for convincing me to pursue graduate studies.

Thanks are extended to my colleagues at the Whiteshell Laboratories of AECL who assisted in this endeavour: Dr. David Dixon, Mr. David Hnatiw, Mr. Lawrence Johnson, Mr. Nazeer Khan, Ms. Susan Miller, Mr. Barry Shenton, Ms. Thanh To and Dr. Alan Wan.

Many people at AECL participated in the construction and installation of the high-pressure gas-breakthrough apparatus including: Mr. Kevin Borgford, Mr. Louis David, Mr. Glen Graham, Mr. Len Hiebert and Mr. Len Kroeker.

Mr. Randy Herman is thanked for the cation exchange capacity and exchangeable cation analyses and Ms. Diane Doern for the XRD traces. Figures 4.2, 4.4 and 6.3 were photographed by Mr. Art Dutka, Figures 4.1, 4.5 and II.1 were drawn by the staff of Flying Pigment Design Studio and Figure 4.3 by Mr. Len Hiebert.

The financial support of the Canadian Nuclear Fuel Waste Management Program, which is jointly funded by AECL and Ontario Hydro, and of the Natural Sciences and Engineering Research Council made this work possible and is gratefully acknowledged.

Last, I wish to thank my parents for their continued support, despite my infrequent visits during the past three years.

TABLE OF CONTENTS

Page

LIST OF TABLES

LIST OF FIGURES

LIST OF SYMBOLS

A	cross-sectional area
A_c	area of contact
A_e	effective pore area
A_f	attractive unit force
A_s	surface area
b	initial pressure in an increasing-pressure gas-breakthrough experiment
B	Ostwald constant
c	concentration
c_g	concentration in the gaseous phase
c_l	concentration in the liquid phase
c_o	concentration in bulk solution
d	spacing between crystal planes
D	dielectric constant
D_e	effective or steady-state diffusion coefficient
D_{mean}	mean of the measured differences
g	acceleration due to gravity
G_{grav}	Gibb's free gravitational energy
G_{se}	Gibb's free surface energy
h	head
h_s	specimen height
h_0	digital display reading at the bottom of the cell
h_1	digital display reading at the top of the first layer of clay
h_2	digital display reading at the top of the second layer of clay
i	hydraulic gradient
$\{I\}$	unit tensor
k	hydraulic conductivity
k_B	Boltzmann constant
k_o	pore shape factor
L	distance or length
L_e	effective length
m	rate of pressure increase in an increasing-pressure gas-breakthrough test
M	mass of wet soil
M_s	mass of dry soil
M_w	mass of water
n	porosity
n_B	Bragg's law index
n_D	number of samples used in a statistical analysis of the population difference

n_o	number of cations per unit volume in the bulk solution
n_x	number of cations per unit volume at a distance x from the clay surface
N'	component of force normal to a plane
N_R	Reynolds number
p	pressure
p_b	gas-breakthrough pressure
p_c	pressure in constant-pressure gas-breakthrough tests
p_i	inlet gas pressure at breakthrough
p_o	outlet gas pressure at breakthrough
P_t	total force on soil particles
q	volumetric flux
Q	quantity diffused
r	capillary or pore radius
r_h	mean hydraulic radius
R	gas constant
R^2	coefficient of determination
R_f	repulsive unit force
s_D	standard deviation of the differences
S_m	specific surface area
S_r	degree of saturation
t	time
t_b	gas-breakthrough time
$t_{0.025}$	student's t value for a 95% confidence interval
T	absolute temperature
T'	component of force parallel to a plane
T_s	surface tension
u	pore water pressure
v	velocity of flow
v'	velocity of flow in a glass capillary or clay pore
V	total specimen volume
V_a	volume of air
V_s	volume of solids
V_v	volume of void space
V_w	volume of water
w	mass water content
w_{100}	mass water content when $S_r = 100\%$
x	distance from the clay surface
X	generic parameter
Y	range about X that gives a 95% confidence interval for X
z	cation valence
Z	air-penetration distance
α	wetting angle
β	pressure transducer calibration constant
χ	voltage

ε	charge on the electron
γ	pressure transducer calibration constant
η	viscosity
κ	inverse of the centre of gravity of the diffuse double layer
λ	wavelength
π	osmotic pressure
θ	angle between x-ray beam and crystal planes
ρ	density
ρ_c	effective clay dry density
ρ_d	soil dry density
ρ_s	soil particle density
ρ_w	water density
σ	total stress
σ'	effective stress
σ_i'	interparticle contact stress
σ'_{in}	effective stress on the inlet surface of the clay plug
σ'_{out}	effective stress on the outlet surface of the clay plug
τ	tortuosity

1. INTRODUCTION

1.1 Canadian Nuclear Fuel Waste Disposal Concept

Canadians are currently examining a concept for the safe disposal of nuclear fuel waste. The concept is described in an environmental impact statement (EIS) that was submitted to the Canadian Environmental Assessment Agency (AECL 1994). Nuclear fuel waste is currently stored in water-filled pools and concrete canisters. This can only be a temporary solution as it requires regular monitoring. The principle of sustainable development imposes an ethical responsibility to either detoxify hazardous materials or place them where they cannot enter the environment at a future time. The generation that benefits from electricity produced in nuclear reactors has a moral obligation to dispose of the waste. The Canadian nuclear fuel waste disposal concept addresses these issues by proposing a method of permanent waste disposal.

In the EIS, it is proposed that a disposal vault be excavated in a granite pluton 500 to 1000 m below the surface of the Canadian Shield (AECL 1994). Vertical shafts would connect the surface facilities with the vault. The disposal vault would consist of a network of horizontal tunnels and disposal rooms. The tunnels and disposal rooms would be several metres wide and high. The total area of the disposal vault would likely be several

square kilometres (Simmons and Baumgartner 1994). A possible disposal centre layout is illustrated in Figure 1.1.

Engineered barriers would be used, in addition to the natural barrier provided by the rock, to slow the movement of radioisotopes and chemically toxic substances to the biosphere (AECL 1994). The radioactivity of nuclear waste decreases with time, due to the decay of radioisotopes to stable isotopes. Therefore, any barrier that slows the movement of radioisotopes also reduces the amount of radioactivity that can enter the biosphere. Used fuel bundles would be placed in corrosion-resistant metal containers (Figure 1.2) designed to last at least 500 years. After 500 years, the radioactivity of the used fuel will be <0.0005% its value at the time of removal from the reactor. Containers made of both Cu and Ti have been studied. The containers could be placed on the floor of the disposal rooms (in-room emplacement) or in boreholes drilled in the floors (borehole emplacement).

Clay-based materials are important components of the disposal concept (Johnson et al. 1994b). The material surrounding the containers, termed buffer, would be comprised of 50% Avonlea bentonite clay (also known as Saskatchewan bentonite) and 50% graded silica sand, by dry mass. In the borehole-emplacement concept, the buffer would first be compacted. A hole with a slightly greater diameter than the disposal container would be augered into the buffer. Following emplacement, fine sand would be placed in the gap around the circumference of the container; this would limit the volume into which the buffer could swell and provide a pathway for the conduction of heat away from the

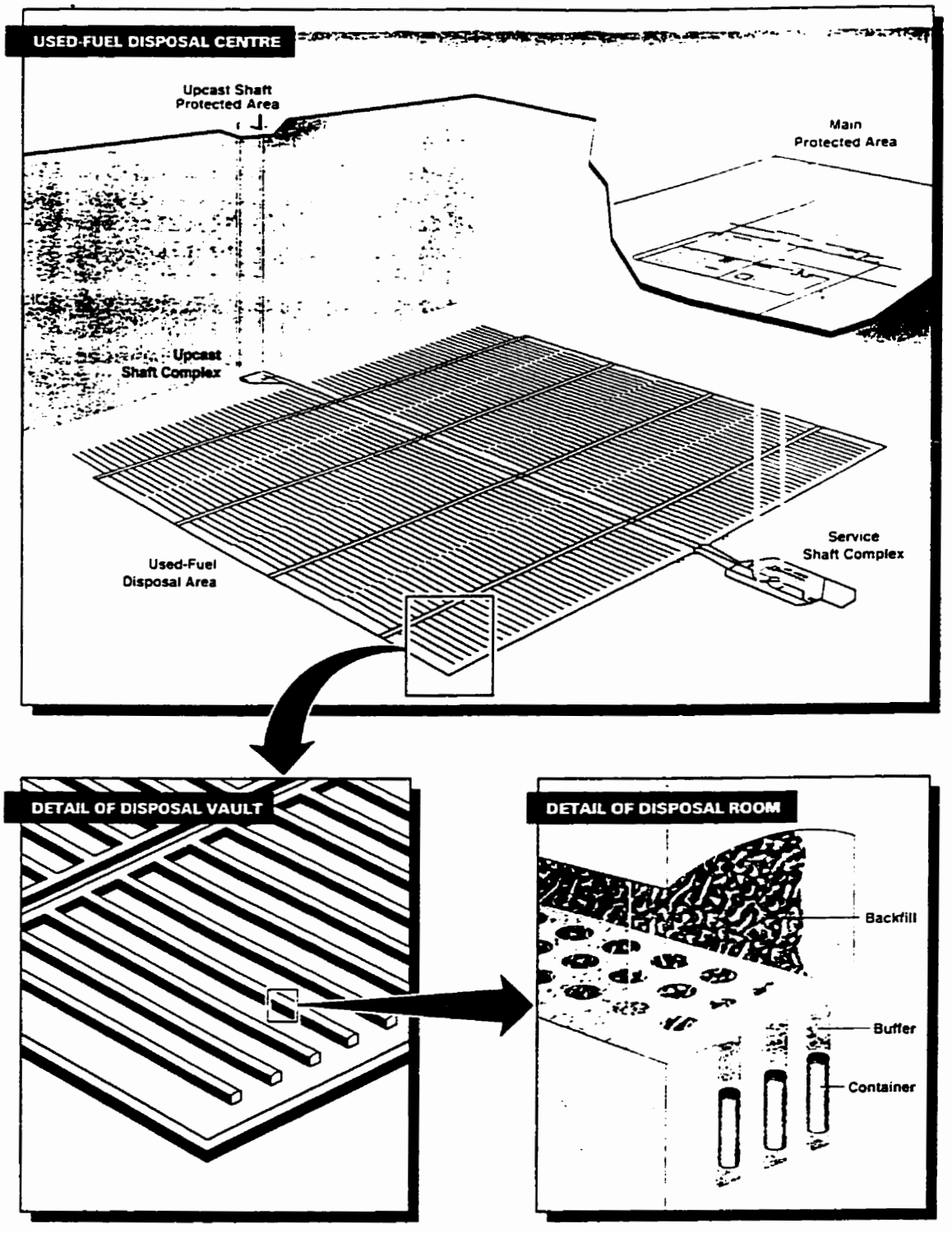

Figure 1.1 Possible layout of a used-fuel disposal centre (from Johnson et al. 1994a).

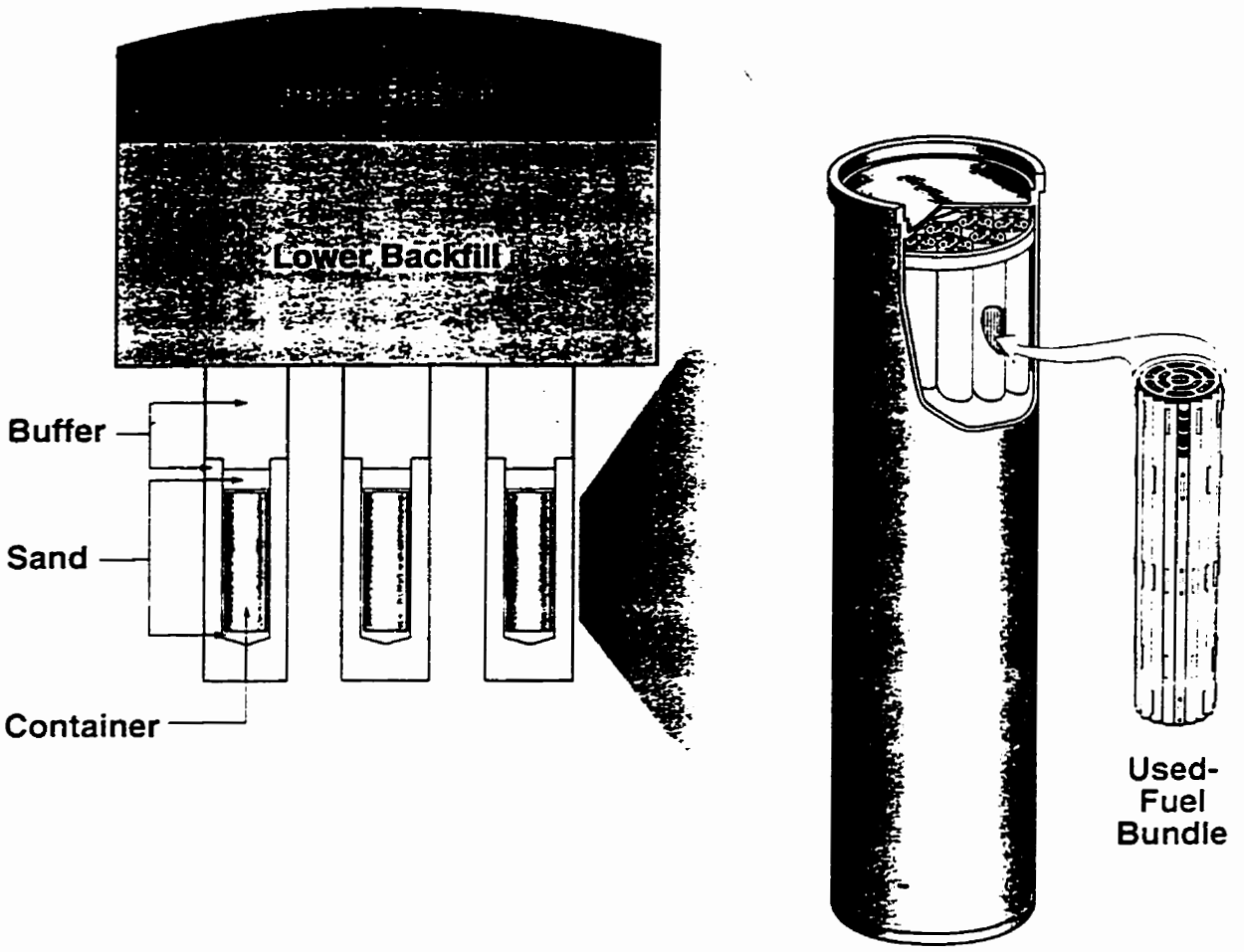

Figure 1.2 Cross-section of a disposal room showing disposal containers in boreholes (from Johnson et al. 1994a).

container. Compacted buffer would also surround the containers in the in-room-emplacement concept. In both concepts the disposal rooms and tunnels would be back-filled, likely with clay-based materials. The lower portion of the backfill would be composed of 75% crushed granite aggregate and 25% Lake Agassiz clay by dry mass. This material would be mechanically compacted to increase its density. As the machinery for compaction would require about two metres of vertical space, it is proposed that the

upper parts of the tunnels and disposal rooms be backfilled pneumatically. The composition of the upper backfill would be similar to that of the buffer. Figures 1.1 and 1.2 show the possible appearance of a disposal vault and how clay-based materials would be used to help seal the vault.

Concrete bulkheads would be placed at disposal room entrances and at critical locations in the access tunnels and shafts (Johnson et al. 1994b). The bulkheads would be grouted to the rock walls. Walls constructed of highly compacted bentonite blocks would likely be placed next to the concrete bulkheads for additional sealing. These composite seals would retain the clay-based materials in the rooms and tunnels where they were placed. They would also direct contaminant migration into the low-permeability rock by limiting movement to the surface via tunnels and vertical shafts.

A conceptual model has been developed that describes the most likely scenario by which radioisotopes could reach the biosphere (Johnson et al. 1994a). Void spaces in the disposal vault, such as the small pore spaces between clay particles in the buffer and backfill, will eventually fill with water (saturate). The containers and fuel bundles will slowly corrode and perforate. Radioisotopes in the gap between the fuel pellet and sheath, in cracks in the pellet and between grains in the fuel pellet would dissolve relatively quickly in the groundwater. (Fuel pellets and the sheath containing them are visible in the used-fuel bundle in Figure 1.2.) The large majority of the radioisotopes would be released slowly from the UO_2 fuel matrix and the Zr-alloy fuel sheaths, as they dissolve. The contaminants, dissolved in groundwater, could then move through pores in the buffer and

backfill materials, into the surrounding granite, and then to the biosphere. Once radioisotopes reach the biosphere, human exposure could result from activities such as drinking well water, consuming fruits and vegetables grown in the soil, consuming livestock that grazed on plants grown in the soil, or inhaling. The barriers described previously are designed to limit the movement of contaminants from a disposal vault to the biosphere.

Dissolved contaminants might migrate through the pores of the buffer and backfill due to advection or diffusion, or both. Advection, also known as convection, is the flow of groundwater through a porous medium due to a hydraulic gradient (defined in section 2.4). Diffusion is the movement of a substance, in this case dissolved contaminants, from a region of high concentration to a region of low concentration due to random molecular movement. The relevance of these two processes to the nuclear fuel waste disposal concept has been studied. Given the low hydraulic conductivity of the buffer (defined in section 2.4; Dixon 1995), and the low hydraulic gradients expected in a disposal vault (Chan 1989), diffusion is likely to be the dominant migration mechanism in the buffer (Johnson et al. 1994a). Both diffusion and advection may occur in the backfill, although diffusion will likely dominate (Johnson et al. 1994a). A mathematical model of this process has been developed to demonstrate how contaminant transport in the buffer and backfill can be quantified. However, the effect of a gas phase on contaminant transport in clay-based materials has not been included in either the conceptual or mathematical models. This forms the topic studied in this thesis.

1.2 Gas Sources

A number of potential gas sources have been identified in the proposed nuclear fuel waste disposal vault. Some sources are more likely to produce significant quantities of gas than others. The gas sources can be divided into four classes: gases present at the time of vault sealing, and those produced chemically, radiochemically and biochemically.

1.2.1 Gases Present at the Time of Vault Sealing

Immediately following emplacement, both the buffer and backfill pores would contain air. The containers would have air inside unless they are internally supported by solid metal (that is, molten metal is poured into the containers to fill the void spaces, before they are sealed). The buffer and backfill would be moist before emplacement and, as a result, their void spaces would be at least partially filled with water after compaction. This water would contain air dissolved at its solubility limit at atmospheric pressure. The remaining voids contain air which would gradually be replaced with water from the rock surrounding the disposal vault. A typical water from the Canadian Shield contains about 1.6×10^{-3} M dissolved N_2 (Gascoyne 1992). The gases He, Kr and Xe are present as stable isotopes in used nuclear fuel (AECL 1994) and they would be released when the containers and fuel bundles are perforated. Radon-222, a radioactive gas produced in the natural decay of ^{238}U, would also be released into the vault when the containers and fuel bundles are breached.

1.2.2 Gases Produced Chemically

Johnson et al. (1994a) predict that the disposal vault will become anaerobic between 8 and 300 years after it is closed. Under anaerobic conditions some metals can oxidize, by reaction with water, with H_2 being produced in the reaction. As Cu and Ti are potential container materials, these metals must be considered. The Zr-alloy fuel bundles are another potential source of H_2 from this mechanism. Steel may be used for various purposes in a disposal facility and therefore Fe should also be considered. In the absence of S^{2-}, the thermodynamic stability of Cu precludes any reactions with water in a disposal vault (Pourbaix 1966). Titanium reacts with water under anaerobic conditions (Johnson et al. 1994a)

$$Ti + 2\ H_2O \rightarrow TiO_2 + 2\ H_2 .$$

The corrosion rate of Ti plate in bentonite pore water is 2 nm/year (Mattsson and Olefjord 1984). Little appears to be known about the anaerobic behaviour of the Zr alloy used in fuel bundles. In anaerobic conditions, the Fe in steel may react according to

$$3\ Fe + 4\ H_2O \rightarrow Fe_3O_4 + 4\ H_2$$

or

$$Fe + 2\ H_2O \rightarrow Fe(OH)_2 + H_2$$

(Voinis et al. 1992). Which reaction will occur depends on parameters such as pH, E_h and temperature in the disposal vault. Voinis et al. (1992) report that the rate of corrosion of stainless steel plate ranges from 0.1 to 100 μm/year depending on the experimental conditions. The corrosion rate of carbon steel is likely greater.

1.2.3 Gases Produced Radiochemically

Gamma irradiation of clay slurries produces H_2, O_2, CO_2 and CH_4, while irradiation of air produces N_2O (Voinis et al. 1992). The O_2 would react with reduced chemical species in an anaerobic environment and, depending on the type of concrete used for the bulkheads, CO_2 may precipitate by the reaction

$$CO_2 + Ca(OH)_2 \rightarrow CaCO_3 + H_2O\ .$$

This reaction could be beneficial if the $CaCO_3$ plugs the buffer and backfill pores, thus reducing water movement (Rees 1992). The other gases produced by gamma irradiation might persist in the vault. Following container and fuel bundle corrosion, alpha radiolysis of water can produce O_2 and H_2 (Christensen and Bjergbakke 1982). Alpha particle decay will generate He. Although not strictly a radiochemical product, the absorption of radiation by matter generates heat. This heat in turn could cause water vaporization and may cause the release of dissolved gas from liquids and sorbed gas from geologic materials.

1.2.4 Gases Produced Biochemically

Microbial processes in a disposal vault may also produce gas. Carbon is present in both the buffer and backfill clays (Oscarson and Dixon 1989). It may also be introduced during operation of the vault from, for example, hydrocarbon leaks from equipment used underground. Microbes may convert the C to CO_2 or CH_4. However, Sheppard et al. (1996) have been unable to produce CH_4 in anaerobic clay slurries. Other microbes

known as methanogens can use CO_2 to produce CH_4 and methanotrophs can oxidize CH_4 (Sheppard et al. 1996). Sulphate is present in the disposal-vault clays and sulphur-reducing bacteria can convert this to H_2S in an anaerobic environment (Sheppard et al. 1996). If S^{2-} is produced in significant quantities by microbes, the Cu containers could be another source of H_2.

1.3 Consequences of Gas Generation

Gas generation in a disposal vault has several potential problems and at least one possible benefit. Although most of the gases discussed in section 1.2 are not radioactive when formed, they may become so after the containers and fuel bundles are breached. Substitution of a stable atom by a radioisotope could occur. For example, in H_2 and CH_4 ^1H could be substituted by ^3H, and ^{14}C could substitute for ^{12}C in CH_4 and CO_2. Neutrons emanating from used fuel could generate radioisotopes from stable isotopes. Therefore, radioactive and non-radioactive gases may both be present in a disposal vault.

Johnson et al. (1994a) showed that the rate of gas generation in the Canadian nuclear fuel waste disposal concept is likely to exceed the rate at which gas can move out of the vault by diffusion. Therefore the groundwater will become saturated with gas and bubbles may form.

The theory of gas movement in porous media is not as well developed as the understanding of contaminant movement by diffusive and advective transport.

Nevertheless, direct and coupled transport mechanisms can both be envisioned. Direct transport is the movement of a gas phase to the biosphere. There may indeed be possible benefits from intentionally reducing the pressure in a disposal vault by permitting the gas to vent. This appears to contradict conventional vault design theory that assumes the vault should be sealed to minimize water movement. Venting of gas would only be acceptable if the gas was not radioactive, toxic or hazardous. However, as mentioned previously, likely repository gases may become radioactive following formation. Given the gases most likely to be produced, as described in section 1.2, high toxicity is unlikely to be a problem. However, both H_2 and CH_4 are explosive if present in sufficient concentration. Kroth et al. (1992) state that 4% H_2 is the lower explosive limit in air. It appears, therefore, that movement of gas to the surface could potentially have design and performance implications.

Coupled transport mechanisms include enhanced advection or diffusion due to the presence of gas. Advective transport depends upon the hydraulic conductivity and hydraulic gradient present in the disposal facility. Because both are expected to be low, especially when the vault is unsaturated, advective transport is unlikely to occur in the buffer and should be of minor importance in the backfill. However, hydraulic gradients may increase due to gas pressure in a disposal vault. As well, the passage of gas through the buffer or backfill may cause changes to the structure of these materials, such as pore dilation or fracturing, leading to increases in the hydraulic conductivity. Due to changes in the fabric of the materials, gas passage could also increase diffusion rates.

If high gas pressures are not released from the vault, container failures might occur sooner than predicted, leading to earlier than expected dissolution of radioisotopes in the groundwater. Conversely, if gas forms next to the container surface and remains there, it could limit water access to the container. This might reduce container corrosion and result in longer container lifetimes. Container corrosion would not be stopped completely because the gas would dissolve in groundwater up to its solubility limit and slowly diffuse away.

Given that gases will likely form in a disposal vault and that the understanding of the fate of these gases is limited, the study of gas migration in clay is important. This research continues and develops work started by Kirkham (1995). Using a specially-designed apparatus, Kirkham measured the pressure required to force gas through wet, compacted illitic clay (gas breakthrough) at various clay densities. The tests were performed by increasing the gas pressure in short-duration increments until breakthrough occurred. He also conducted six tests on water-saturated buffer material, but obtained gas breakthrough in only one specimen before reaching the pressure limit of the equipment. Others have done similar work using different apparatus and materials (section 2.6).

As noted, Avonlea bentonite is the clay component of the buffer material proposed in the Canadian nuclear waste disposal concept. This research has examined the gas-breakthrough pressure of Avonlea bentonite. Special efforts were made to understand the mechanisms of gas movement in bentonite. This was done so that the relevance of gas to contaminant migration from a nuclear fuel waste disposal vault can be more accurately

assessed. This should facilitate a decision as to whether gas generation and migration must be included in future conceptual and mathematical models of contaminant transport.

1.4 Overview

Some basic ideas and concepts about clays, from both soil science and geotechnical engineering perspectives, are introduced in the early sections of the literature review (chapter 2). Hydraulic conductivity is discussed later in the chapter. Building on the mathematics of hydraulic conductivity, models of the gas-breakthrough process obtained from the literature are presented followed, for consistency, by some original modeling by the author. The literature review concludes with a summary of gas-breakthrough results presented by other researchers.

Chapter 3 briefly describes the materials that were used in the gas-breakthrough experiments. A short description of a low-pressure gas-breakthrough apparatus used for the early tests starts chapter 4, followed by an explanation of the experimental procedures. A high-pressure gas-breakthrough apparatus that was constructed for this research is described later in chapter 4, along with procedures for operating the equipment.

The experimental results are presented in chapter 5 and a discussion of their significance in chapter 6. An attempt is made in the discussion to understand the experimental results using the theoretical models described in the literature review. Possible mechanisms for gas-breakthrough, and the theoretical gas-breakthrough behaviour assuming such

mechanisms, are compared with the data obtained. The summary chapter (7) consists of a brief review of the research and the major findings.

2. LITERATURE REVIEW

2.1 Clay Science

2.1.1 Introduction

With respect to mass transport from the vault, the active component of the buffer proposed for use as a seal in the Canadian nuclear fuel waste disposal concept is Avonlea bentonite clay; silica sand is essentially an inert filler (Dixon et al. 1987). Therefore, contaminant migration in buffer can be better understood with a knowledge of clay mineralogy and chemistry. The term 'clay' can refer to soil particle size, soil type and specific soil minerals. By definition, soil particles less than two micrometres equivalent spherical diameter constitute the clay-size fraction (Craig 1994). Most particles of this size are clay minerals, although there are exceptions (for example, rock flour particles can be this size or smaller). If more than about 50 weight percent of the particles in a soil are clay size, the behaviour of the soil is dominated by the clay particles; the larger soil particles (silt, sand, et cetera) have only a minor influence (Holtz and Kovacs 1981). (The precise percent value depends on the type of clay mineral.) Soils composed of more than 50% clay-size particles have properties characteristic of clay soils. Clay minerals are largely defined by their crystal structure, which is described in the next section. Whether

the term 'clay' refers to particle size, soil type or mineral can usually be determined from the context in which it is used.

2.1.2 Clay Mineralogy

Clays are secondary minerals formed from primary minerals by weathering processes (McBride 1994). Physical weathering breaks the primary mineral into progressively smaller particles, with an ever increasing surface area on which chemical weathering can occur. Chemical weathering occurs simultaneously with physical weathering and causes the mineral to slowly dissolve. Clays are often formed when the dissolved material recrystallizes from solution (McBride 1994). The type of clay mineral formed depends on thermodynamic and kinetic factors.

When viewed with an electron microscope, dry clay particles appear as flakes (Holtz and Kovacs 1981). This accounts in part for some of the synonyms by which clays are known: layer silicates (or layer aluminosilicates), sheet silicates (or sheet aluminosilicates) and phyllosilicates. Each dry particle is composed of many layers (Holtz and Kovacs 1981), much like a stack of paper is composed of individual sheets. In some clays (swelling clays) these layers separate when the particle is placed in aqueous solution, whereas in non-swelling clays the layers remain bonded together (McBride 1994). Swelling clays are proposed in the nuclear fuel waste disposal concept because their expansive properties will assist in sealing the vault. Some swelling and non-swelling clay minerals are identified in section 2.1.5.

In the most common clay minerals, each layer is composed of one or two sheets of silica tetrahedra and one sheet of alumina octahedra (Craig 1994). A silica tetrahedron (triangular-base pyramid) consists of a central Si^{4+} cation surrounded by four O^{2-} anions as illustrated in Figure 2.1(a). All three basal O^{2-} are shared with adjacent tetrahedra (Figure 2.1(b)), resulting in a very large sheet with the chemical formula $Si_2O_5^{2-}$. A schematic representation of the silica sheet is shown in Figure 2.1(c); it will be used later to illustrate the arrangement of sheets in some common clay minerals (section 2.1.5). When viewed perpendicular to the plane of the sheet, a hexagonal-shaped hole known as the ditrigonal cavity is present between the bases of the silica tetrahedra (Figure 2.1(d)). The alumina sheet consists of octahedra of OH^- anions surrounding Al^{3+} cations, as shown in Figures 2.2(a) and (b). Figure 2.2(c) shows a schematic representation of an alumina sheet. As each OH^- in the octahedron is shared by two Al^{3+}, the chemical formula of the alumina sheet is $Al(OH)_3$. Both the alumina and silica sheets have large surface areas, but they are relatively thin perpendicular to the plane of the sheet.

The silica sheet is bonded to the alumina sheet through the O^{2-} ions at the apex of the tetrahedron (apical O^{2-}; McBride 1994). One OH^- ion is missing from each $Al(OH)_3$ molecule because the apical O^{2-} from the silica tetrahedron is also bonded to two Al^{3+} ions (McBride 1994). The stoichiometry of the formation of a 1:1 clay (one silica sheet and one alumina sheet) is

$$Si_2O_5^{2-} + 2\ Al(OH)_3 \rightarrow Si_2Al_2O_5(OH)_4 + 2\ OH^- .$$

In this clay, one surface of each layer has hydroxyls exposed (from the alumina sheet) and the opposite surface is composed of basal O (from the silica sheet). A 2:1 clay, which

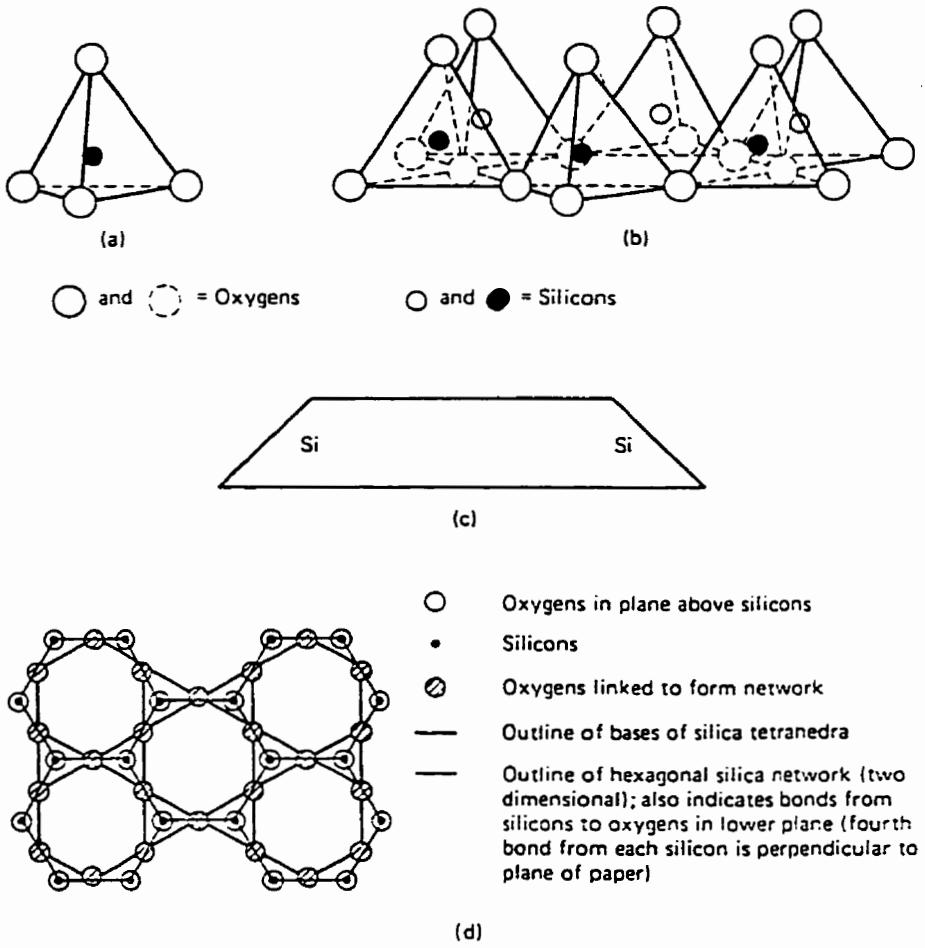

Figure 2.1 (a) A silica tetrahedron. (b) Six silica tetrahedra bonded together. (c) Schematic representation of a silica sheet. (d) View perpendicular to the sheet showing five ditrigonal cavities. (From Holtz and Kovacs 1981.)

consists of an alumina sheet sandwiched between two silica sheets, would be formed by reaction of the previous product with another $Si_2O_5^{2-}$ ion

$$Si_2Al_2O_5(OH)_4 + Si_2O_5^{2-} \rightarrow Si_4Al_2O_{10}(OH)_2 + 2\ OH^-\ .$$

Both surfaces of the layers of 2:1 clays are identical, consisting of the outward-facing basal O of silica tetrahedra.

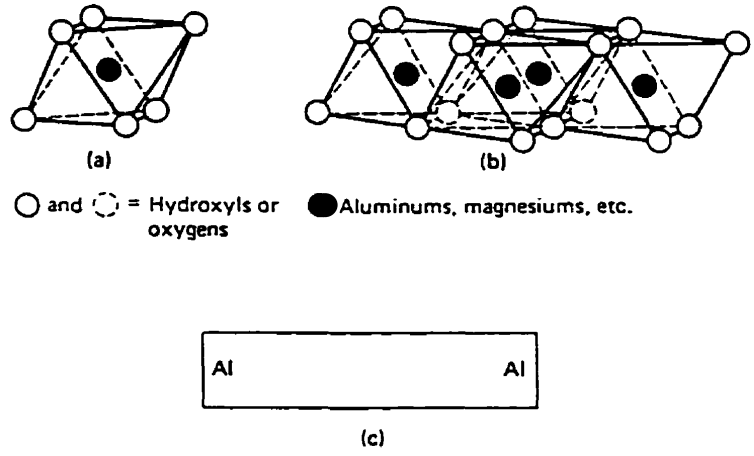

Figure 2.2 (a) An alumina octahedron. (b) Alumina octahedra bonded together. (c) Schematic representation of an alumina sheet. (From Holtz and Kovacs 1981.)

2.1.3 Isomorphous Substitution and the Diffuse Double Layer

Substitution of other cations for Si^{4+} (in the tetrahedral sheet) or Al^{3+} (in the octahedral sheet) is common. This is known as isomorphous substitution because the basic anion structure of the sheet remains relatively unchanged (McBride 1994). The most common substitutions are Al^{3+} for Si^{4+} in the tetrahedral sheet and Mg^{2+} or Fe^{2+} for Al^{3+} in the octahedral sheet (Mitchell 1976). Because the substituting ion has a valence less than the ion being replaced, a clay with isomorphous substitution has a net negative charge on its structure. This charge is neutralized by cations which are tightly bound to the structure when the clay is dry (Mitchell 1976), much like Na^+ and Cl^- are strongly bonded in crystalline NaCl.

When some clays are immersed in water, charge-balancing cations dissociate from the negatively-charged structure and concentrate near the particle, forming an adjacent region of solution that is positively charged (Mitchell 1976). This is analogous to the dissociation into Na^+ and Cl^- ion pairs that occurs when NaCl is dissolved in water, except that with clays the negative charge is on the clay particle. Mitchell (1976) states "The negative surface and the distributed charge in the adjacent phase are together termed the diffuse double layer."

The Gouy-Chapman mathematical model has been developed to describe the distribution of ions in the diffuse layer. According to Mitchell (1976), the model assumes that:

(1) the ions in solution can be considered as point charges that do not interact,

(2) the charge on the clay surface is uniform,

(3) the dimensions of the clay surface are much greater than the thickness of the aqueous ion double layer in the direction perpendicular to the surface, and

(4) the dielectric constant of the water is constant.

With these assumptions, the distribution of ions in solution next to the clay is given by the Boltzmann equation and the characteristics of the electric field surrounding the clay can be described by the Poisson equation (Yong and Warkentin 1975).

Using the Gouy-Chapman model, Yong and Warkentin (1975) calculated the concentration of cations near a clay particle from

$$n_x = n_o(\coth(1.6z(c_o)^{0.5}x))^2 , \qquad [1]$$

where n_x and n_o are the number of cations per unit volume (both in the same units) at a distance x from the surface (in nm) and in the bulk solution, respectively; z the valence of the cation in solution and c_o the concentration (mol/L) in the bulk solution. To calculate the relative thickness of the positively-charged solution surrounding a clay particle, Mitchell (1976) provided the equation

$$1/\kappa = (Dk_BT/8\pi n_o\varepsilon^2z^2)^{0.5}, \qquad [2]$$

where $1/\kappa$ is the centre of gravity of the layer (a relative measure of thickness), D the dielectric constant, k_B the Boltzmann constant, T the absolute temperature and ε the charge on the electron.

The assumptions of the Gouy-Chapman model clearly include approximations and, therefore, results obtained from [1] and [2] should be considered approximate. For example, the assumptions lead to the predicted concentration of cations next to the clay particle being so high that they cannot physically fit onto the available surface area (Mitchell 1976). The Stern model, a modification of the Gouy-Chapman model, corrects for this by assuming that the first layer is composed of close-packed cations (Yong et al. 1992).

The cation layer may be replaced (exchanged) if a different cation species is added to a suspension of clay in water (Mitchell 1976). The exchangeable cation composition of a clay can be determined by displacing the existing cations and analyzing the solution for the common naturally-occurring cations like Na^+, K^+, Ca^{2+} and Mg^{2+} (Thomas 1982).

The cation exchange capacity of a clay is an important chemical property. For example, cation exchange will slow the migration of some contaminant species from a nuclear fuel waste disposal vault to the biosphere. To measure the cation exchange capacity of a clay, a homoionic clay, in which all the exchange sites are occupied by one cation species, is prepared. The cation exchange capacity is measured by displacing all the cations on the homoionic clay with a different cation, and determining the quantity of cations that were replaced (Rhoades 1982).

Richards (1974) discussed four possible mechanisms of interaction between water molecules and clays.

(1) Due to the relative electronegativities of the atoms, the O to H bond is polarized. The electron density is disproportionately located in the region of the O, producing a slight negative charge on the O and a slight positive charge on the H. Therefore, the H atoms in water molecules can be electrostatically attracted to the outward-facing basal O atoms of silica sheets in 1:1 and 2:1 clays. As well, the O atoms of water molecules are drawn towards the hydroxyl H atoms that are present on the exposed alumina surface of 1:1 clays. This process is known as hydrogen bonding.

(2) Interactions can occur between the positive dipoles of water molecules and the negatively-charged clay. Richards (1974) refers to this as polar adsorption.

(3) Cations are hydrated to varying degrees when in solution, and the charge balancing cations present on some dry clays attract water molecules as they dissociate from the clay structure when wetted.

(4) Weak London forces (also known as van der Waals forces) between water molecules and the clay surfaces can play a part in the wetting of clays.

Hydrogen bonding (point (1) above) is likely the dominant mode of interaction between water and clay (Yong and Warkentin 1975). However, whatever the mechanism, water forms a hydration shell around clay. This raises another potential problem with the Gouy-Chapman model. The particle surface is most likely covered with a combination of cations and water molecules, the composition depending on the pore fluid chemistry. Interactions between water molecules and the clay surface are not considered in the Gouy-Chapman model (Mitchell 1976).

Regardless of the mechanism of interaction between clay and water, it is important to note that the hydration shell does not neutralize the negative charge on clay. In those mechanisms where there is an assumed separation of charge in the water molecules surrounding the clay, the magnitude of the positive and negative charges are exactly equal.

Dixon (1995) summarized several evaluations of the thickness of hydration shells. Thicknesses between 0.5 and 10 nm have been reported, which corresponds to a layer of water two to about 35 molecules thick. Yong and Warkentin (1975) stated "Each successive layer is held less strongly, and the bonding quickly decreases to that of free water." Therefore, it would be wrong to envision several molecular layers of water strongly bonded to the clay surface and to each other, followed by an abrupt transition to water with the properties of bulk water. Rather, the strength of bonding decreases

continuously, as the distance from the clay surface increases, until the bonding is the same as that in bulk water. Since different experimental techniques measure different amounts of bound water, it is not surprising that a range of measured values has been reported for the thickness of the hydration shell.

Just as the Gouy-Chapman model is limited because it does not consider the presence of water, a model that considers hydration water in isolation is also incomplete. A total picture must include all three components: negatively-charged clay, polarizable water molecules and cations. Interactions among all three components must be considered in a complete description of the system (Yong et al. 1992).

With respect to gas breakthrough in clay, the important point is that the strength of bonding between layers of water molecules decreases with increasing distance from the clay surface. Therefore, the number of water layers that are mobile in a gas-breakthrough experiment may depend on the applied gas pressure. If gas is moving through a pore in the clay, the effective size of the opening (and therefore the flux) might increase as more of the water bound to the surfaces of the clay particles surrounding the pore is mobilized. As a result, the effective pore size and the gas flux may depend on the gas pressure.

2.1.4 Specific Surface Area

As noted, clay particles are small and they are often electrically charged. For these and other reasons, many clays are surface active. Therefore the specific surface area (S_m;

surface area per unit mass) is an important property. For example, the amount of water associated with a clay particle depends, in part, on S_m (Holtz and Kovacs 1981). For a non-swelling clay, there is little difference in S_m between wet and dry samples. However, as the layers of a swelling clay separate on wetting, S_m can increase substantially. With a swelling clay it is therefore important to consider whether the wet or dry surface area is most appropriate to the problem being studied (Carter et al. 1986). Given that a nuclear fuel waste disposal vault is expected to saturate with water some time after sealing, S_m of wet clay is relevant.

To measure S_m, a material (sorbate) that forms a monomolecular layer on the clay (sorbent) at equilibrium is required. The sorbate and sorbent are combined and left to equilibrate. Provided the surface area covered by a unit mass of the sorbate is known, S_m can be calculated from the starting mass of dry clay and equilibrium mass of retained sorbate. However, S_m depends on the procedure that is used for the measurement. For example, different sorbates may give different results due to variations in the bonding mechanism to the clay. Evidence shows that both ethylene glycol and ethylene glycol monoethyl ether form a monolayer on clay, and that the surface area accessible to these two compounds is similar to that accessible to water (Carter et al. 1986). These two sorbates are often used to determine S_m. However, S_m is normally measured on loose clay and, therefore, the values are not directly applicable to compacted clay. For example, some pores accessible to the sorbate when the clay is loose may be inaccessible (occluded) in compacted clay. Caution is necessary when S_m measurements obtained on loose clay are applied to compacted specimens.

2.1.5 Clay Minerals

Most of the dozens of clay minerals that have been identified are formed from combinations of alumina and silica sheets (Holtz and Kovacs 1981). The differences among clay minerals arise from different ratios of silica to alumina sheets (for example, 1:1 or 2:1), isomorphous substitution and different types of bonding between the layers (Yong and Warkentin 1975). Although the clay minerals are numerous, five of the more common are: kaolinite, illite, montmorillonite, vermiculite and chlorite. Only the first three are described because, as the results presented in section 3.1.4 will show, they are the clay minerals present in the Avonlea bentonite used for the gas-breakthrough experiments.

Kaolinite consists of one silica and one alumina sheet. Ideally it has the chemical formula $Si_2Al_2O_5(OH)_4$ (McBride 1994). There is very little isomorphous substitution in kaolinite and hence it has a low cation exchange capacity (0.01 to 0.15 mol/kg (McBride 1994)). A typical kaolinite crystal consists of 70 to 100 layers stacked one on top of the other (Holtz and Kovacs 1981), perpendicular to the plane of the sheets, as shown in Figure 2.3(a). The positively-charged H atoms on the exposed hydroxyls of the alumina sheet are electrostatically attracted to the O atoms on the base of the adjacent silica sheet that have a slight negative charge. This hydrogen bonding holds the layers of a kaolinite crystal together, even in a polar solvent like water (McBride 1994). The result, on a macroscopic scale, is that kaolinite does not swell when wetted. It has a relatively low specific surface area of 5 to 20 m^2/g (McBride 1994).

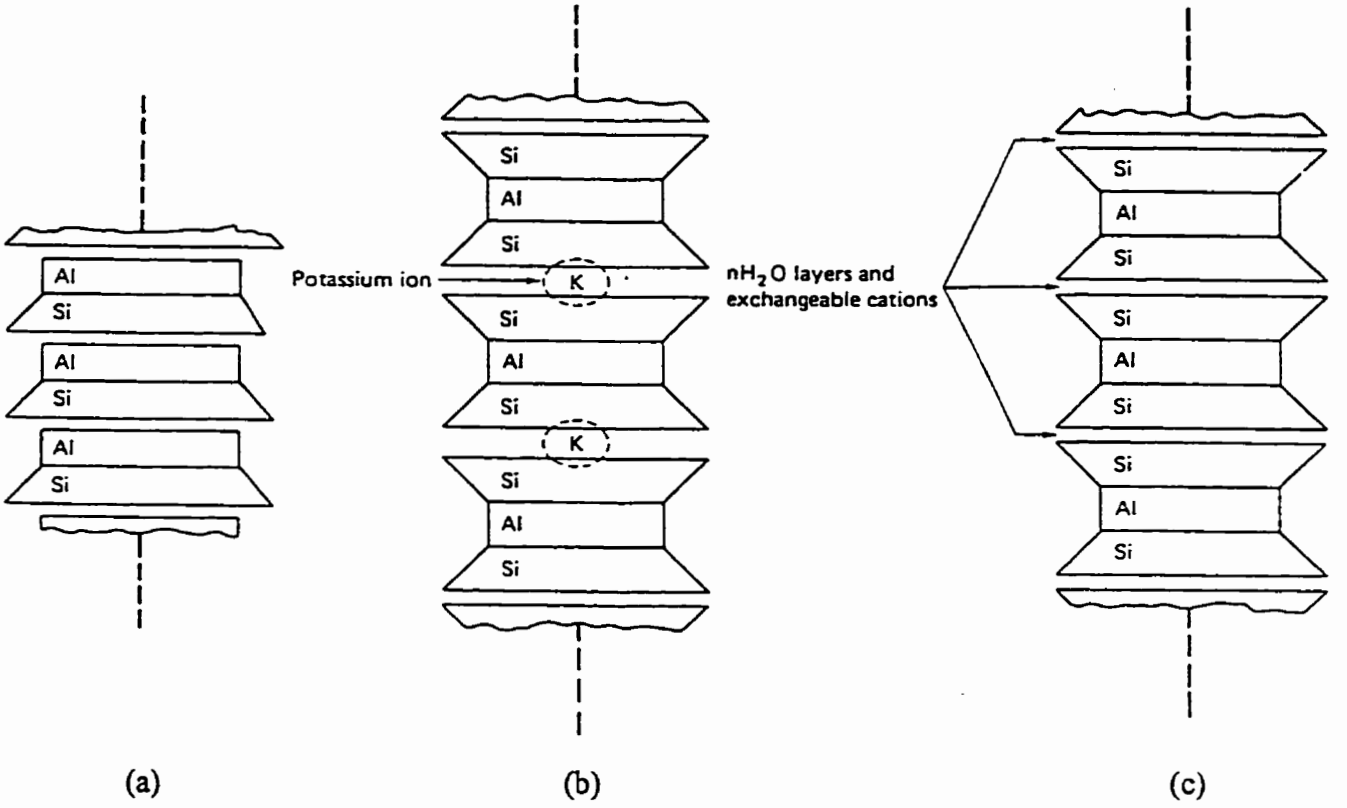

Figure 2.3 (a) Kaolinite. (b) Illite. (c) Montmorillonite. (Adapted from Holtz and Kovacs 1981.)

Illite, also known as hydrous mica, is a 2:1 clay as shown in Figure 2.3(b). It is actually several clay minerals that are grouped together because they have similar properties and are difficult to distinguish. Two of the more common minerals in the illite group are muscovite and biotite. If there was no isomorphous substitution in illite, both muscovite and biotite would have the formula $Si_4Al_2O_{10}(OH)_2$. However, in muscovite 25% of the Si^{4+} in the tetrahedral sheet are substituted by Al^{3+}, and K^+ neutralizes the net negative charge, resulting in the formula $(Si_3Al)Al_2O_{10}(OH)_2K$ (Mitchell 1976). The tetrahedral sheet of biotite is substituted the same as the tetrahedral sheet of muscovite. In addition,

the octahedral sheet contains some combination of Mg^{2+} and Fe^{2+} ions totaling three, rather than two Al^{3+}, so the biotite formula is $(Si_3Al)(Mg,Fe)_3O_{10}(OH)_2K$ (Mitchell 1976). Illite has the most isomorphous substitution of any clay mineral, but it has a moderate cation exchange capacity of 0.1 to 0.4 mol/kg (McBride 1994). The reason for this is that the unhydrated, charge-neutralizing K^+ ions are the correct size to fit in the ditrigonal cavities in the silica sheets of two adjacent layers (Mitchell 1976). The bonding between the K^+ cation and the 12 O atoms ringing the ditrigonal cavities is therefore strong (Mitchell 1976). Moreover, the heat of hydration of K^+ is 322 kJ/mol, which is low relative to other common exchangeable cations (Cotton and Wilkinson (1980)). Therefore, due to the relative sizes of K^+ and the ditrigonal cavity and the low solvation energy of K^+, bonding to the clay is thermodynamically favoured. This strong bonding limits the amount of layer separation that occurs when illite is placed in water. The above explanation accounts for the moderate specific surface area of illite (80 to 150 m^2/g (McBride 1994)) and its limited swelling when wetted.

Smectite is the name of a group of clay minerals that swell significantly in water; montmorillonite is the most common mineral in this group. Soils that are composed mostly of Na-montmorillonite are known as bentonites (Holtz and Kovacs 1981). Like illite, montmorillonite consists of an alumina sheet sandwiched between two silica sheets (Figure 2.3(c)). In montmorillonite, isomorphous substitution of Al^{3+} by Mg^{2+} occurs in the octahedral sheet. The formula of montmorillonite is $Si_4(Al_{2-x}Mg_x)O_{10}(OH)_2M_y$ where x is between 0.5 and 1.2 (Mitchell 1976). (The symbol M represents any cation present to neutralize the negative charge on the clay structure. The value of y is equal to x if M is

monovalent and it is equal to 0.5x if M is divalent.) Montmorillonite has a relatively large specific surface area when wet (700 to 800 m^2/g (McBride 1994)), because the layers separate. The cation exchange capacity of montmorillonite is greater than either kaolinite or illite. The theoretical cation exchange capacity calculated from the above formula ranges from 1.3 to 3.1 mol/kg (assuming M = Na). However, McBride (1994) reported measured values between 0.7 and 1.2 mol/kg.

2.1.6 X-ray Diffraction

As described in section 2.1.2, most clay minerals are composed of sheets of silica tetrahedra and alumina octahedra that are bonded together to form layers. A clay particle consists of a stack of these layers. Due to the stacking of the layers, repeating planes of atoms exist within the particles. The presence of recurrent atomic planes allows clay minerals to be identified by x-ray diffraction (Whittig 1976).

The principle of x-ray diffraction will be described with reference to Figure 2.4. Imagine the incident x-ray beam AB rotating clockwise from a point parallel and to the left of the crystal planes, to a point perpendicular and above the planes. Assume that the points D and P are fixed. If the distance between crystal planes is d, the ray BPB' travels a distance that increases from zero to 2d further than ADA', depending on the angle between the incident beam and the atomic planes (θ). At certain θ, diffracted beams are observed. If the wavelength of the x-rays is λ, it can be shown that diffraction peaks will be obtained whenever the value of n_B in Bragg's law

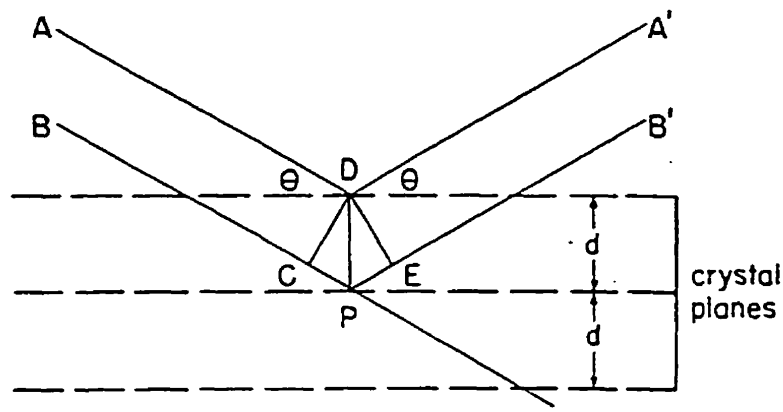

Figure 2.4 X-ray diffraction from crystal planes (from Whittig 1976).

$$n_B\lambda = 2d\sin\theta \qquad [3]$$

is integral. Since λ is fixed and θ is known following an experiment, d can be calculated if values of n_B are obtained by trial and error.

When combined with chemical treatment of the clay, clay minerals can often be identified from the x-ray diffraction pattern of parallel-oriented samples (Whittig 1976). Table 2.1 lists the d(001) spacings (that is, the value of d when $n_B = 1$) of the five clay minerals mentioned in the previous section. The air-dry d(001) values for chlorite, montmorillonite and vermiculite are all about 1.4 nm. However, solvating a sample with ethylene glycol causes montmorillonite to expand to about 1.7 nm, while chlorite and vermiculite are unchanged. Saturating the exchange complex with K^+ and heating to 500°C causes montmorillonite and vermiculite to collapse to about 1.0 nm, but chlorite is unaffected. Kaolinite becomes amorphous to x-rays when heated to 500°C. Thus x-ray diffraction can be used to distinguish between these five common clay minerals in a sample. Identification

Table 2.1 d(001) spacings of some common clay minerals[a]

Mineral	Air-dry (nm)	Glycolated (nm)	K^+/500°C (nm)
Kaolinite	0.7	0.7	-
Illite	1.0	1.0	1.0
Montmorillonite	1.4	1.7	1.0
Vermiculite	1.4	1.4	1.0
Chlorite	1.4	1.4	1.4

[a]From Moore and Reynolds (1989).

of the minerals present in a clay sample is important because, as noted, each clay mineral has distinct properties.

2.2 Soil Mechanics

2.2.1 Introduction

Soil mechanics provides a conceptual framework that is useful for the study of the mechanical properties of clay. Whereas clay chemistry and mineralogy are applicable to both loose and dense specimens, soil mechanics is primarily concerned with compacted specimens or natural samples where the void spaces between the particles are small.

From an engineering perspective, compacted soil consists of solid particles with void spaces (pores) between them (Holtz and Kovacs 1981). A macroscopic analogy for this would be a bag of corn flakes, with the flakes representing soil particles and the volume

between them corresponding to the void spaces between soil particles. The pores in soil may be completely filled with air or water, or partially filled with both (Holtz and Kovacs 1981). When the void space is completely filled with water, the soil is said to be saturated; otherwise it is unsaturated. The mathematical model of advective transport through a porous medium (section 2.4) assumes that the pore structure is constant spatially and temporally (Mitchell 1976). The same assumption is required for mathematical models of gas breakthrough (section 2.5). In the context of the gas-breakthrough research that is the subject of this thesis, the structure and properties of the void space are therefore as important, if not more important, than those of the solid phase.

2.2.2 Soil Mechanics Definitions and Derived Relationships

Although not possible in reality, it is sometimes helpful to imagine a volume of soil in which the solid particles are idealized as shown in Figure 2.5. The void volume is assumed to be filled with a combination of air and water.

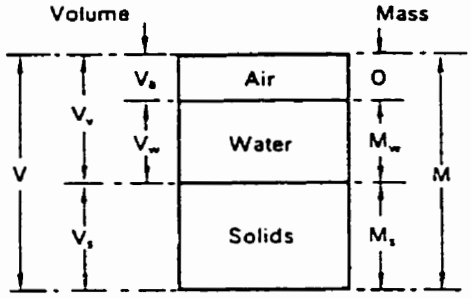

Figure 2.5 Schematic representation of a soil sample divided into three phases (from Craig 1994).

With reference to Figure 2.5, the mass water content (w) is defined as

$$w = M_w/M_s \,, \qquad [4]$$

where M_w is the mass of water in a specimen and M_s the mass of dry soil. The mass of water to be added to a given M_s, to obtain a desired w, can be obtained from [4]. Since wet soil consists of air (mass $\approx$ 0), water and dry soil, an operational definition of w is

$$w = (M - M_s)/M_s \,, \qquad [5]$$

where M is the mass of wet soil. The water content of soil is measured by drying a sample at 105 to 110°C to constant mass (American Society for Testing and Materials 1992).

If V_w and V_v are the volumes of water and void space, respectively, the degree of saturation (S_r) of a compacted soil is defined as

$$S_r = V_w/V_v \,. \qquad [6]$$

The degree of saturation is limited to values between 0 and 1 or, equivalently, 0 and 100%. The porosity of compacted soil (n) is defined as

$$n = V_v/V \,, \qquad [7]$$

where V is the total specimen volume.

Dry density (ρ_d) and particle density (ρ_s) are defined as

$$\rho_d = M_s/V \,, \qquad [8]$$

and

$$\rho_s = M_s/V_s \,, \qquad [9]$$

where V_s is the volume of solids. As noted, the buffer material is a mixture of clay and sand. The effective clay dry density (ρ_c) of buffer is defined as the mass of clay divided by the volume of the clay plus voids; the volume of clay plus voids is equal to the total specimen volume less the volume of sand. Since the tests described in this thesis were performed on pure clay specimens, ρ_d and ρ_c are numerically equal. The symbol ρ_c will be substituted for ρ_d in the remainder of the thesis when referring to the dry density of clay specimens. In this work ρ_s for the Avonlea bentonite clay is assumed to be 2.70 Mg/m^3 (Lambe and Whitman 1979).

From Figure 2.5, it can be shown that the water content of a saturated specimen (w_{100}) is

$$w_{100} = (1 - (\rho_c/\rho_s))(\rho_w/\rho_c) , \qquad [10]$$

where ρ_w is the density of water (1.00 Mg/m^3). At the end of a gas breakthrough experiment, the author determined w (from [5]) and ρ_c (from [8]). Equation [10] can then be used to determine the theoretical w_{100}, and S_r can be obtained from

$$S_r = w/w_{100} . \qquad [11]$$

If w is known, and it is assumed that a specimen is saturated (that is, $w = w_{100}$), ρ_c can be obtained from

$$\rho_c = 1/((w_{100}/\rho_w) + (1/\rho_s)) , \qquad [12]$$

which is obtained by rearranging [10].

The fraction of the total volume of a specimen that is occupied by clay particles is ρ_d/ρ_s. Therefore n can be determined from

$$n = 1 - (\rho_d/\rho_s) . \qquad [13]$$

2.2.3 Geotechnical Soil Classification

From an engineering perspective, the behaviour of a soil is more important than its mineralogical composition or chemistry. The unified soil classification system is a method of categorizing soils according to their properties and is widely used in geotechnical engineering (Casagrande 1948). To classify a soil using this system, the particle-size distribution is required and the Atterberg limits, which are a measure of the effect of water on soil behaviour, are often needed (Atterberg 1911).

Gravel, sand, silt and clay are defined by particle size. The definition of these fractions depends on the system used. Gravel is often defined as having particle sizes between 75 and 4.75 mm, sand from 4750 to 75 μm, silt between 75 and 2 μm, and clay particles are <2 μm equivalent spherical diameter. Particle-size analysis of the coarse fraction of a soil (sand, gravel and larger particles) is done by sieving (American Society for Testing and Materials 1992). The distribution of particle sizes in the fine fraction can be determined by measuring the density of a clay suspension over time (known as hydrometer analysis), but this is not necessary for classification using the unified system. If >50% by mass of a soil sample consists of coarse material, the soil can be classified using the particle-size distribution and a chart describing the unified soil classification system.

If <50% of a soil sample is coarse material, the Atterberg limits are required to classify it. The liquid limit is numerically equal to the water content at which a slurry begins to flow when subjected to a standard shear stress. It is reached when a groove, cut into a clay slurry in a standard cup using a standard tool, closes over 13 mm after 25 10-mm drops of the cup onto a standard surface (American Society for Testing and Materials 1992). To determine the plastic limit, a soil sample is formed into a 6-mm-diameter thread using the index finger and thumb of one hand. The thread is then rolled between the tips of the fingers and a glass plate. The plastic limit is equal to the water content at which the thread crumbles at a diameter of 3 mm (American Society for Testing and Materials 1992). The plastic index is defined as the difference between the liquid and plastic limits. Fine-grained soils are classified according to the unified soil classification system using the liquid limit, plastic index and a graph such as the one in Figure 2.6.

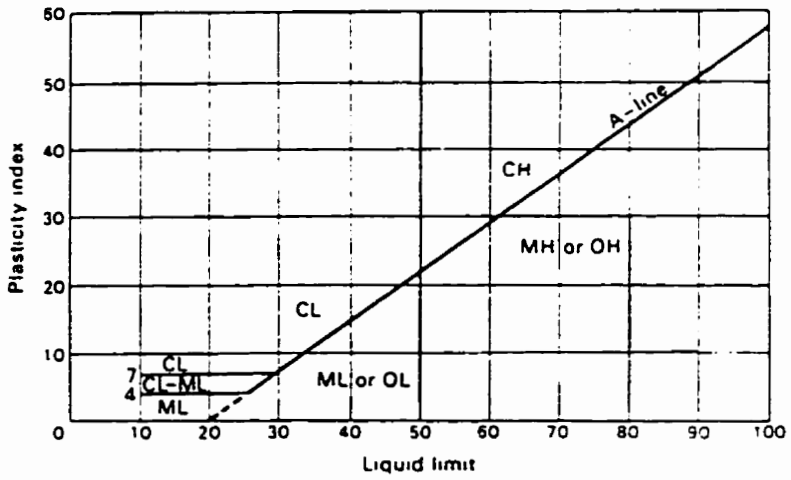

Figure 2.6 Plasticity chart for classifying fine-grained soils according to the unified system (from Craig 1994).

2.2.4 Compression

When a soil compresses, V decreases. At the pressures used in these gas-breakthrough tests, the particles themselves are incompressible, so the reduction in V is due to a reduction in V_v. As a result ρ_c increases (see Figure 2.5 and [8]). Two words are used to describe soil compression: compaction and consolidation. Compaction is defined as an increase in ρ_c resulting from a decrease in the volume of air (V_a) with w remaining constant (Craig 1994). This can only occur in an unsaturated soil. For ρ_c of saturated soil to increase, water must be removed from the specimen (V decreases due to a reduction in V_w). This process, in which the sample remains saturated while V decreases, is known as consolidation (Craig 1994). Soil compaction occurs relatively rapidly during the period that compactive effort is applied. Consolidation is a time-dependent process that may take many years in full-scale field applications (Holtz and Kovacs 1981).

In compaction or consolidation, for ρ_c to increase the soil particles must rearrange as V_a or V_w decreases. When soil particles move, the structure of the pore space changes. This is important with respect to gas breakthrough because the models of the process (section 2.5) assume the pore structure is unchanging. If the soil particles rearrange, deviations from the models might be expected.

2.2.5 Effective Stress Concept

When considering stresses in saturated soils, it is necessary to separate the total stress into the portion that is carried by the soil particle framework and the portion that is transmitted in the water phase (Terzaghi 1936). Figure 2.7 shows a number of soil particles with some of their contact points indicated. The total force applied normal to the wavy plane indicated by the dashed line is P_t, and the cross-sectional area is A. (Given the small size of soil particles, on a macroscopic scale the wavy plane indicated by the dashed line is nearly flat.) The interparticle force at every point of contact on the wavy plane can be resolved into components that are normal (N') and parallel (T') to the plane. If the pores contain water, pore-water pressure (u) can also transmit some of the applied force. Pore-water pressure can act on the exposed surface of the soil particles, which is $A - A_c$ where A_c is the area of particle contact. Resolution of the forces across the wavy plane yields

$$P_t = \Sigma N' + (A - A_c)u \, . \qquad [14]$$

Dividing each term in the above equation by A converts the forces to stresses,

$$P_t/A = \Sigma N'/A + (A - A_c)u/A \, , \qquad [15]$$

or

$$\sigma = \sigma' + (1 - (A_c/A))u \, , \qquad [16]$$

where σ and σ' are the total and effective stresses, respectively. Assuming that the area of particle contact is very small, A_c/A approaches zero and the term $(1 - (A_c/A))$ approaches unity. Equation [16] can then be simplified to

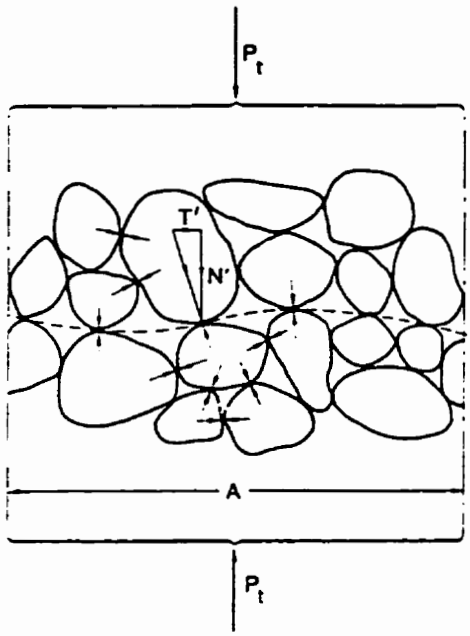

Figure 2.7 Illustration of an applied force being transmitted through soil particles in contact (from Craig 1994).

$$\sigma = \sigma' + u \,, \qquad [17]$$

which is known as the effective stress equation (Terzaghi 1936). Equation [17] is only valid in one dimension; a more general effective stress equation is

$$\{\sigma\} = \{\sigma'\} + u\{I\} \,, \qquad [18]$$

where the parentheses designate tensor quantities and $\{I\}$ is the unit tensor. Both σ and u can be measured, but σ' can only be obtained by calculation from the effective stress equation (Holtz and Kovacs 1981).

Given that Avonlea bentonite particles are surrounded by hydration shells when wet (section 2.1.3), there may be little interparticle contact; therefore [18] must be revised for application to this clay. Graham et al. (1992) suggest that $\{\sigma'\}$ be redefined as

$$\{\sigma'\} = \{\sigma_i'\} + \{R_f - A_f\} , \qquad [19]$$

where σ_i' is the interparticle contact stress discussed previously and $R_f - A_f$ is the difference between the repulsive and attractive unit forces (stresses) acting between hydrated particles. Repulsion arises from Coulomb and osmotic forces, while London (van der Waals) forces attract particles together (Graham et al. 1992). If there is no interparticle contact $\{\sigma'\} = \{R_f - A_f\}$ and [18] can be rewritten as

$$\{\sigma\} = \{R_f - A_f\} + u\{I\} . \qquad [20]$$

As with [18], only σ and u can be measured in [20]; the difference between σ and u is the net of the repulsive and attractive forces. The effective stress is a very important quantity in soil mechanics. For example, work on soil settlement, soil strength and slope stability relies on the effective stress concept.

Examining gas breakthrough requires gas-pressure gradients to be applied across soil specimens. The application of gas pressure causes an increase in σ in the specimen being tested. If the specimen is small, and assuming that the gas pressure is applied parallel to the direction that gravity is acting, the stress resulting from the specimen mass is often negligible compared with the total applied stress. If so, and there is no other externally applied loading, σ is equal to the applied stress resulting from the gas pressure. These assumptions will be used in examining the gas-breakthrough experiments described later in this thesis.

2.2.6 Pore-Size Distributions

Mercury intrusion porosimetry has been used to study pore-size distributions in relatively small soil specimens with masses of a few grams, or less (Diamond 1970). In the instrument, the Hg pressure is increased and with the rising pressure Hg enters progressively smaller pores. A plot of incremental (differential) intrusion against pore size can be obtained. The plot provides data on the sizes of the pores in a sample and the total volume of each pore size. Wan (1996) described the use of Hg intrusion porosimetry to study pore-size distributions in compacted bentonite. Figure 2.8 shows the results of a typical test on Avonlea bentonite. From Oscarson et al. (1990), ρ_c of the specimen was likely about 1.2 Mg/m^3. Within the limits of the instrument, pore diameters between about 0.003 and 0.3 μm were detected with a maximum incremental intruded pore volume of 0.023 mL/g at about 0.03 μm.

There are potential problems with the application of Hg intrusion porosimetry to clays. Mitchell (1976) lists these as: (1) the specimen pores must be dry, (2) occluded pores are not detected, (3) large pores accessed through small pores will be detected as small pores, and (4) the pressure limit of the apparatus is insufficient to detect the smallest pores. Danielson and Sutherland (1986) identified several other possible problems including (1) uncertainty in the value of the Hg-clay contact angle, (2) air trapped in the sample after evacuation, and (3) collapse of pores due to the Hg pressure. Given these limitations, results obtained by Hg intrusion porosimetry, while valuable, must be used with caution.

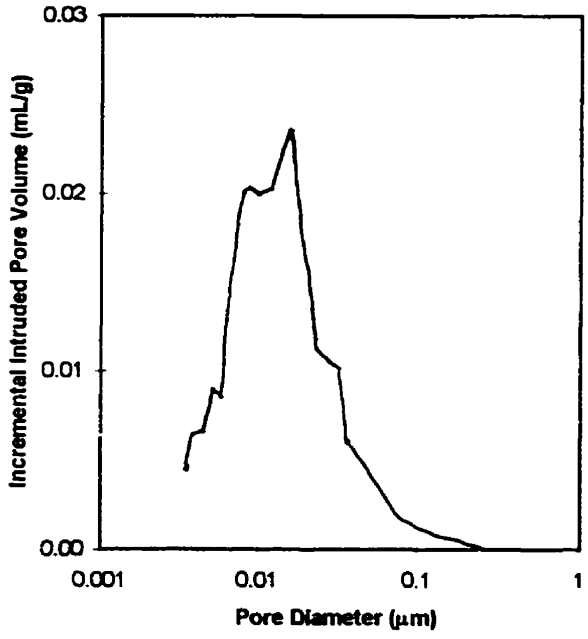

Figure 2.8 Result of Hg intrusion porosimetry test on Avonlea bentonite (adapted from Wan 1996).

2.3 Water Movement in Unsaturated Soils

Several mechanisms cause water to move in unsaturated soils, in addition to the interactions between water and clay surfaces described in section 2.1.3. To simplify this discussion, it will be assumed that there are no temperature gradients present in the soil. With this assumption, authors such as Richards (1974) and Mitchell (1976) have proposed three mechanisms for unsaturated flow: capillarity, osmosis and gravity. Yong and Warkentin (1975) add two more mechanisms, one of which is particularly relevant to water flow in gas-breakthrough experiments: gas pressure.

If a capillary tube is considered to be an analogy for a soil pore, then capillary theory can be applied to the soil pores. It is known that when a capillary is inserted into a beaker of liquid, any fluid that wets the capillary walls will rise in the tube. The height of rise depends on the liquid and the capillary radius (Barrow 1979); Taylor (1948) also adds the angle between the liquid and the glass (the wetting angle) as a dependent variable. An equation for the height of capillary rise can be derived assuming an equilibrium between the weight of liquid and the attractive force between the liquid and capillary walls (Barrow 1979). The wetting of capillary walls can be viewed as a chemical process and, as with any chemical reaction, a free energy change is involved (Barrow 1979). As described by Barrow (1979), and including the wetting angle (Taylor 1948), the differential surface energy (dG_{sc}) that is lost by the wetting of an infinitesimal surface area dA_s is

$$dG_{sc} = T_s(dA_s)\cos(\alpha) = T_s 2\pi r(dL)\cos(\alpha)\,, \qquad [21]$$

where T_s is the surface tension of the liquid, α the wetting angle and r the radius of the capillary. With reference to Figure 2.9, the differential potential energy that is gained in raising a small volume $\pi r^2(dL)$, with a density ρ, to a height L (dG_{grav}) is

$$dG_{grav} = \pi r^2 \rho g L(dL)\,, \qquad [22]$$

where g is the acceleration due to gravity.

Letting [21] equal [22] gives

$$2T_s\cos(\alpha)/r = L\rho g\,. \qquad [23]$$

The wetting angle in glass capillaries and soil is often assumed to be approximately 0°, and thus $\cos(\alpha)$ is about one. The height of a vertical column of water that exerts a pressure (p) equal to the water pressure at a given point is defined as the head (h) at that point.

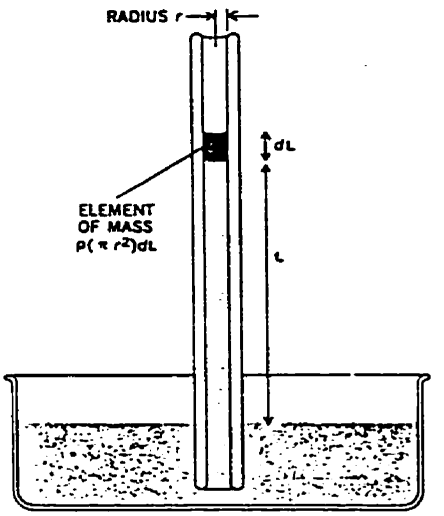

Figure 2.9 Schematic drawing of liquid rise in a capillary (adapted from Barrow 1979).

The head is related to p by

$$h = p/\rho_w g \qquad [24]$$

(Holtz and Kovacs 1981). Rearranging gives

$$p = h\rho_w g \,. \qquad [25]$$

If the fluid is water, h can be substituted for L and ρ_w for ρ in [23], and substituting [25] for the right side of [23] yields

$$p = 2T_s/r \,. \qquad [26]$$

It is noted that the capillary pressure is a negative pressure (suction) because water moves spontaneously into the capillary (soil pore). If it is assumed that the surface tension of water in soils is a constant, regardless of pore diameter, from [26] it is apparent that the greatest suction is developed in the smallest capillaries. Thus, in the absence of other driving forces, water will move from larger to smaller voids in an unsaturated soil.

Because of the negative charge on many clays, cations are held near the clay surface as discussed in section 2.1.3. This results in a solute concentration gradient between the surface water and the water further away. The result is that an osmotic pressure (π) develops, given by

$$\pi = cRT \qquad [27]$$

where c is the concentration and R the gas constant.

Provided there is void space for the water to enter, water in unsaturated soils will tend to flow in a gravitational field. The water pressure at any elevation in a water column was given by [25].

Lastly, water will flow under an air or gas pressure gradient. This mechanism is not operational in most agricultural soils. However, it is important with respect to gas-breakthrough experiments, because a gas-pressure gradient must be applied across a specimen to cause gas breakthrough to occur. Similarly, if gas pressure develops in a nuclear fuel waste disposal vault, this mechanism may be significant.

2.4 Water Movement in Saturated Soils

The flow of fluid through saturated soil is a result of a hydraulic gradient; in the case of the nuclear fuel waste disposal concept the fluid is groundwater. Saturated flow, known as advection, occurs through the pores between soil particles. If contaminants are dissolved in the groundwater, they will be transported in the flow. The mathematics of

advection are described because some of the models for gas breakthrough (section 2.5) will build on the advection model.

The driving force for advection is the hydraulic gradient (i), defined as

$$i = dh/dL\ , \qquad [28]$$

where dh is the difference in head, and dL the distance, between two points (Holtz and Kovacs 1981). Substituting [24] into [28], with ρ_w and g constant, gives

$$i = dp/\rho_w g(dL)\ . \qquad [29]$$

As shown in Figure 2.10, at low i the velocity of fluid flow in pipes or in the voids of large-grained soils such as coarse gravels (v) is linearly related to i. At high i, the flow becomes turbulent and the linear relationship no longer exists. At high i, the rate of increase of v is less than it is at low i. The reason for this is that more energy is required for turbulent flow than for laminar flow, due to internal energy dissipation (Holtz and Kovacs 1981).

Assuming the fluid is water, whether the flow will be laminar or turbulent can be estimated by calculating the Reynolds number,

$$N_R = 2r\rho_w v/\eta\ , \qquad [30]$$

where r is the effective radius, v the velocity and η the viscosity of the water. At low values of N_R, laminar flow is obtained; as N_R increases, a transition to turbulent flow occurs. The transition between laminar and turbulent flow occurs in circular pipes at an N_R value between 1000 and 2200 (Hillel 1980). In a curved tube with variable diameter,

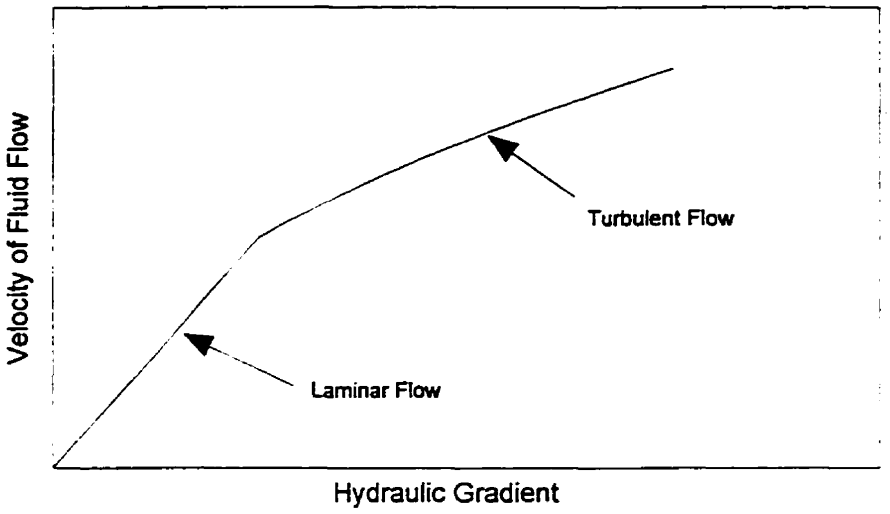

Figure 2.10 Relationship between hydraulic gradient and the velocity of fluid flow for laminar and turbulent flows.

which is assumed to be analogous to a soil pore, laminar flow is only assured if the value of N_R is less than one (Hillel 1980) or less than one to ten (Corey 1986).

The equation

$$v = ki \qquad [31]$$

expresses the empirical relationship shown in Figure 2.10 at low i. The constant k is known as the hyraulic conductivity and varies between soils. Equation [31] is known as Darcy's law after Darcy (1856) who derived it following a study of water flow through clean sands. Darcy's law is also relevant to advective transport in all fine-grained soils, though care must be taken when studying flow through bentonite (Dixon 1995).

The rate of flow (volume per unit time) is the flux (q). For one-dimensional flow, q is given by

$$q = vA\,, \qquad [32]$$

where A is the cross-sectional area perpendicular to the flow (Holtz and Kovacs 1981). Substituting [31], [28] and [24]

$$q = kiA = kA(dh)/dL = kA(dp)/\rho_w g(dL)\,. \qquad [33]$$

The hydraulic conductivity is a measure of the ease with which fluid moves through a soil. The value of k can vary many orders of magnitude between different types of soil. It is generally high in large-grained soils such as gravels and low in fine-grained clay soils (Holtz and Kovacs 1981). For a given material, the ease of fluid flow decreases as ρ_d increases, because the pores through which the liquid moves become progressively smaller. Dixon (1995) provided a state-of-the-art review of hydraulic conductivity testing for clays. For compacted Avonlea bentonite, Dixon (1995) gave the following empirical equation for obtaining k,

$$\log k = 4.537n - 14.597\,. \qquad [34]$$

This equation provided the best fit of experimentally-obtained advection data.

2.5 Mathematics of Gas Breakthrough in Porous Media

2.5.1 Introduction

This section presents mathematical models of the gas-breakthrough process. Two basic types of model are developed. In one the gas-breakthrough pressure (p_b) is calculated and in the other the gas-breakthrough time (t_b). Some of the steps involved in the derivation of these models follow from the discussion of advective transport in section 2.4. The models all assume the pore structure remains constant throughout the gas-breakthrough test.

The three pressure models (sections 2.5.2 to 2.5.4) all start with the capillary rise equation. They assume that a clay pore is analogous to a capillary tube. On this assumption, the pressure required to pass gas through a clay plug is equal to the pressure required to force water out of a capillary of the same effective radius. Once the capillary is clear of water, gas can pass more freely through the clay plug. The time needed for gas breakthrough is not a variable in any of these models.

Four models have been developed on the assumption that gas breakthrough is an advection process (sections 2.5.5 to 2.5.8). Again the reasoning is that once water is expelled from a pore, gas will readily pass through the clay. In these sections, equations are derived to calculate t_b. The development of one of these models starts with Darcy's law and the other three begin with the Poiseuille equation (Barrow 1979). Pressure (or

the rate of pressure increase) is a dependent variable in the time models. Although the time models are original, they are included here because they logically follow the pressure models, which were obtained from the literature.

2.5.2 Pore-Radius Pressure Model

Assuming that the pressure required for gas breakthrough in compacted clay is equal to the pressure needed to push water out of a capillary of equivalent size, the breakthrough pressure (p_b) can be substituted for p in [26],

$$p_b = 2T_s/r\,. \qquad [35]$$

The breakthrough pressure is positive because pressure must be applied to the top of the capillary in Figure 2.9 to push the water down to the level in the beaker.

As described in section 2.6, some researchers (for example, Pusch et al. 1987 and Lineham 1989) have used [35] to calculate theoretical pore sizes after gas breakthrough. From [35], the pressure required to force fluid from a capillary is directly related to T_s and inversely related to r. Since water is the only fluid considered in this work, T_s is a constant 0.07275 N/m at 20°C (Barrow 1979), and therefore p_b depends only on r. The interpretation of this model with respect to gas breakthrough is that water will be forced out of the largest capillary in a clay plug if sufficient pressure is applied. After the water has been pushed out of a pore, gas can move through the specimen at a rate determined by the gas conductivity of the clay. As p_b depends on r, this is named the pore-radius pressure model.

2.5.3 Hydraulic-Radius Pressure Model

In studies of fluid flow in non-circular pipes, it has been shown that the mean hydraulic radius (r_h) should be used in the Poiseuille equation instead of r (Wyllie and Spangler 1952). In this section, r_h will be substituted for r in the pore-radius pressure model ([35]).

The mean hydraulic radius of a non-circular pipe is defined as the volume of a given length divided by the wetted surface area (Wyllie and Spangler 1952). For a circular pipe of radius r and length L, the relationship between r_h and r is

$$r_h = \pi r^2 L / 2\pi r L = r/2 \; . \qquad [36]$$

The radius in the pore-radius pressure model ([35]) can be replaced with r_h using this relationship, resulting in

$$p_b = T_s / r_h \; . \qquad [37]$$

This is named the hydraulic-radius pressure model.

In a porous medium such as compacted clay, r_h is the pore space per unit volume divided by the surface area per unit volume (Wyllie and Spangler 1952). It is apparent from [7] that the pore space per unit volume of clay is equal to n. Specific surface area is usually quoted on a dry mass basis (section 2.1.4), so ρ_c is needed to convert it to a volume basis,

$$r_h = n / S_m \rho_c \; . \qquad [38]$$

2.5.4 Kozeny-Carman Pressure Model

Further development of the gas-breakthrough models requires the elimination of r_h in [37] by incorporating the Kozeny-Carman equation (Wyllie and Spangler 1952, Thomas et al. 1968, Davies 1991). The derivation of the Kozeny-Carman equation is described briefly below.

Some authors have considered a bundle of capillaries to be analogous to a compacted clay plug. The Poiseuille equation for the flow velocity through a capillary bundle (v'), given a pressure differential of dp, is

$$v' = r^2(dp)/8L\eta \,, \qquad [39]$$

where r is the equivalent radius of the capillary bundle, L their length and η the viscosity of the flowing medium. The Poiseuille equation requires modification before it can be applied to a compacted clay specimen. Using [36], r can be replaced with r_h

$$v' = r_h^2(dp)/2L\eta \,. \qquad [40]$$

Thomas et al. (1968) stated that the number '2' in the denominator of [40] should be replaced by a variable k_o, known as the pore shape factor. As well, the effective pore length (L_e) should replace L, because $L_e > L$. These two substitutions give

$$v' = r_h^2(dp)/k_oL_e\eta \,. \qquad [41]$$

The value of v' in the pores of a clay specimen is unknown, so a substitution must be made for it. The flux averaged over the entire cross-sectional area of the plug is

$$q = vA = vV/L \quad [42]$$

where V and L are the volume and length of the specimen. The flux is also given by

$$q = v'A_e = v'V_v/L_e \quad [43]$$

where A_e is the effective pore area. Setting [42] equal to [43] and solving for v' gives

$$v' = vVL_e/V_vL \, . \quad [44]$$

From the definition of porosity ([7]), 1/n can be substituted for V/V_v, and therefore

$$v' = vL_e/nL \, . \quad [45]$$

If [45] is substituted into [41], one unknown variable (v') would be replaced with another (v). Darcy's law can be used to express v in terms of known constants, the hydraulic conductivity (k) and the pressure differential (dp). Since the plug length is a constant, dL in [29] can be replaced with L, and combining with [31] gives

$$v = ki = k(dp)/L\rho_w g \, . \quad [46]$$

Substituting [46] into [45] yields

$$v' = kL_e(dp)/nL^2\rho_w g \, . \quad [47]$$

Setting [41] equal to [47] and solving for r_h^2 produces

$$r_h^2 = kk_o\eta \, L_e^2/n\rho_w g \, L^2 \, , \quad [48]$$

which is one form of the Kozeny-Carman equation (Thomas et al. 1968).

Bear (1972) defined the tortuosity of a porous medium (τ) as

$$\tau = (L/L_e)^2 \, . \quad [49]$$

Substituting $1/\tau$ for $(L_e/L)^2$ and taking the square root of both sides of the Kozeny-Carman equation results in

$$r_h = (kk_o\eta/n\rho_w g\tau)^{0.5} . \quad [50]$$

Equation [50] can be substituted for r_h in the hydraulic-radius pressure model ([37]) to form the Kozeny-Carman pressure model

$$p_b = T_s(n\rho_w g\tau/kk_o\eta)^{0.5} . \quad [51]$$

The ρ_c of a specimen can be determined following a gas-breakthrough experiment from [8] and n can then be calculated using [13]. The τ value can be estimated from the equation

$$\tau = -0.24\rho_c + 0.41 , \quad [52]$$

provided ρ_c is expressed in units of Mg/m^3. Given that [52] was obtained from Γ diffusion experiments in compacted Avonlea bentonite (Oscarson and Hume 1994), its applicability to gas-breakthrough experiments is admittedly questionable, but there are no other data available. The hydraulic conductivity of Avonlea bentonite can be calculated from [34]. The value of k_o ranges between 2.0 and 3.0 for most non-circular conduits, so the selection of an intermediate value (2.5) will not introduce a large error (Thomas et al. 1968). The viscosity of bulk water is known to be 1.002×10^{-3} kg/m·s at 20°C (CRC 1978), and if this is assumed to be the viscosity of water in the pores of compacted Avonlea bentonite, then η is known. Therefore, an estimate of p_b at specified values of n is possible with the Kozeny-Carman pressure model given in [51].

2.5.5 Darcy's-Law Time Models

The first of the time models, all of which have been derived by the author, is based on Darcy's law. Starting the derivation with Darcy's law assumes that gas breakthrough is an advection process. As gas enters the clay the length of water-filled pore decreases, and therefore the hydraulic gradient increases. This is, therefore, a model for a specific type of hydraulic-conductivity test.

If the pressure is constant, h and p can replace dh and dp in [33], and defining Z as the distance of air penetration into the plug, yields

$$q = kiA = kAh/(L - Z) = kAp/\rho_w g(L - Z) . \qquad [53]$$

The flux can also be given as

$$q = v'nA . \qquad [54]$$

By definition, v' is

$$v' = dZ/dt , \qquad [55]$$

where t is time. Replacing v' in [54] gives

$$q = nA(dZ)/dt . \qquad [56]$$

Setting [53] equal to [56] produces

$$(L - Z)(dZ) = kp(dt)/\rho_w gn . \qquad [57]$$

A program to integrate the above equation numerically is given in Appendix I.1. The program, which is written in the 'C' language, calculates dZ for a user-specified value of dt. The calculated dZ is then subtracted from L and, if the resulting value of L is ≤ 0, the

program terminates. The total elapsed time is calculated as Σdt and, if the simulation is of an increasing-pressure test, the program checks whether the end of the pressure increment has been reached; if so, the pressure is incremented and the program continues. Another iteration of a program loop occurs with the same variable values if neither of the above apply.

Equation [57] can be integrated analytically for constant-pressure tests from $Z = 0$ at $t = 0$ to $Z = L$ at $t = t_b$ (that is, the length of air-filled pore in a clay plug increases from 0, at the start of an experiment, to the plug length at the time of breakthrough). Solving the resulting expression for t_b

$$t_b = L^2\rho_w g n/2kp_c\,, \qquad [58]$$

where p has been replaced with p_c to indicate a constant-pressure test in which pressure is a dependent variable. This equation is the Darcy's-law time model for constant-pressure tests.

Equation [57] can be modified for increasing-pressure tests and integrated analytically. In the increasing-pressure gas-breakthrough tests described in chapters 4 to 6, the pressure was set at the first increment at time zero and increased at regular intervals throughout the test. If m is the rate of pressure increase, and b the starting pressure, then p at any t is approximately

$$p = mt + 0.5b\,. \qquad [59]$$

To simplify the mathematics, [59] is shortened to

$$p = mt\ . \qquad [60]$$

The accuracy of this simplification increases as the difference between mt and b rises. Substituting [60] into [57] gives

$$(L - Z)(dZ) = kmt(dt)/\rho_w gn\ . \qquad [61]$$

Using the same integration limits as in [58], and solving for t_b, results in

$$t_b = (L^2\rho_w gn/km)^{0.5}\ , \qquad [62]$$

which is the Darcy's-law time model for increasing-pressure tests.

2.5.6 Pore-Radius Time Models

As mentioned previously, a capillary is often considered to be analogous to a pore in a clay plug. If gas breakthrough is an advection process, the time required for gas to pass through the clay will equal the time for water to be expelled from the pore by advection. The flux through a capillary is

$$q = v'A = v'\pi r^2, \qquad [63]$$

and if p is constant the Poiseuille equation [39] can be rewritten as

$$v' = pr^2/8(L - Z)\eta\ , \qquad [64]$$

where L has been replaced with (L - Z) because the length of fluid-filled pore is not constant. Combining the previous two equations gives

$$q = p\pi r^4/8(L - Z)\eta\ . \qquad [65]$$

Substituting [55] into [63] gives

$$q = \pi r^2(dZ)/dt \, . \qquad [66]$$

Setting [65] equal to [66] and separating variables

$$(L - Z)(dZ) = pr^2(dt)/8\eta \, . \qquad [67]$$

The previous equation is integrated numerically by a program that is listed in Appendix I.2. The program operates much like the Darcy's-Law time model program described previously. Integrating [67] from $Z = 0$ at $t = 0$ to $Z = L$ at $t = t_b$, and replacing p with p_c,

$$t_b = 4L^2\eta/p_c r^2 \, , \qquad [68]$$

which is the pore-radius time model for constant pressure.

For increasing pressure, [60] can be combined with [67],

$$(L - Z)(dZ) = mr^2t(dt)/8\eta \, , \qquad [69]$$

and integrated to give

$$t_b = (8\eta L^2/mr^2)^{0.5} \, , \qquad [70]$$

which is the pore-radius time model for increasing pressure.

2.5.7 Hydraulic-Radius Time Models

As with the pressure models, r_h can be substituted for r. Making this replacement in [67] produces the differential equation

$$(L - Z)(dZ) = pr_h^2(dt)/2\eta \, . \qquad [71]$$

A numerical solution of [71] is given in Appendix I.3. The algebraic solution of the hydraulic-radius time model for constant pressure is

$$t_b = L^2\eta/p_c r_h^2 , \qquad [72]$$

and

$$t_b = (2\eta L^2/m r_h^2)^{0.5} , \qquad [73]$$

is the hydraulic-radius time model for increasing pressure.

2.5.8 Kozeny-Carman Time Models

Following the same process used in the derivation of the pressure models, r_h in [71] can be replaced with the Kozeny-Carman equation ([50]). This gives

$$(L - Z)(dZ) = pkk_o(dt)/2n\rho_w g\tau , \qquad [74]$$

for which a numerical solution is in Appendix I.4. The following analytical solution

$$t_b = L^2 n\rho_w g\tau/p_c k k_o , \qquad [75]$$

is the Kozeny-Carman time model for constant pressure, and

$$t_b = (2L^2 n\rho_w g\tau/mkk_o)^{0.5} , \qquad [76]$$

is the Kozeny-Carman time model for increasing pressure.

All the models are listed in Table 2.2. It is interesting to note the similarity of the Darcy's-law and Kozeny-Carman time models. The only differences between the constant pressure models ([58] and [75]) are the addition of τ to the numerator and the replacement of the number '2' by the variable k_o in the denominator. Comparing [62] and [76] (the increasing-pressure models), the number '2' and the variable τ are added to the numerator and k_o is added to the denominator.

Table 2.2 Summary of analytical gas-breakthrough models.

Model Name	Pressure Model	Constant-Pressure Time Model	Increasing-Pressure Time Model
Darcy's Law	NA[a]	$t_b = L^2\rho_w gn/2kp_c$	$t_b = (L^2\rho_w gn/km)^{0.5}$
Pore Radius	$p_b = 2T_s/r$	$t_b = 4L^2\eta/p_c r^2$	$t_b = (8\eta L^2/mr^2)^{0.5}$
Hydraulic Radius	$p_b = T_s/r_h$	$t_b = L^2\eta/p_c r_h^2$	$t_b = (2\eta L^2/mr_h^2)^{0.5}$
Kozeny Carman	$p_b = T_s(n\rho_w g\tau/kk_o\eta)^{0.5}$	$t_b = L^2 n\rho_w g\tau/p_c kk_o$	$t_b = (2L^2 n\rho_w g\tau/mkk_o)^{0.5}$

[a]NA = not applicable

2.6 Review of Previous Gas-Breakthrough Research

Although there have been several desk studies of gas breakthrough in clay, the number of experimental studies is limited. Experimental studies have been conducted by researchers in Sweden, the U.K., Japan and Canada. This section reviews the procedures that were used in the experiments, and the results that were obtained.

The first papers on gas migration in clay, as it pertains to nuclear waste disposal, were published by Pusch and colleagues in Sweden. MX-80 bentonite was used in the experiments. Pusch and Forsberg (1983) studied the gas conductivity of water-saturated clay after gas breakthrough. The definition of the gas conductivity was analogous to that of the hydraulic conductivity ([31]). The S_r value of the specimens was ≈100% after the tests, and therefore the gas must have passed through a few small openings.

Pusch et al. (1985) examined the swelling pressure, k and p_b (termed the critical pressure by them) of bentonite. Eight tests were done on water-saturated bentonite between $\rho_c \approx$ 1.1 and 1.8 Mg/m^3. The gas pressure was increased incrementally at one- to five-day intervals. The magnitude of the pressure increments varied among the tests. The authors concluded that there is a critical gas pressure below which gas will not pass through compacted bentonite. It was noted that this pressure was of the same order of magnitude as the swelling pressure generated by the compacted bentonite. The reason for this remains unclear.

Pusch et al. (1987) reproduced data on the p_b of saturated MX-80 bentonite from a report published in Swedish. The data appear in Table 2.3. No description was given of the procedure used in these experiments. Equation [35] was used to calculate the pore size corresponding to the experimentally measured p_b.

Table 2.3 Gas-breakthrough pressure for MX-80 bentonite.

ρ_c (Mg/m^3)	p_b (MPa)
0.87	0.015
0.95	0.060
1.00	0.060
1.08	0.16
1.40	1.6
1.46	2.4
1.62	5.0
1.71	5.0
1.75	11
1.78	19
1.79	21

Lineham (1989) studied gas breakthrough in saturated London and Kimmeridge clays. London clay was reported to be illitic with small amounts of smectite and kaolinite; the mineralogy of Kimmeridge clay was not reported. Before gas-breakthrough testing, the samples were consolidated in the test apparatus, at a given load, until consolidation ceased. Because of the consolidation procedure, a saturation step was not required. Three low-pressure tests (maximum pressure =1.0 MPa) were performed on London clay at $\rho_c \approx 1.5$ Mg/m^3. In these tests, a typical gas-pressure increment was 0.2 MPa; the duration of each increment was not stated. In the low-pressure experiments, gas passed slowly through the clay plug; this was attributed to diffusive transport. The pressure increments were typically 0.34 MPa in eight high-pressure tests (maximum pressure =12.4 MPa) and the duration of each increment was >8 h. Tests were done on both London and Kimmeridge clays, but the ρ_c of the specimens were not reported. Contrary to the results reported by Pusch and Forsberg (1983), Lineham (1989) found that the volume of water expelled by the passage of gas was approximately equal to the void volume of the specimen. The pressure at which rapid gas breakthrough occurred, named the critical gas-breakthrough pressure, was between 3.5 and 6.2 MPa. Lineham used the pore-radius pressure model ([35]) to estimate the size of the pores through which the gas passed.

Experiments conducted by the British Geological Survey are described by Volckaert et al. (1993) and Horseman and Harrington (1994). Five tests were performed (three perpendicular and two parallel to the bedding planes) on Boom clay at $\rho_c \approx 1.63$ Mg/m^3. These experiments included saturating with a synthetic pore solution, hydraulic conductivity tests, gas-breakthrough tests and gas-flow-rate measurements after

breakthrough. To obtain gas breakthrough, water was pumped into the bottom of a 500-mL gas-filled vessel at a rate of 375 μL/h, causing the gas volume in the vessel to decrease and the gas pressure to increase. The gas-breakthrough pressure varied between 1.2 and 1.9 MPa perpendicular to bedding and from 0.5 to 1.0 MPa parallel to bedding. It was noted that after the tests $S_r \approx 100\%$.

In Japan, preliminary tests have been performed on Kunigel V1 bentonite (K. Tanai, Power Reactor and Nuclear Fuel Development Corporation, personal communication). Swelling pressure, p_b and gas permeability tests were conducted on saturated clay. The gas pressure was increased stepwise until breakthrough occurred. The p_b increased from about 1.4 to 3.6 MPa as ρ_c increased from 1.6 to 1.8 Mg/m^3.

Kirkham (1995) reported the results of gas-breakthrough tests on an illitic clay with the commercial name Sealbond. The clay was wetted with distilled water before testing; both saturated and unsaturated samples were examined. In the breakthrough tests, the gas pressure was increased by 0.2 MPa every five minutes. Gas-breakthrough pressures between 0.2 and 6.4 MPa were observed. Kirkham concluded that the p_b of Sealbond increases with both ρ_c and S_r. It was also noted that at $S_r < 80\%$, there is little resistance to gas breakthrough.

Six tests on saturated buffer material at $\rho_d \approx 1.67$ Mg/m^3 ($\rho_c \approx 1.22$ Mg/m^3) were conducted by Kirkham (1995) using the same procedures. Breakthrough was obtained in only one of the tests (at 9.4 MPa) before the pressure limit of the equipment was reached.

On the basis of [35], it was concluded that the apparatus was not capable of measuring the breakthrough pressure of Avonlea bentonite at the ρ_c of the buffer material (1.22 Mg/m^3). This thesis describes gas-breakthrough work on Avonlea bentonite that is a continuation of the work begun by Kirkham.

3. MATERIALS[1]

3.1 Avonlea Bentonite Chemistry and Mineralogy

3.1.1 Introduction

As noted in section 1.1, Avonlea bentonite is the clay component of the buffer material in the Canadian Nuclear Fuel Waste Disposal Concept. This clay was used for all the gas-breakthrough tests described here. Avonlea bentonite comes from the Bearpaw Formation, which was deposited during the Upper Cretaceous age in southern Saskatchewan (Oscarson et al. 1990). It was obtained in powdered form from Canadian Clay Products, Wilcox, SK.

3.1.2 Exchangeable Cation Composition and Cation Exchange Capacity

The exchangeable cation composition of Avonlea bentonite was measured by Analytical Science Branch staff at the Whiteshell Laboratories of AECL using the ammonium acetate method (Thomas 1982). The cations Na, Ca, Mg and K were present (0.61, 0.28, 0.020 and 0.0076 mol(+)/kg, respectively). Analysis was performed for Fe, but it was undetectable (<0.0002 mol(+)/kg).

[1] This section contains information published in Hume (1997) and Hume et al. (1997).

The cation exchange capacity was also determined by Analytical Science Branch personnel. A homoionic clay saturated with Ca was prepared and Mg was used as the displacing cation (Jackson 1975). Triplicate measurements gave 0.734, 0.757 and 0.748 mol(+)/kg, which results in a mean value of 0.75 mol(+)/kg. This result is intermediate between the 0.82 mol(+)/kg reported by Quigley (1984) and the 0.60 mol(+)/kg reported by Oscarson et al. (1992). The cation exchange capacity value is less than the sum of the concentrations of the exchangeable cations, likely due to the dissolution of soluble salts in the exchangeable cation analysis (Oscarson and Hume 1993).

3.1.3 Specific Surface Area

The specific surface area of Avonlea bentonite was measured with 2-ethoxyethanol on loose clay as described by Carter et al. (1986). Triplicate tests gave results of 5.59, 5.57 and 5.10×10^5 m^2/kg. The mean specific surface area was 5.4×10^5 m^2/kg. This result is less than the 6.3×10^5 m^2/kg quoted by Quigley (1984) but greater than the 4.8×10^5 m^2/kg reported by Oscarson et al. (1992).

3.1.4 X-ray Diffraction Analysis

An x-ray diffraction pattern of a parallel-oriented, ethylene-glycol-treated sample of Avonlea bentonite is shown in Figure 3.1. The sample was prepared by the author and scanned by Geochemistry Research Branch staff at the Whiteshell Laboratories of AECL.

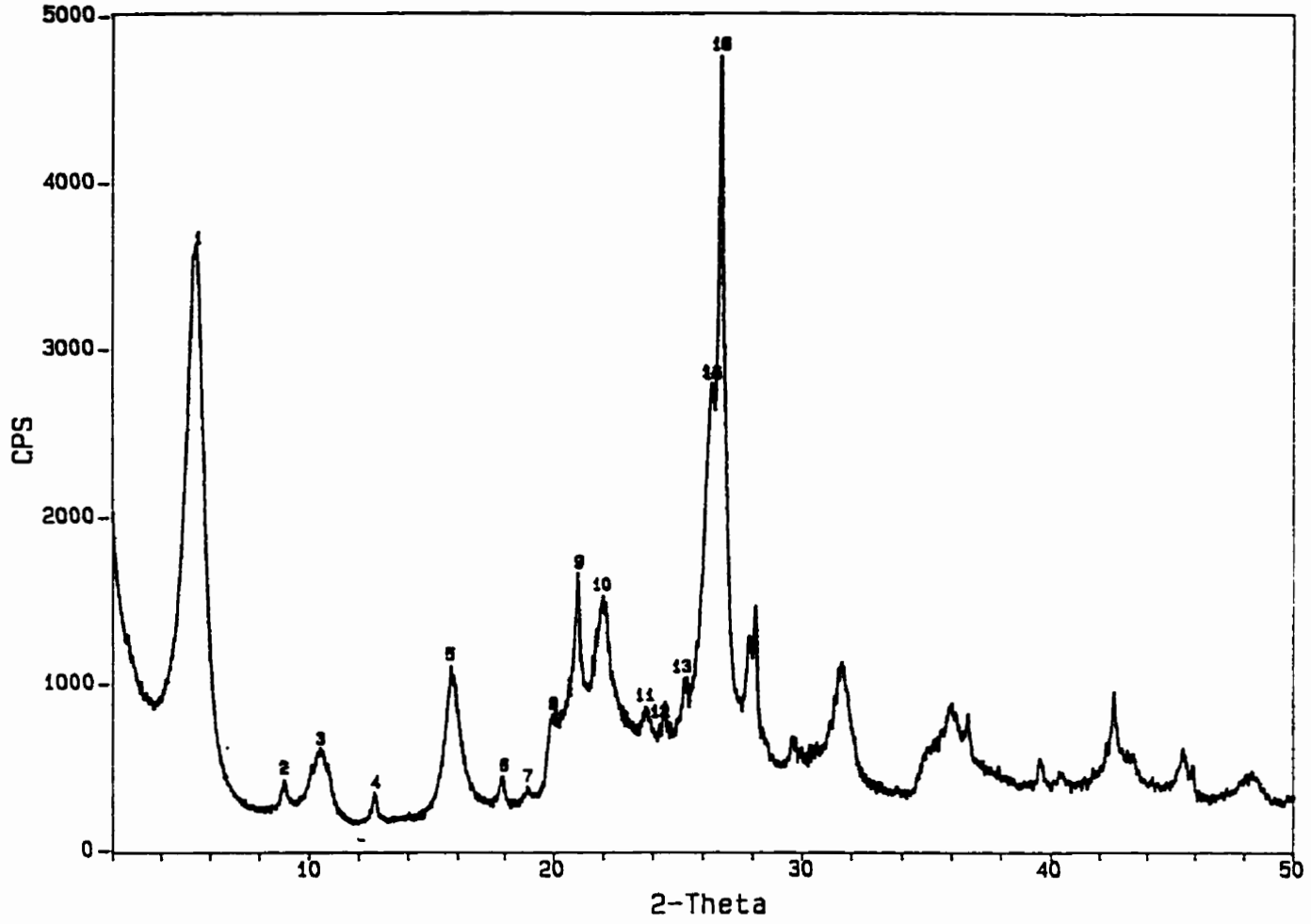

Figure 3.1 X-ray diffraction pattern of parallel-oriented, ethylene-glycol-treated Avonlea bentonite.

The sample was scanned with a Rigaku D/max-B diffractometer, from 2 to 50° 2θ at 1° per minute, using Ni-filtered Cu-K_α radiation (0.15418 nm) generated at 50 kV and 150 mA. Table 2.1 was used to identify the clay-mineral peaks, and the non-clay-mineral peaks were identified as described by Moore and Reynolds (1989); the results are in Table 3.1. Identification was not continued beyond the 0.336 nm peak, even though some clay-mineral peaks are present, because many non-clay-mineral peaks also occur in this region.

Table 3.1 Identification of minerals in a parallel-oriented, ethylene-glycol-treated sample of Avonlea bentonite.

Peak Number	°2θ	d[a] (nm)	n_B	d(001)[b] (nm)	Mineral
1	5.45	1.620	1	1.620	Smectite (001)
2	9.00	0.982	1	0.982	Illite (001)
3	10.49	0.843	2	1.686	Smectite (002)
4	12.63	0.700	1	0.700	Kaolinite (001)
5	15.74	0.563	3	1.689	Smectite (003)
6	17.94	0.494	2	0.988	Illite (002)
7	18.93	0.468	NA	NA	NA
8	19.98	0.444	NA	NA	NA
9	20.99	0.423	4/ NA	1.692/ NA	Smectite (004)/ Quartz
10	21.99	0.404	NA/ NA/ NA	NA/ NA/ NA	Albite/ Anorthite/ Cristobalite?
11	23.73	0.375	NA	NA	Anorthite
12	24.40	0.364	NA	NA	Albite
13	25.32	0.351	2	0.702	Kaolinite (002)
14/15/16	26.53	0.336	5/ 3/ NA	1.680/ 1.008/ NA	Smectite (005)/ Illite (003)/ Quartz

[a]From [3].
[b]$d(001) = d \times n_B$ (for clay minerals).

As there was no 1.4 nm peak, preparation and analysis of a sample saturated with K^+ and heated to 500°C, to differentiate between vermiculite and chlorite, was not required.

The clay minerals smectite, illite and kaolinite were identified, which are the same clays present in the sample tested by Oscarson and Dixon (1989). The non-clay minerals quartz, albite and anorthite were also identified, and cristobalite may have been present. Since the smectite peak is dominant in the x-ray diffraction pattern, and Na is the major

exchangeable cation, classification of this clay as a bentonite is appropriate given the definition in section 2.1.5.

3.2 Geotechnical Classification of Avonlea Bentonite

Dixon (1995) has reported some geotechnical analyses of Avonlea bentonite. Particle size analysis by method D422-63 (American Society for Testing and Materials 1992) gave a sand, silt and clay composition of <3, 20 and >77% by mass, respectively. A water content of 10% gave the maximum compacted ρ_c when tested according to D1557-78. The free swell volume (the volume of a sample with access to unlimited water) was >9 cm^3/g.

Since >50% of the mass of Avonlea bentonite is silt and clay, it must be classified using Atterberg limits. The liquid limit and plasticity index (D4318-84) are 257 and 208%, respectively (Dixon 1995). Using the plasticity chart for the unified soil classification system in Figure 2.6, Avonlea bentonite is classified as CH.

3.3 Other Materials

In all the gas-breakthrough tests, the specimens were wetted with distilled water. Argon with a quoted purity of >99% was used as both the breakthrough and back-pressure gas. Although CO_2 may be produced in a disposal vault, it was not chosen because of its high solubility and pH-altering properties. Both H_2 and CH_4 may be generated in a vault, but

they were not used because of safety concerns. Compressed Ar was selected because it has a low solubility and is an inert gas.

4. EQUIPMENT AND PROCEDURES

4.1 Low-Pressure Gas-Breakthrough Apparatus

4.1.1 Introduction

Three gas-breakthrough systems were used: two low pressure and one high pressure. They were designed to determine the resistance that compacted clays have to the one-dimensional flow of gas. The two low-pressure systems were assembled by T.L. Kirkham and are described in detail in Kirkham (1995). They are located in the Geotechnical Laboratory of the Department of Civil and Geological Engineering at the University of Manitoba. The remainder of section 4.1 provides a brief description of the components of the low-pressure systems and an explanation of the low-pressure test procedures.

4.1.2 Components

A schematic drawing of one of the systems is shown in Figure 4.1. The apparatus consists of a cell, water- and gas-supply systems, and instrumentation. Each cell consists of a central sleeve and two end flanges. After the sleeve and bottom flange are bolted together, porous Ni and filter paper discs are placed in the cell. Following compaction of

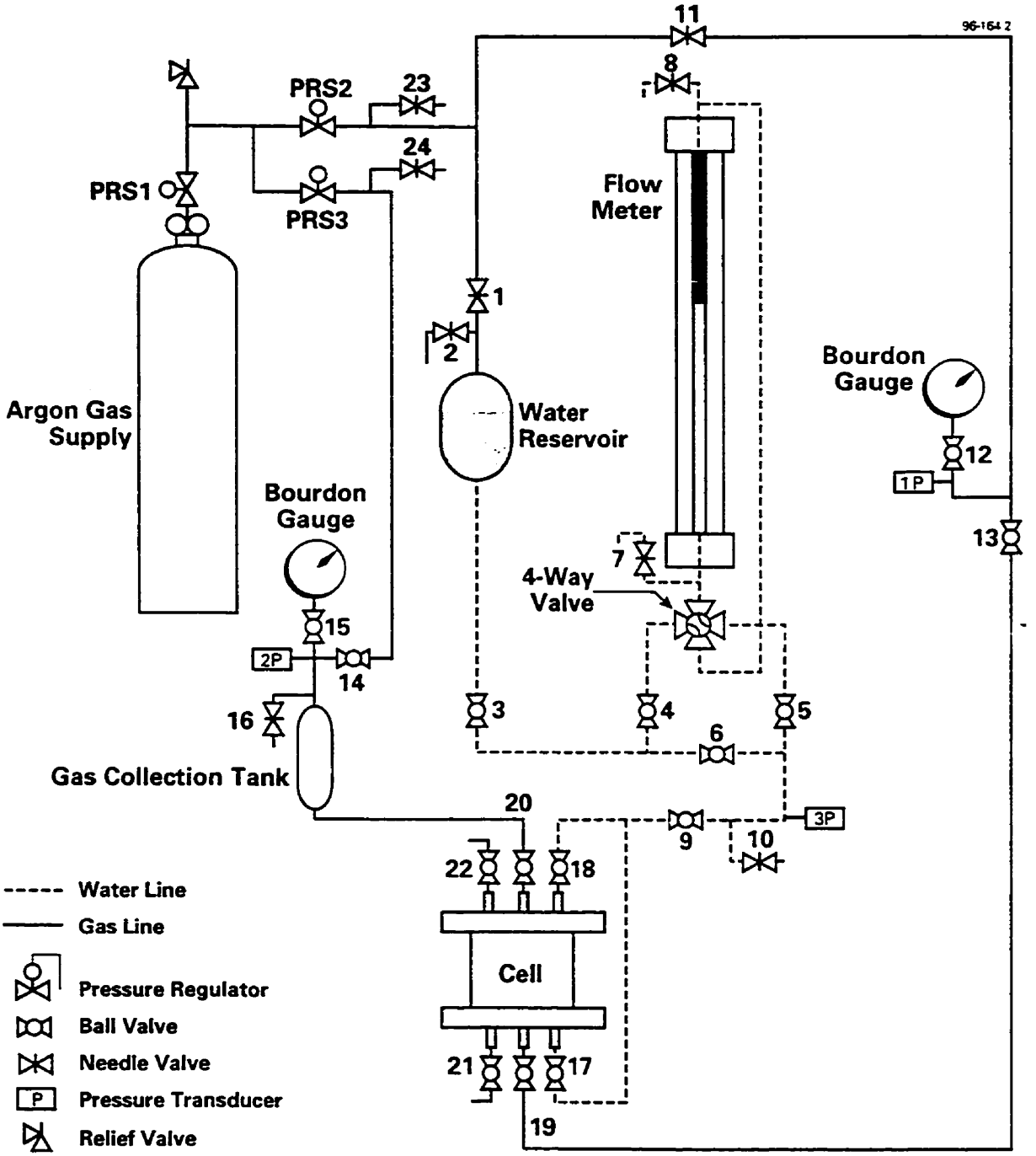

Figure 4.1 Schematic of the low-pressure gas-breakthrough apparatus.

the clay specimen, filter paper and porous Ni discs are placed on top. The top flange is placed on top of the sleeve and the complete cell is bolted together. When fully assembled the cell has a cavity 24.0-mm long, which is also the target height of the clay plug. The cavity is 50.7 mm in diameter and therefore the volume is 48.5 mL.

In some tests the clay plug is wetted towards full saturation after compaction into the cell, while in other experiments the gas-breakthrough pressure is measured on as-compacted clay. The water systems, each consisting of a water reservoir, flow meter, pressure transducer and associated tubes and valves, are used in those tests that include further wetting after compaction. The purpose of the flow meter is to measure the volume of water absorbed by the clay. When combined with measurements of the clay water content both before wetting and after gas breakthrough, in theory the volume of water expelled by the passage of gas can be calculated. A connection between the water- and gas-supply systems permits the water pressure to be increased, thus reducing the time required to wet the clay.

Gas from the Ar cylinder can be directed to both the top (outlet) and bottom (inlet) of each cell. The connection to the outlet is used to apply a back pressure, as described in section 4.1.3. As shown in Figure 4.1, the inlet pressure is monitored with transducer 1P and the outlet pressure with transducer 2P. Bourdon gauges are present on the apparatus, but they are only for emergency use and have not been needed. The pressure transducers are connected to an analog-to-digital converter; the converter is connected to a computer running LabTech Notebook data-acquisition software. Each test is continued until gas

breakthrough occurs or until the pressure limit of the apparatus (about 10 MPa) is reached. The raw data are transferred to a spreadsheet program for manipulation and plotting.

4.1.3 Procedures

Before being prepared for compaction, the Avonlea bentonite is dried in a 110°C oven to constant mass. The clay is cooled to 4°C in a desiccator to prevent the sorption of atmospheric moisture. The mass of water calculated from [4], for a chosen w and M_s, is added to the clay in a 4°C room and mixed until it appears homogeneous. The mass of each batch is enough to prepare several plugs. The moist clay is equilibrated in sealed double plastic bags for a minimum of two days before use. The mass of wet clay required to achieve a target ρ_c is

$$M = \rho_c V(1 + w) . \qquad [77]$$

Each clay plug is statically compacted in four layers into the cell using a piston driven by a hand-operated hydraulic jack. The tops of each of the first three layers are scored to improve the adhesion between lifts. A caliper scale is used to measure the piston travel; it is mounted so that one part moves with the piston and one part is anchored to a stationary reference point. Following clay compaction, the cell is assembled as described in the previous section, connected to the remainder of the apparatus with stainless steel tubing and all the valves are closed.

For those tests which include a wetting phase following compaction, valves 2, 3, 6 and 9 are opened. Valve 18 is opened and valve 22 repeatedly opened and closed to dislodge all air from the void space at the top of the cell. The two valves are then closed. A similar technique is used with valves 17 and 21 to remove air from the void space at the bottom of the cell. Valve 2 is closed and the cylinder valve opened. Regulator PRS1 (which supplies both low-pressure test systems) is adjusted to about 10 MPa, which is the pressure limit imposed by the relief valve. The data-acquisition system is started, valve 1 opened and regulator PRS 2 adjusted until the water pressure is 0.2 MPa. This was the water pressure used in earlier work by Kirkham (1995), and for consistency the same pressure was used for these tests. Once again air is flushed from the cell using valves 18 and 22 on the top, and valves 17 and 21 on the bottom. The flow meter is pressurized by slowly opening valve 4, and then the valve is closed. Valves 17 and 18 are opened briefly to ensure that the cell is pressurized, then valves 17, 18 and 6 are closed. Valve 4 is opened slowly, followed immediately by valves 5, 17 and 18. The volume of water entering the cell is recorded from the displacement of an oil column in the flow meter. After the wetting phase, which generally lasts about 42 h, all the valves are closed.

Following the wetting phase, or immediately following connection of the cell to the rest of the apparatus for those tests without a wetting phase, valves 11, 13 and 14 are opened and the data-acquisition system is started. If not already done, the cylinder valve is opened and PRS1 adjusted to 10 MPa. Regulators PRS2 and PRS3 are set at 0.2 MPa, as measured by transducers 1P and 2P and displayed on the data-acquisition monitor. For those tests which include a wetting phase, the water is removed from the void spaces at

the top and bottom of the cell before gas-breakthrough testing starts. Valve 20 is opened and valve 22 repeatedly opened and closed until only gas flows from the cell. A similar procedure is used on the bottom of the cell with valves 19 and 21. For either type of test, valves 19 and 20 are opened briefly to apply the back pressure to both sides of the clay plug, then closed. The inlet pressure is increased to 0.4 MPa, the data-acquisition system stopped and valve 14 shut.

At the beginning of the test, the data-acquisition system is re-started and valves 19 and 20 opened at about the same time. After five minutes the inlet pressure is increased to 0.6 MPa using regulator PRS2. The pressure is incremented at a rate of 0.2 MPa every five minutes for the remainder of the test. The test continues at least until gas passes through the plug, as evidenced by an increase in the outlet pressure, or until the pressure limit of the apparatus is reached.

At the end of the test, the clay plug is extruded from the sleeve using the same hydraulic press used to compact it. The plug is cut approximately in the middle to make inlet and outlet discs; four peripheral pieces are cut from each disc leaving an approximately square central piece. The two central samples (inlet and outlet) and the two peripheral samples (inlet and outlet) are dried in a 110°C oven to constant mass. The water contents are calculated from [5] and ρ_c from [77] with $w = 0$.

4.2 High-Pressure Gas-Breakthrough Apparatus[1]

4.2.1 Introduction

As will be described in section 5.2, no gas breakthrough was obtained on wetted Avonlea bentonite at $\rho_c > 0.90$ Mg/m^3 before the pressure limit of the low-pressure equipment was reached. The results were evaluated in the context of the pore-radius pressure model ([35]), which was the gas-breakthrough theory in use at that time. It was concluded that the capacity of the low-pressure equipment was insufficient to obtain breakthrough at the effective clay density of the buffer material ($\approx$1.22 Mg/m^3). The author coordinated the design, construction and installation of a 50-MPa test system at the Whiteshell Laboratories of AECL.

4.2.2 Components

4.2.2.1 Cell. The design of the new high-pressure cell is based on that of the earlier low-pressure cell so results can be compared. Whereas the low-pressure cell is limited to 10 MPa, the high-pressure cell is operated at pressures up to about 50 MPa. The cell is designed so that experiments can be conducted at temperatures between 20 and 95°C. Although they have not yet been done, the purpose of high-temperature tests would be to replicate the temperatures expected in a disposal vault (Mathers 1985). To provide a margin of safety, the cell is designed to withstand temperatures up to 150°C and pressures

[1] This section contains information published in Hume (1997).

as great as 62.7 MPa. The cell is designed according to ASME Section VIII, Division I, Boiler and Pressure Vessel Code (1995). It was fabricated according to CSA B51-M1995 (Boiler, Pressure Vessel and Pressure Piping Code).

The cell consists of two end flanges and a central sleeve (Figures 4.2 and 4.3). Stainless steel was chosen for the cell material because of its corrosion resistance, strength, ease of machining, low cost and ready availability. The sleeve is 200.0 mm in diameter and 38.0 mm thick. There is a 50.8-mm-diameter hole through the centre of the sleeve. Each of the two flanges is 200.0 mm in diameter; the thickness increases in one step from 76.0 mm near the circumference to 79.0 mm next to the cell cavity. A piston-like insert ensures that each flange is centred on the sleeve; the inserts are 50.6 mm in diameter and 4.0 mm long. The end of each insert is grooved, as shown in Figure 4.2, so that any introduced gas or water is distributed over the end of the plug. Eight equally-spaced holes are located around the circumference of both flanges and the sleeve.

Two holes through the lower flange are aligned with threaded holes in the bottom of the sleeve. Small bolts in these holes hold the sleeve and lower flange together while the specimen is being prepared.

There are four threaded holes on the top of the upper flange and three on the bottom of the lower flange. A channel connects each of the holes to internal openings on the flange insert, next to the specimen. A 7.9-mm-diameter o-seal straight-thread to 3.2-mm tube-fitting adapter fits all the holes on the bottom flange and three of the holes on the top

Figure 4.2 The high-pressure gas-breakthrough cell shown partially assembled.

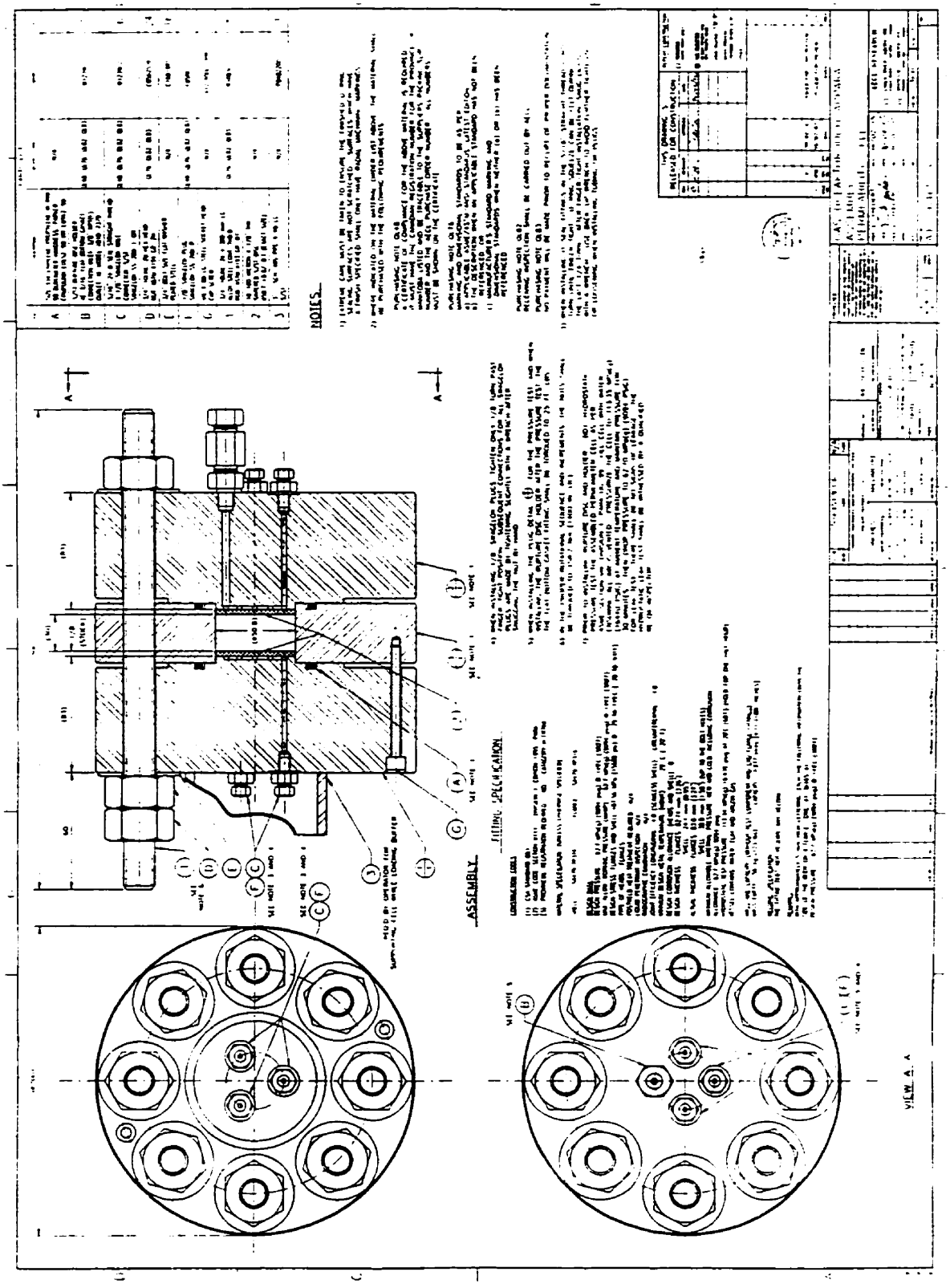

Figure 4.3 Blueprint of the high-pressure gas-breakthrough cell.

flange. Stainless-steel tubing connects one pair of adapters (one on each of the upper and lower flanges) to a water-supply system. A second pair of adapters on the upper and lower flanges is connected to the gas outlet and inlet, respectively. The final pair of adapters is connected to valves that vent to the atmosphere.

The fourth opening on the top of the cell (4.8 mm in diameter) is fitted with a rupture disc assembly (Autoclave Engineers model 1010-7379). Free water should be expelled from the cell before it is heated. If the cell is not drained before heating, expansion of the water could produce dangerous pressure. The rupture disc provides a 'soft' failure point for the cell.

The cell is sealed by ethylene propylene o-rings (90 durometer hardness) between each flange and the sleeve. When the cell is completely assembled there is a 23.1-mm-long (46.8-mL) cavity where the specimen is located. A 50.0-mm-diameter filter-paper disc (Whatman #40) is located on each side of the clay plug. A porous stainless-steel disc (Pall Trinity Micro Corporation, 3.2 mm thick and 50.0 mm in diameter, porosity type H) is located between each filter and the flange insert. The cell is held together by eight 19.0-mm-diameter threaded rods, and corresponding nuts, passing through the eight holes around the perimeter of the cell.

The cell, without the rupture disc, was hydrostatically tested to 113 MPa before use. The o-rings were deformed by the pressure test but the cell did not fail. The o-rings are not deformed by repeated use at pressures up to approximately 50 MPa.

The fully-assembled cell is shown in Figure 4.4. The water, gas and vent tubes are shown connected to the remainder of the apparatus in the figure. The water- and gas-supply systems, and the vent valves, are fastened to a sheet of plywood. Figure 4.5 shows a schematic diagram of the connections between the cell and the rest of the test system.

4.2.2.2 Water-Supply System. The water system is visible in the photograph of the high-pressure apparatus (Figure 4.4) and is illustrated in the schematic (Figure 4.5). A gas regulator (PRS1 in Figure 4.5; Matheson model 3536-580) controls the gas pressure to the water system. The regulator is visible in Figure 4.4 near the left edge of the plywood panel. A pressure relief valve (RV2; Nupro model SS-RL3S4) protects the water system from the potentially damaging pressure in the gas cylinder. Valve V3 is used to vent gas from the water reservoir and the line leading to the water reservoir. A 500-mL Whitey stainless-steel cylinder (TK3; model 304L-HDF4-500CC), located to the left of the flow meter (Figure 4.4), serves as a water reservoir. A length of clear plastic tubing next to the cylinder is used to indicate the height of water in the vessel.

A flow meter was included in the design of the apparatus to measure the volume of water absorbed in the clay plug. The flow meter consists of a clear glass tube mounted in front of a calibrated scale. The volume of water passing through the flow meter can be measured from the displacement of a column of coloured mineral oil. Filling of the flow meter with distilled water and the introduction of an oil column is described by Kirkham (1995). The design of the flow meter, and the associated valves, is the same as that used in hydraulic conductivity experiments by Dixon (1995).

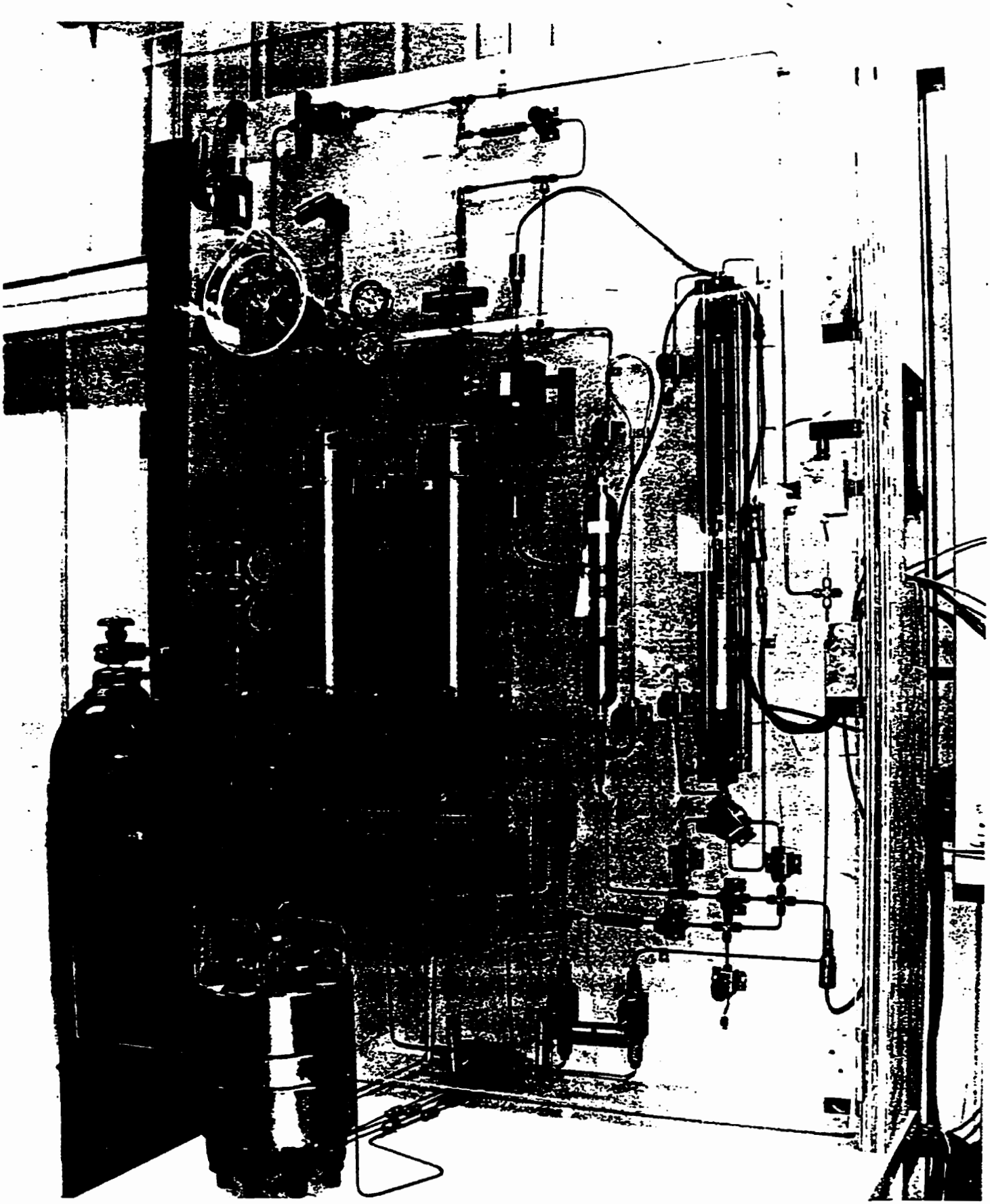

Figure 4.4 Assembled cell connected to the remainder of the gas-breakthrough apparatus.

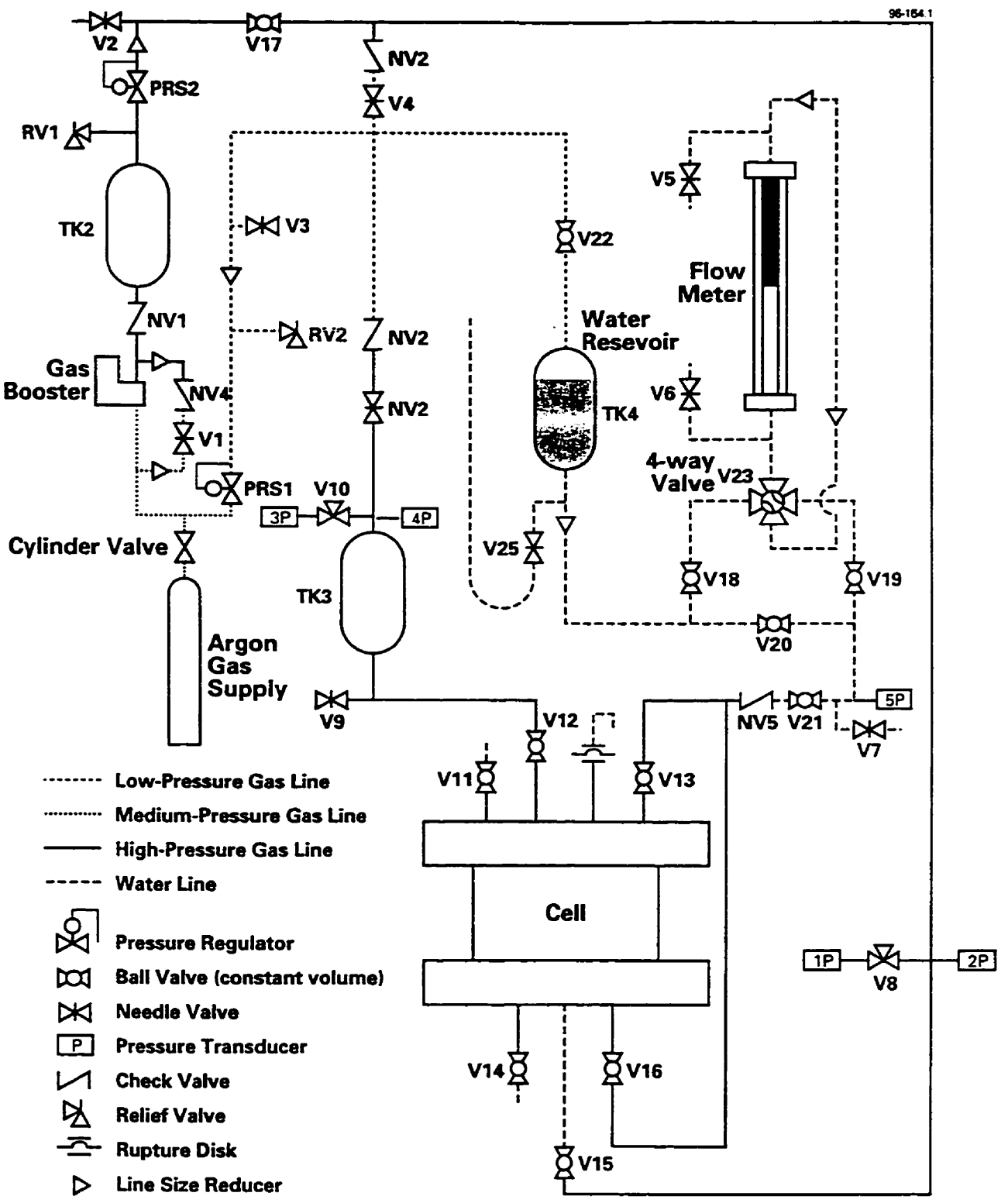

Figure 4.5 Schematic drawing of the complete high-pressure gas-breakthrough apparatus.

The flow meter cannot be used as planned when the equipment was designed. The original experimental procedure included a measurement of the volume of water expelled from the plug by the passage of gas. This volume was to have been obtained as the difference between the volume of water in the clay at the beginning of a gas-breakthrough test (the water in the clay at compaction plus the water absorbed in the specimen as measured by the flow meter) and the volume of water remaining in the plug after a gas-breakthrough test (as measured gravimetrically by drying in an oven). This is not practicable because the leads to the cell cannot be filled with water without having some water absorbed by the clay at the same time. Secondly, the 3.5-mL volume chosen for the flow meter, which is the same as that used in the low-pressure apparatus, is inappropriate for the ρ_c used. For example, at $\rho_c = 0.9$ Mg/m^3, the volume of void space in a plug is about 31 mL. Assuming that the initial clay water content is zero, this corresponds to about nine flow-meter volumes. Lastly, the water content of the plug can change either because water is expelled from the specimen by gas or because the particle structure is consolidated, thus reducing the volume of void space. As a result, the flow meter is only used occasionally, and its use is restricted to determining whether the flow of water into the cell has ceased. If another gas-breakthrough apparatus is constructed, elimination of the flow meter should be considered.

Check valve NV5 (Autoclave Engineers SW02200) allows water to flow into the cell but prevents the possibly hazardous pressure in the cell from entering the water system, which is not designed for high pressure. A vacuum pump (not shown in any of the figures) can

be used to evacuate air from the cell before wetting the plug. A belt-drive vacuum pump (Marvac Scientific Manufacturing Co. model A10) is used for this purpose.

The gas line leading to the water reservoir is connected to the high-pressure gas inlet to the cell and to the gas outlet from the cell. These connections are used to purge water from the void spaces at both ends of the clay plug between the wetting and gas-breakthrough phases of an experiment. The connection to the cell outlet is also used to apply a back pressure on the specimen. The connection to the cell inlet can also be used as the gas inlet for low-pressure tests, using pressure regulator PRS1 to control the pressure. Check valves NV2 and NV3 (Autoclave Engineers SW02200) allow gas to pass from the low- to the high-pressure regions, but not in the reverse direction.

The needle valves on the low-pressure side of the check valves are Whitey model SS-0RS2 or Whitey SS-1RS4 and the ball valves are Swagelok SS-41S2. The two ball valves between check valve NV5 and the cell are Autoclave Engineers model BSW2021. The four-way valve associated with the flow meter is manufactured by Whitey (model SS-43YFS2-049). The tubing on the low-pressure side of the check valve is 3.2 mm outside diameter (O.D.) with a 0.5-mm wall thickness or 6.4 mm O.D. with a wall thickness of 0.9 mm. On the high-pressure side of the check valve, the tubing has an O.D. of 3.2 mm and a 0.9-mm-thick wall. All connections are either threaded or tube fittings.

4.2.2.3 Gas-Supply System. A diaphragm gas compressor (mounted on the floor and not visible in Figure 4.4) is used to boost the gas pressure from that in the cylinder to the

pressure needed for the experiments. The compressor (Pressure Products Industries model 46-14025-2) operates on the laboratory 0.7-MPa compressed-air system. The maximum output pressure is 70 MPa, but the compressor can be stopped at a lower pressure by turning off the supply of compressed air.

The output of the compressor is into the left cylinder in Figure 4.4 (TK1). It is an Autoclave Engineers vessel (model OR0050SS11) with a volume of 500 mL. This vessel serves as a high-pressure gas reservoir. It also buffers pressure pulses that might occur if the compressor is operated while a test is in progress. Valve V1 opens a bypass that allows the gas reservoir to be filled with Ar to the pressure in the gas cylinder, thus reducing the compressor operation time. Check valves NV1 and NV4 prevent high-pressure gas from flowing into the Ar cylinder and creating a dangerous pressure inside the bottle.

Relief valve RV1 (Autoclave Engineers model 10RV9072) releases if the pressure increases above about 50 MPa, as could happen if the compressor is operated unattended. High-pressure regulator PRS2 (Tescom model 26-1021-24-008) controls the pressure to the cell. The high-pressure regulator is connected to the inlet on the bottom of the cell with tubing. A needle valve (V2) is used for venting the gas reservoir and the inlet line to the cell. Valve V17 isolates the compressor from the inlet line when water is being expelled from the void space below the clay plug.

The outlet (top) of the cell is connected to a second Autoclave Engineers model OR0050SS11 pressure vessel (TK2). Valve V9 is used for purging the outlet side of the cell and valve V23 separates the low- and high-pressure gas systems.

Heavy-duty valves and tubing are used on the high-pressure side of the compressor. All the valves are manufactured by Autoclave Engineers: the ball valves are model BSW2021 and the needle valves are model 10V2081. The stainless-steel tubing between the Ar cylinder and the compressor is 6.4 mm O.D. and the wall is 0.9 mm thick. From the compressor to the high-pressure regulator, the tubing is 6.4 mm O.D. and the wall is 1.7 mm thick. From the pressure regulator to the cell, and from the cell outlet to check valve NV3, tubing with a wall thickness of 0.9 mm and an O.D. of 3.2 mm is used. Connections between tubes are with tube fittings; tubing and other components are joined with either threaded or tube fittings.

4.2.2.4 Instrumentation and Data-Acquisition System. A Microgage P-102 pressure transducer rated for 0 to 14 MPa operation is connected to the water system (5P in Figure 4.5). On both the gas inlet and outlet, a low- or high-pressure transducer can be selected by rotating a three-way valve (Autoclave Engineers model BSW2023). The low-pressure transducers (1P and 3P) are Microgage P-102 rated for 0 to 14 MPa and the high-pressure transducers (2P and 4P) are Microgage P-102 rated for 0 to 70 MPa. The low-pressure transducers provide greater precision than the high-pressure ones at pressures <14 MPa. The high-pressure transducers allow the apparatus to be used up to its limit of about 50 MPa. If the low-pressure transducers are exposed to high pressure,

they will likely be damaged but they should not fail. The transducers are powered by 5.00 V from a Hewlett Packard dual dc power supply (model 6255A).

The five pressure transducers were calibrated with a dead-load calibration apparatus. The output voltage from the transducers (χ) was measured with a voltmeter for several pressures and an equation of the form $p = \beta(\chi + \gamma)$ was determined by linear regression for each transducer. The constants β and γ are used in the data-acquisition software (described in the following paragraph) so that the pressure is output in SI units.

The output of the transducers is connected to a μMAC-5000 analog-to-digital converter manufactured by Analog Devices. The analog-to-digital converter is connected to a personal computer with a 486 processor running LabTech Notebook version 7.2.1W data-acquisition software. The data-acquisition system displays the inlet and outlet gas pressures and the water pressure on a monitor graphically as a function of time, and numerically. The pressures and elapsed time are recorded on a computer disk every 10 s. The recorded data from an experiment are transferred into Microsoft Excel version 5.0c for plotting of the inlet and outlet pressures against time.

As recommended by Kirkham (1995), an outlet pressure gauge is not installed on this apparatus. An inlet gauge is present as it was integrated with pressure regulator PRS2. During routine operation an outlet gauge is not needed. However, during commissioning of the equipment it would provide confidence that the pressure transducers are operating. An outlet pressure gauge should be included on a future gas-breakthrough apparatus.

4.2.3 Procedures

4.2.3.1 Plug Preparation. As described in sections 5.2 and 6.2, low-pressure tests showed that changes in the compaction water content did not cause variations in the gas-breakthrough pressures of specimens that were further wetted towards saturation (in the cell) before testing. (This finding is similar to that of Dixon (1995), who found that changes in the compaction water content did not cause changes in the hydraulic conductivity of compacted Avonlea bentonite.) As a result, two series of tests were conducted on specimens prepared with air-dry clay.

It has been reported in the literature that the compaction water content is often an important parameter in soil testing. For example, Pacey (1956) reported that changes in the compaction water content causes changes in clay particle orientation. Sloane and Kell (1966) published electron micrographs showing how clay fabric changes with compaction water content. Barden and Sides (1970) reported the results of geotechnical engineering tests as a function of the compaction water content. Diamond (1970 and 1971), Garcia-Bengochea et al. (1979) and Garcia-Bengochea and Lovell (1981) reported that the pore-size distribution in compacted clays depends on the compaction water content. Wan (1987) and Wan et al. (1990) concluded that the compaction water content influenced the results of geotechnical engineering (triaxial) tests they conducted on buffer material. In Wan (1996), the results of mercury intrusion porosimetry tests on compacted Avonlea bentonite are described; it is concluded that the compaction water content affects the

pore-size distribution. Delage and Graham (1996) review the evidence supporting a relationship between compaction water content and soil properties.

Given the results presented in the previous paragraph, there was concern about the validity of gas-breakthrough results obtained on specimens that were compacted using air-dry clay. Therefore, two sets of tests were conducted in which the clay was wetted before compaction. The procedure for wetting the clay before compaction was similar to that described for the low-pressure tests, except that the clay and water were mixed in a room temperature laboratory, as a 4°C room was not available at Whiteshell Laboratories. The precise wetting procedure used for each set of high-pressure tests is described in chapter 5.

The clay specimens are statically compacted using a Materials Testing System model 810 hydraulic press. The sleeve is bolted to the bottom flange of the cell. A porous-stainless-steel disc and a filter-paper disc are placed in the bottom of the cavity before compacting the plug. The partially-assembled cell is placed on a base that can be elevated, and a 50.0-mm-diameter ram is threaded into a load-sensing cell directly above. The base is raised until the ram contacts the bottom of the cell as evidenced by a change in the output from the load cell on the digital display. An arbitrary reading of the base height (h_o) is obtained from the digital display. Twenty-five percent of the mass of clay calculated using [77] is added to the cell. As the plugs are prepared in four layers, the base is raised until the value on the digital display (h_1) is

$$h_1 = h_0 + (0.2\ V/mm)(h_s)/4 \qquad [78]$$

where h_s is the total height of the clay specimen in millimetres and 0.2 V/mm is the change in potential per unit upward movement of the base. Each layer, except the top layer, is scored before adding the next layer to improve the adhesion between layers.

The second layer is compacted much like the first layer except that h_1 and h_o in [78] are replaced by h_2 and h_1, respectively, where h_2 is the display value to which the base should be raised to compact the second layer to the correct ρ_c. Layers three and four are compacted similarly. Following compaction, filter-paper and porous-stainless-steel discs are placed on top of the plug. The top flange is placed on the cell and the cell bolted together.

Stainless-steel tubes are connected to the adapters on the top and bottom of the cell following assembly. The opposite ends of the tubes are connected to the water, gas and purge lines as shown in Figures 4.4 and 4.5.

4.2.3.2 Wetting Phase. All the high-pressure tests were conducted on clay that was further wetted after compaction. An initial series of tests was done on specimens that were wetted with a gas pressure of 0.2 MPa applied to the water reservoir for 2 d. This pressure was chosen for consistency, since 0.2 MPa was applied during the wetting phase of the low-pressure tests. It was later determined that wetting at a pressure of 0.2 MPa resulted in a 0.9 Mg/m^3 Avonlea bentonite specimen having a $S_r < 1.0$ (Table 4.1). Subsequent testing showed that 0.6 and 1.2 Mg/m^3 bentonite plugs wetted for 2 d at a

Table 4.1 Results of tests to determine the effect of various wetting-phase parameters on S_r in compacted Avonlea bentonite.

ρ_c (Mg/m^3)	Cell Evacuated?	Water Pressure (MPa)	Duration (d)	S_r
0.9	No	0.2	2	0.89
0.9	No	1.1	2	0.89
0.6	No	5.0	2	0.97
1.2	No	5.0	2	1.06
1.3	Yes	0.2	1	0.79
0.9	Yes	1.0	2	0.98
1.3	Yes	1.0	2	1.02

pressure of 5.0 MPa have a $S_r \approx 1.0$ (Table 4.1). Black and Lee (1973) and Craig (1994) suggest evacuating specimens as a method of increasing S_r. It was found that 0.9 and 1.3 Mg/m^3 bentonite plugs that were evacuated and then wetted for 2 d with an applied gas pressure of 1.0 MPa have a $S_r \approx 1.0$ (Table 4.1).

It was decided to change the wetting procedure, even though the results would not be comparable to earlier tests. A series of tests was conducted on clay specimens that were wetted at 1.0 MPa following evacuation. Two sets of experiments were performed on clay that was wetted at 5.0 MPa without evacuation.

If the cell is to be evacuated before wetting, the vacuum pump is connected to the top and bottom of the cell via purge valves V11 and V14. The valves are opened and the cell is evacuated for 15 minutes to remove air. Following evacuation, valves V11 and V14 are closed and the vacuum pump is disconnected.

Before wetting, valves V3, V22 and V24 are opened. The height of water in the reservoir is observed in the adjacent clear plastic tubing. If necessary, more water is added as described in the following paragraph. If more water is not required, the valves are closed. To add more water to the reservoir, a 60-mL syringe full of water is connected near valve V7 using a length of plastic tubing with a tube fitting on one end and a tubing-to-syringe adapter on the opposite end. Valves V7 and V20 are opened and water is transferred into the reservoir until the syringe is nearly empty. Valve V20 is closed while the syringe is refilled and then the procedure is repeated. This procedure is continued until the reservoir is full as indicated by the height of water in the clear plastic tube. All the valves are closed and the syringe is disconnected.

The oil column should be near the top of the flow meter before the wetting of the specimen begins. If necessary, the oil column can be moved to the top of the flow meter. The four-way valve is rotated so that it points to the right. Valves V3, V22, V18 and V19 are opened. Valve V7 is opened slightly and the oil column allowed to rise slowly until it reaches the top of the flow meter. If the oil column begins to separate, the flow rate is reduced by closing valve V7 a little. All the valves are closed when the oil column nears the top of the flow meter.

Air must first be removed from the void spaces at the top and bottom of the cell, if the clay is wetted without evacuating the cell. Valves V3, V22, V20 and V21 are opened. Valve V13 is opened and V11 repeatedly opened and closed to displace air from the top of the cell. Both valves are closed when only water flows from the cell. The same

procedure is used on the bottom of the cell with valves V16 and V14. All the valves are then closed. The valve on the Ar cylinder and valves V22, V20 and V21 are opened. The data-acquisition system is started and the water pressure is adjusted to 0.2 MPa with pressure regulator PRS1. Again air is dislodged from the cell using valves V13 and V11 on the top of the cell and valves V16 and V14 on the bottom.

If not already done, the valve on the Ar cylinder and valves V22, V20 and V21 are opened and the data-acquisition system is started. The chosen wetting pressure is obtained by adjusting regulator PRS1. Valves V13 and V16 are opened to allow water to flow from the reservoir to the cell.

The flow meter is used sometimes on the second day of wetting to determine if the flow of water into the plug has stopped. It is generally operated with the flow downwards as this minimizes the separation of the oil column (hence the reason for positioning the oil column near the top of the flow meter). When valve V20 is open, with valves V18 and V19 closed, water bypasses the flow meter when flowing from the water reservoir to the cell. When valves V18 and V19 are open, and valve V20 is closed, the flow of water is directed through the flow meter. The four-way valve at the base of the flow meter rotates through 90°. When the four-way valve is pointing down, water flows downwards through the flow meter as illustrated schematically in Figure 4.5. When the four-way valve is pointing to the right, as in Figure 4.4, water flows through valve V18 and upwards through the flow meter. It then passes through V19 and V21 and into both the top and bottom of the cell.

After two days of wetting, valves V13, V16, V21, V20 (or V19 and V18) are shut and data acquisition is stopped. Pressure regulator PRS1 is set to zero and valve V3 is opened to vent gas from the line and water reservoir. Valves V22 and V3 are closed when Ar stops venting to the atmosphere.

4.2.3.3 Gas-Breakthrough Phase. Water is purged from the void spaces in the top and bottom of the cell before the gas-breakthrough phase of the experiment begins. Valves V4 and V23 are opened, the data-acquisition system is started and pressure regulator PRS1 is adjusted to 0.2 MPa. Purge valve V11 is opened and valve V12 is repeatedly opened and closed to dislodge water from the top of the cell. Valves V11 and V12 are closed when only gas flows from the cell. Similarly on the bottom of the cell, valve V14 is opened and valve V15 alternately opened and closed; both valves are shut when no further water is expelled from the cell. Valves V12 and V15 are simultaneously opened for a brief time to ensure that the pressure is 0.2 MPa on both the top and bottom of the specimen. Before starting the gas-breakthrough phase of the experiment, data acquisition is suspended and valves V4 and V23 are closed. Pressure regulator PRS1 is adjusted to zero and valve V3 is opened; when Ar stops venting the valve is closed.

Valve V1 is opened until the gas reservoir (TK1) is filled with Ar to the same pressure as in the cylinder, and then the valve is closed. The Ar pressure in TK1 is increased to about 50 MPa using the gas compressor. Valve V17 is opened and pressure regulator PRS2 is adjusted to the starting pressure. The data-acquisition system is re-started and valves V15 and V12 are opened at about the same time.

Two types of tests were conducted: in some cases the pressure to the cell was initially set at 1 MPa and then increased 1 MPa every five minutes while in other experiments the pressure was maintained at the starting pressure and the time to breakthrough was measured. If the pressure in TK1 drops significantly, it is boosted to 50 MPa with the compressor. The test continues until gas passes through the specimen, as evidenced by an increase of pressure on the outlet side of the cell, or until the pressure limit of the apparatus is reached.

At the end of the experiment the data-acquisition system is shut off. The Ar-cylinder valve is closed and valves V2 and V9 are carefully opened to vent the bottom and top of the cell, respectively. When Ar has finished venting, all the valves on the apparatus are closed and the pressure regulators are adjusted to zero. The cell is disconnected from the rest of the apparatus. The tubes are removed from the cell and it is disassembled. The plug is extruded from the sleeve with the same hydraulic press used to compact it.

The specimen is cut into pieces to determine the water content distribution. Sometimes the plug is cut as described in the procedure for the low-pressure apparatus; alternatively it is sliced perpendicular to the direction of gas flow. The pieces are dried at 110°C to constant mass and the w and ρ_c are determined as described in section 4.1.3. The data are imported into a spreadsheet program and the inlet and outlet pressures plotted against time.

5. GAS-BREAKTHROUGH EXPERIMENT RESULTS

5.1 Incremental Low-Pressure Unsaturated Tests[1]

Gas-breakthrough tests were conducted on unsaturated Avonlea bentonite specimens using a pressure increment of 0.2 MPa and an increment duration of five minutes. These specimens were tested as compacted; that is, they were not further wetted towards saturation after compaction into the gas-breakthrough cell. A preliminary set of tests (series A) was conducted between $\rho_c = 0.9$ and 1.2 Mg/m^3 in collaboration with K.S. Gelmich Halayko (1998). Table 5.1 shows the target, initial (at the time of compaction) and final (after completion of the gas-breakthrough test) values of w and ρ_c. The final w value in Table 5.1 is the mean of the inlet periphery, inlet centre, outlet periphery and outlet centre values in Table 5.2. The values of w are obtained from [5]. The initial ρ_c is calculated from [77] using the measured initial w value and the known M value, assuming that the correct mass of clay was placed in the cell and that none was lost during compaction. The final ρ_c is obtained from [8] after drying the plug.

Statistics are used frequently in this chapter, and chapter 6, to determine if results are significantly different. In all cases, the method of paired samples is used (Wonnacott and

[1] This section contains information published in Hume et al. (1997).

Table 5.1 Target, initial and final w and ρ_c for series A.

Test	Target w (%)	Target ρ_c (Mg/m^3)	Measured Initial w (%)	Calculated Initial ρ_c (Mg/m^3)	Measured Final w (%)	Measured Final ρ_c (Mg/m^3)
A1	45	0.90	46.83	0.889	46.34	0.836
A2	50	0.90	49.13	0.905	48.19	0.891
A3	55	0.90	54.31	0.904	53.48	0.902
A4	60	0.90	NA	NA	60.71	0.902
A5	45	1.00	44.66	1.002	44.40	0.992
A6	45	1.00	NA	NA	48.65	1.000
A7	50	1.00	51.50	0.990	49.92	0.981
A8	50	1.00	49.36	1.004	52.78	0.996
A9	55	1.00	54.31	1.005	58.38	0.992
A10	60	1.00	59.44	1.004	56.78	1.011
A11	60	1.00	56.69	1.021	58.54	0.998
A12	60	1.00	57.59	1.015	59.45	0.991
A13	60	1.03	57.91	1.044	55.23	1.015
A14	50	1.05	50.75	1.045	50.34	1.040
A15	50	1.05	49.06	1.057	49.40	1.047
A16	50	1.05	52.66	1.032	51.71	1.054
A17	55	1.05	56.13	1.042	54.21	1.045
A18	55	1.05	55.88	1.044	56.06	1.000
A19	55	1.08	55.98	1.073	52.81	NA
A20	55	1.08	54.95	1.081	53.27	1.071
A21	55	1.08	56.35	1.071	53.27	1.063
A22	45	1.10	44.66	1.103	46.68	1.078
A23	50	1.10	48.06	1.115	49.42	1.100
A24	50	1.10	49.13	1.107	49.59	1.098
A25	50	1.10	50.75	1.095	50.51	1.087
A26	50	1.13	52.04	1.115	50.77	1.097
A27	45	1.15	48.18	1.125	47.88	1.121
A28	50	1.15	53.32	1.125	48.89	1.117
A29	45	1.20	48.69	1.170	46.97	1.160

Table 5.2 Final water contents of clay samples (%) for series A.

Test	Gas Inlet (Periphery)	Gas Inlet (Centre)	Gas Inlet (Mean)	Gas Outlet (Periphery)	Gas Outlet (Centre)	Gas Outlet (Mean)	Difference[a]
A1	NA	NA	NA	NA	NA	NA	NA
A2	47.49	48.37	47.93	48.17	48.74	48.46	-0.53
A3	NA	NA	NA	NA	NA	NA	NA
A4	62.79	62.19	62.49	59.49	58.38	58.94	3.85
A5	45.25	43.93	44.59	44.34	44.10	44.22	0.37
A6	51.14	46.62	48.88	50.04	46.80	48.42	0.46
A7	50.00	50.46	50.23	49.52	49.68	49.60	0.63
A8	NA	NA	NA	NA	NA	NA	NA
A9	60.05	58.25	59.15	57.88	57.36	57.62	1.53
A10	NA	NA	NA	NA	NA	NA	NA
A11	58.51	57.78	58.14	58.89	58.98	58.94	-0.80
A12	NA	NA	NA	NA	NA	NA	NA
A13	57.60	58.77	58.18	52.24	52.30	52.27	5.91
A14	50.69	50.28	50.48	50.19	50.19	50.19	0.29
A15	49.20	49.53	49.36	49.48	49.37	49.42	-0.06
A16	51.90	51.83	51.86	51.38	51.74	51.56	0.30
A17	53.93	54.19	54.06	54.30	54.41	54.36	-0.30
A18	56.42	55.48	56.45	56.36	55.98	56.17	0.28
A19	54.92	NA	54.92	54.46	49.04	51.75	3.17
A20	53.44	53.39	53.42	53.10	53.15	53.12	0.30
A21	54.84	55.02	54.93	52.90	52.67	52.78	2.15
A22	NA	NA	NA	NA	NA	NA	NA
A23	53.75	51.96	52.86	46.16	45.79	45.98	6.88
A24	50.27	49.76	50.02	49.45	48.88	49.16	0.86
A25	50.24	50.27	50.26	50.87	50.65	50.76	-0.50
A26	51.48	51.44	51.46	50.13	50.03	50.08	1.38
A27	47.83	47.24	47.54	48.56	47.89	48.22	-0.68
A28	50.70	50.37	50.54	47.12	47.37	47.24	3.30
A29	48.37	47.55	47.96	46.28	45.68	45.98	1.98

[a]Difference = Gas Inlet (Mean) - Gas Outlet (Mean)

Wonnacott 1977). A 95% confidence interval is obtained from

$$\Delta X = D_{mean} \pm t_{0.025} s_D / n_D^{0.5}, \qquad [79]$$

where ΔX is the average difference between two populations for parameter X, D_{mean} the mean of the measured differences, $t_{0.025}$ the appropriate student's t value, s_D the standard deviation of the differences and n_D the number of samples. A result reported as $\Delta X = D_{mean} \pm Y$ is a 95% confidence interval for the difference, not the average difference plus or minus the standard deviation. The difference in results is statistically significant, at the 95% confidence level, only if the interval does not include zero.

In general, the target ρ_c values agree well with both the initial and final values. However, the initial ρ_c is slightly larger than the final one ($\Delta\rho_c = 0.013 \pm 0.006$ Mg/m^3). This difference is attributed to clay losses during compaction, extrusion and slicing. As the majority of these losses likely occurred after the test (during the extrusion and slicing procedures), the calculated initial ρ_c is considered the more accurate of the values. No initial ρ_c value is available for tests A4 and A6 and, therefore, the final value is used. These two values both agree well with the target value. There is no statistically significant difference between the initial and final w values ($\Delta w = 0.46 \pm 0.79\%$). (That is, with 95% confidence Δw is between -0.33 and 1.25%. All subsequent equations of this format should be interpreted similarly). Therefore the best value of w is assumed to be the average of the two.

Gas breakthrough is defined arbitrarily as the first sustained outlet pressure that is greater than the back (outlet) pressure applied at the beginning of the experiment (p_o). The gas-breakthrough pressure (p_b) is defined as the difference between the inlet pressure at breakthrough (p_i) and p_o

$$p_b = p_i - p_o \,. \qquad [80]$$

It is not obvious if the above definition of breakthrough is the best one. However, the definition can be applied consistently to all of the experiments. The p_b results from all specimens are listed in Table 5.3 along with the ρ_c, w, S_r and t_b of the specimens. The S_r value is calculated from [10] and [11]. Because it is difficult to determine the precise time of breakthrough for some tests, t_b is the mid-point time of the pressure increment in which breakthrough occurred. In none of the experiments was there any visible evidence of damage to the clay plug, when the cell was disassembled, as a result of the passage of gas.

The data in Table 5.3 include those from Tables 5.1 and 5.2. Test A13 has been added to the target 1.05 Mg/m^3 group of tests and tests A26, A27 and A28 have been combined with the target 1.10 Mg/m^3 tests. The largest ρ_c range for a group is 0.031 Mg/m^3, and this is for a group in which the target ρ_c was the same for all of the tests (1.00 Mg/m^3). For each ρ_c, the tests are listed in order of increasing S_r.

Two rates of gas breakthrough are observed in this set of experiments: slow and rapid. Those tests that had slow breakthrough are indicated in Table 5.3. Whether a test has slow or rapid breakthrough is decided arbitrarily after examining the data.

A second set of tests (series B) was conducted between ρ_c = 0.95 and 1.45 Mg/m^3, in 0.05 Mg/m^3 increments. The expanded ρ_c range brackets the ρ_c of reference buffer material (1.22 Mg/m^3). As with series A, the clay was wetted before specimen preparation; no additional wetting was done before gas-breakthrough testing. Tests were conducted at w

Table 5.3 Summary of experimental results for series A.

Test	Calculated Initial ρ_c (Mg/m^3)	Mean w (%)	S_r (%)	p_b (MPa)	t_b (h)
A1	0.889	46.58	61.74	0.2	0.04
A2	0.905	48.66	66.24	0.2	0.04
A3	0.904	53.90	73.25	0.2	0.04
A4	0.902	60.72	82.25	0.2	0.04
Mean	0.90		70.9		
A5	1.002	44.53	70.95	0.2	0.04
A6	1.000	48.65	77.27	0.2	0.04[a]
A7	0.990	50.70	79.25	0.2	0.04
A8	1.004	51.07	81.63	0.2	0.04[a]
A9	1.005	56.35	90.21	0.6	0.2[a]
A10	1.004	58.11	92.88	0.2	0.04
A11	1.021	57.62	94.60	0.6	0.2[a]
A12	1.015	58.52	95.18	>8.8	>3.6
Mean	1.01		85.2		
A14	1.045	50.54	82.45	0.2	0.04
A15	1.057	49.23	85.51	0.2	0.04[a]
A16	1.032	52.18	87.17	0.4	0.1[a]
A17	1.042	55.16	93.60	0.8	0.3
A18	1.044	55.97	95.27	0.6	0.2
A13	1.044	56.57	96.29	7.8	3.2
Mean	1.04		90.0		
A19	1.073	54.40	96.87	1.2	0.5
A20	1.081	54.11	97.55	3.4	1.4
A21	1.071	55.10	97.81	4.6	1.9
Mean	1.08		97.4		
A22	1.103	45.67	85.17	0.2	0.04
A23	1.115	48.74	92.58	>9.2	>3.8
A24	1.107	49.36	92.61	0.6	0.2
A27	1.125	48.03	92.63	0.8	0.3[a]
A25	1.095	50.62	93.24	0.6	0.2[a]
A26	1.115	51.40	97.63	5.4	2.2
A28	1.125	51.10	98.55	>8.6	>3.5
Mean	1.11		93.2		
A29	1.170	47.83	98.75	6.8	2.8

[a]Start of slow breakthrough.

ranging from 30 to 60%, in 5% increments. In series A, breakthrough occurred at the first pressure increment (p_b = 0.2 MPa) in all cases where S_r was <85%. Since series B extends to higher ρ_c, it was thought that p_b might exceed 0.2 MPa at values of S_r < 85%. It was arbitrarily decided to test those combinations of target ρ_c and w that give a S_r between 80 and 100%.

The procedures used for the series B tests differed from those for series A as follows. The clay w was kept more constant by checking it following mixing of the clay and water, but before compaction of the plug. If necessary, the w was adjusted to within ±1% of the target value (for example, if the target was 60%, then 59 to 61% moisture was acceptable) by drying the clay in an open tray at room temperature or by adding more water, as appropriate. Before compaction of the plug w was measured a second time, and the M required to obtain a target ρ_c was calculated from this number. The difference between the target w and that measured before plug preparation exceeded 1% in only four of the tests.

Table 5.4 shows the target and final values of w and ρ_c and the initial values of w for series B. The final ρ_c is less than the target value ($\Delta\rho_c = 0.005 \pm 0.002$ Mg/m^3). The target ρ_c is considered to be the more accurate of the two values. The w of most of the samples, obtained at the end of the experiment, are in Table 5.5. Water contents for the 1.40 and 1.45 Mg/m^3 tests are absent because it was difficult to slice these clay plugs with the equipment available. The final w in Table 5.4 is the mean of the results in Table 5.5. Unlike the series A experiments, in series B the final w is significantly less than the initial

Table 5.4 Target, initial and final ρ_c and w for series B.

Test	Target ρ_c (Mg/m^3)	Target w (%)	Measured Initial w (%)	Measured Final ρ_c (Mg/m^3)	Measured Final w (%)
B1a	0.95	60.0	60.29	0.954	57.55
B1b	0.95	60.0	60.36	0.946	58.51
B1c	0.95	60.0	60.36	0.947	58.92
B2a	1.00	55.0	54.50	1.007	52.63
B2b	1.00	55.0	54.50	1.010	52.61
B2c	1.00	55.0	54.56	1.005	52.86
B3a	1.00	60.0	60.26	0.996	58.83
B3b	1.00	60.0	60.26	0.993	58.39
B3c	1.00	60.0	60.29	0.998	58.67
B4a	1.05	55.0	54.01	1.044	52.49
B4b	1.05	55.0	54.01	1.057	52.50
B4c	1.05	55.0	54.56	1.054	52.80
B5a	1.10	50.0	50.14	1.096	48.64
B5b	1.10	50.0	50.14	1.102	48.45
B6a	1.15	45.0	44.95	1.148	44.10
B6b	1.15	45.0	44.95	1.148	44.02
B7a	1.15	50.0	49.77	1.143	48.35
B7b	1.15	50.0	49.77	1.141	48.48
B8a	1.20	40.0	41.38	NA	39.37
B8b	1.20	40.0	41.38	1.193	39.65
B9a	1.20	45.0	45.32	1.195	44.56
B9b	1.20	45.0	45.32	1.197	44.35
B10a	1.25	40.0	40.53	1.243	39.56
B10b	1.25	40.0	40.53	1.238	39.04

continued...

Table 5.4 (continued).

Test	Target ρ_c (Mg/m^3)	Target w (%)	Measured Initial w (%)	Measured Final ρ_c (Mg/m^3)	Measured Final w (%)
B11a	1.30	35.0	35.90	1.287	34.98
B11b	1.30	35.0	35.90	1.288	35.16
B12a	1.30	40.0	40.67	NA	NA
B12b	1.30	40.0	40.67	NA	NA
B12c	1.30	40.0	40.75	NA	NA
B12d	1.30	40.0	40.75	1.286	39.72
B13a	1.35	35.0	36.09	1.338	35.07
B13b	1.35	35.0	36.09	1.338	35.21
B14a	1.40	30.0	30.16	1.393	29.97
B14b	1.40	30.0	30.16	1.392	29.94
B15a	1.40	35.0	35.90	1.387	35.13
B15b	1.40	35.0	35.90	1.388	35.23
B16a	1.45	30.0	30.23	1.441	30.08
B16b	1.45	30.0	30.23	1.440	30.13

value ($\Delta w = 1.24 \pm 0.21\%$; that is, 1.03 to 1.45%). As with the previous series of tests, there was no visibly observable damage to the clay fabric caused by the passage of gas in any of these tests.

The target ρ_c and initial w were chosen for use in Table 5.6, which also shows the S_r, p_b and t_b values for each test. The calculated S_r is >100% for six of the tests, which is physically impossible. The actual S_r for these tests was probably ≈100%, as the excess water would have been forced out of the clay during preparation of the plugs. This may explain, at least in part, why the average final w value is less than the initial value.

Table 5.5 Final water contents of clay samples (%) for series B.

Test	Gas Inlet (Periphery)	Gas Inlet (Centre)	Gas Inlet (Mean)	Gas Outlet (Periphery)	Gas Outlet (Centre)	Gas Outlet (Mean)	Difference*
B1a	58.48	58.46	58.47	58.35	58.73	58.54	-0.07
B1b	59.00	59.27	59.14	58.63	58.79	58.71	0.43
B1c	57.49	57.85	57.67	57.26	57.59	57.42	0.25
B2a	52.99	52.81	52.90	52.30	52.41	52.36	0.54
B2b	52.58	51.78	52.18	53.11	52.98	53.04	-0.86
B2c	52.80	52.72	52.76	52.93	52.97	52.95	-0.19
B3a	59.00	58.76	58.88	58.54	58.39	58.46	0.42
B3b	58.64	59.00	58.82	58.86	58.81	58.84	-0.02
B3c	58.17	58.59	58.38	58.45	58.36	58.40	-0.02
B4a	52.52	52.73	52.62	53.05	52.88	52.96	-0.34
B4b	52.49	52.43	52.46	52.60	52.44	52.52	-0.06
B4c	52.69	52.72	52.70	52.22	52.39	52.30	0.40
B5a	48.57	48.80	48.68	48.47	48.72	48.60	0.08
B5b	48.44	48.44	48.44	48.45	48.46	48.46	-0.02
B6a	NA	NA	NA	NA	NA	NA	NA
B6b	44.02	43.91	43.96	43.92	44.21	44.06	-0.10
B7a	49.08	48.98	49.03	47.82	47.51	47.66	1.37
B7b	49.10	49.11	49.10	47.98	47.75	47.86	1.24
B8a	39.39	39.50	39.44	39.06	39.53	39.30	0.14
B8b	39.93	39.92	39.92	39.26	39.49	39.38	0.54
B9a	44.61	44.71	44.66	44.34	44.58	44.46	0.20
B9b	NA	NA	NA	NA	NA	NA	NA
B10a	39.68	39.86	39.77	39.21	39.47	39.34	0.43
B10b	38.59	39.03	38.81	39.18	39.35	39.26	0.45
B11a	34.67	35.04	34.86	35.16	35.04	35.10	-0.24
B11b	35.30	35.37	35.34	NA	NA	34.81	0.53
B12a	NA	NA	NA	NA	NA	NA	NA
B12b	NA	NA	NA	NA	NA	NA	NA
B12c	NA	NA	NA	NA	NA	NA	NA
B12d	39.90	39.91	39.90	39.69	39.40	39.54	0.36
B13a	NA	NA	NA	NA	NA	NA	NA
B13b	34.81	34.90	34.86	34.87	36.25	35.56	-0.70

*Difference = Gas Inlet (Mean) - Gas Outlet (Mean)

Table 5.6 Summary of experimental results for series B.

Test	Target ρ_c (Mg/m^3)	Initial w (%)	Initial S_r (%)	p_b (MPa)	t_b (h)
B1a	0.95	60.29	88.37	0.2	0.04
B1b	0.95	60.36	88.47	0.2	0.04
B1c	0.95	60.36	88.47	0.2	0.04
B2a	1.00	54.50	86.56	0.2	0.04
B2b	1.00	54.50	86.56	0.2	0.04
B2c	1.00	54.56	86.65	0.2	0.04
B3a	1.00	60.26	95.71	0.4	0.1
B3b	1.00	60.26	95.71	0.2	0.04[a]
B3c	1.00	60.29	95.75	0.4	0.1
B4a	1.05	54.01	92.80	0.6	0.2
B4b	1.05	54.01	92.80	0.6	0.2
B4c	1.05	54.56	93.74	0.6	0.2
B5a	1.10	50.14	93.07	0.4	0.1[a]
B5b	1.10	50.14	93.07	0.2	0.04[a]
B6a	1.15	44.95	90.04	0.2	0.04[a]
B6b	1.15	44.95	90.04	1.4	0.5
B7a	1.15	49.77	99.70	>8.8	>3.6
B7b	1.15	49.77	99.70	>8.8	>3.6
B8a	1.20	41.38	89.38	0.2	0.04[a]
B8b	1.20	41.38	89.38	0.2	0.04[a]
B9a	1.20	45.32	97.89	1.4	0.5
B9b	1.20	45.32	97.89	1.4	0.5
B10a	1.25	40.53	94.34	2.2	0.9[a]
B10b	1.25	40.53	94.34	0.6	0.2[a]
B11a	1.30	35.90	90.01	0.2	0.04[a]
B11b	1.30	35.90	90.01	0.4	0.1[a]
B12a	1.30	40.67	101.97	>6.2	>2.5
B12b	1.30	40.67	101.97	5.6	2.3
B12c	1.30	40.75	102.17	5.0	2.0
B12d	1.30	40.75	102.17	6.2	2.5

continued...

Table 5.6 (continued).

Test	Target ρ_c (Mg/m^3)	Initial w (%)	Initial S_r (%)	p_b (MPa)	t_b (h)
B13a	1.35	36.09	97.44	3.0	1.2[a]
B13b	1.35	36.09	97.44	4.0	1.6
B14a	1.40	30.16	87.70	0.6	0.2[a]
B14b	1.40	30.16	87.70	0.4	0.1[a]
B15a	1.40	35.90	104.39	>8.4	>3.5
B15b	1.40	35.90	104.39	>8.4	>3.5
B16a	1.45	30.23	94.68	2.4	1.0[a]
B16b	1.45	30.23	94.68	2.2	0.9[a]

[a]Start of slow breakthrough.

Another possible explanation for the final w being less than the initial value is that, before plug preparation, some of those specimens with a calculated S_r <100% may have contained more water than required for specimen saturation after compaction. This could happen if the assumed value for ρ_s or ρ_w, or both, is in error. If ρ_s is less than the assumed 2.70 Mg/m^3, a given M_s would occupy more volume than expected and, therefore, V_v would be reduced. If the ρ_w of bound water is less than the assumed 1.00 Mg/m^3, the volume occupied by a given M_w would be greater than anticipated. Depending on the calculated value of S_r, and the magnitude of the error in ρ_s or ρ_w, either scenario could have caused V_w to exceed V_v. If excess water was present, it would have been squeezed out of the clay during compaction and the final w would have been less than the initial value.

As with series A, both slow and rapid gas breakthrough was observed. Figure 5.1 is an example of the results of a test with rapid breakthrough. In this test p_b = 6.2 MPa at t_b = 2.5 h. However, breakthrough is not always so clearly defined. Figure 5.2 is an example of a test in which an initially slow breakthrough is followed by rapid breakthrough. Using the definition of breakthrough given earlier in this section, and studying the data, it was determined that p_b = 0.6 MPa at t_b = 0.2 h. Note that slow breakthrough is not always followed by rapid breakthrough. As well, the distinction between slow and rapid breakthrough is not always as clear as in these two examples, so discretion is needed in classifying the tests.

There is no trend apparent in the specimens that exhibited slow breakthrough. Slow breakthrough occurred in specimens with ρ_c from 1.00 to 1.45 Mg/m^3 and with a S_r between 77 and 97%. In some cases two different rates of breakthrough can be seen for tests with identical ρ_c and S_r. The current understanding of gas breakthrough is insufficient to explain why different rates of breakthrough are observed.

5.2 Incremental Low-Pressure Wetted Tests

In collaboration with K.S. Gelmich Halayko (1998), low-pressure gas-breakthrough experiments were conducted on Avonlea bentonite that was wetted before compaction and further wetted in the cell after plug preparation. These tests, designated as series C, were conducted between ρ_c = 0.60 and 1.00 Mg/m^3. The duration of each 0.2 MPa pressure increment was five minutes. The objective of wetting the clay was to increase S_r to about

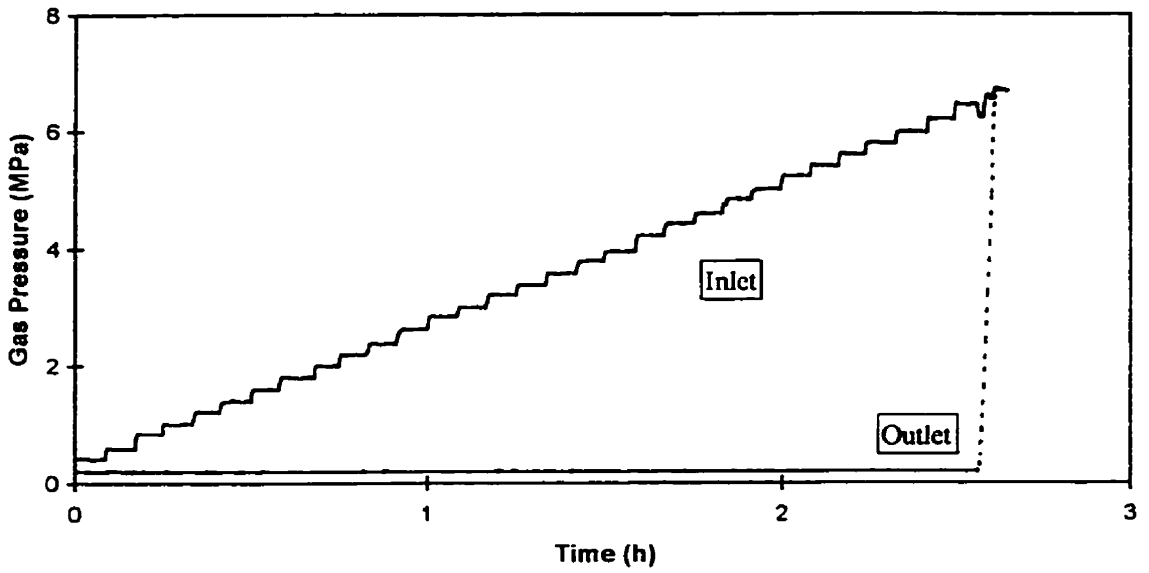

Figure 5.1 Example of an experiment with rapid breakthrough (test B12d).

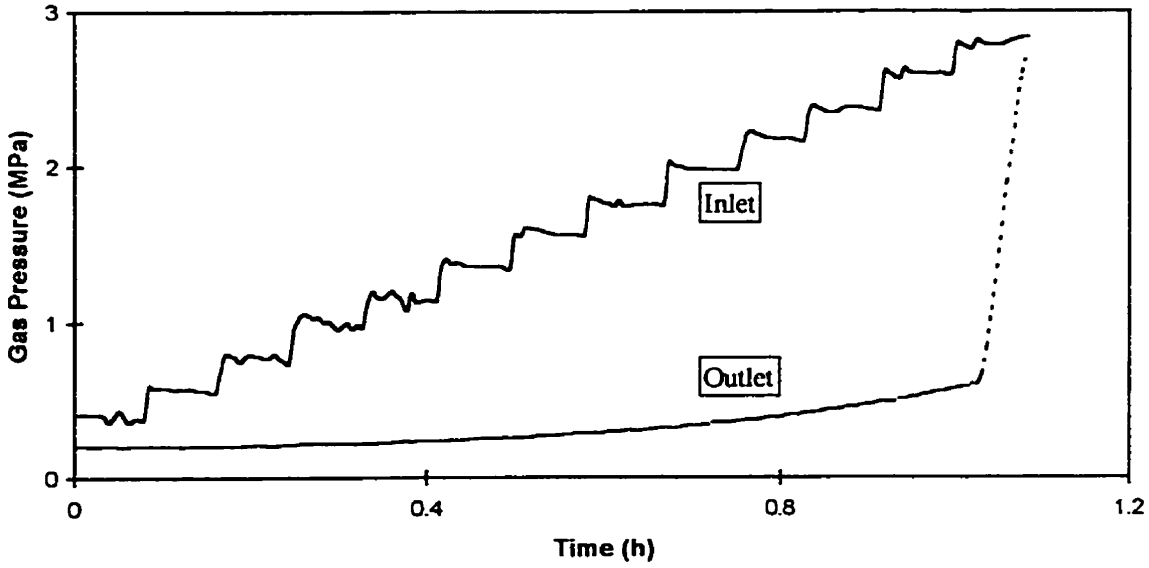

Figure 5.2 Example of an experiment with an initial slow breakthrough (test B10b).

100% but, as described below, this was probably not successful. Hence these tests are termed 'wetted' rather than 'saturated'.

As described in section 4.2.3.1, some authors have noted that the fabric of compacted clay depends, in part, on w at the time of compaction. To determine if the p_b of wetted clay plugs depends on the preparation w, tests were conducted on specimens with different initial w. Regardless of the initial w, each specimen had access to an unlimited supply of water before the gas-breakthrough phase of the test was performed.

Table 5.7 shows the target, initial and final values of w and ρ_c. The final ρ_c of the specimens is 0.024 ± 0.006 Mg/m^3 less than the calculated initial value. Again this is attributed to losses during handling; therefore the calculated initial ρ_c value is probably the more accurate of the two. The p_b results from all specimens are listed in Table 5.8 along with the w, ρ_c, S_r and t_b of the specimens.

5.3 Incremental High-Pressure Wetted Tests

Three series of incremental high-pressure tests were conducted: D, E and F. Air-dry clay was compacted into the cell in series D and E, whereas the clay was wetted before compaction in series F. A different in-cell wetting procedure (which will be described along with the results of each series of experiments) was used for each series of incremental high-pressure wetted tests, and different p_b results were obtained for plugs of comparable ρ_c. This is probably due to the specimens having varying S_r, at the time of

Table 5.7 Target, initial and final w and ρ_c for series C.

Test	Target Initial w (%)	Target ρ_c (Mg/m^3)	Measured Initial w (%)	Calculated Initial ρ_c (Mg/m^3)	Measured Final w (%)	Measured Final ρ_c (Mg/m^3)
C1	50	0.60	46.89	0.613	111.92	0.572
C2	55	0.60	54.60	0.602	114.23	0.573
C3	60	0.65	58.15	0.658	108.23	0.621
C4	50	0.70	48.34	0.708	93.07	0.681
C5	55	0.70	54.28	0.703	96.10	0.661
C6	60	0.70	60.19	0.699	98.25	0.665
C7	60	0.75	58.15	0.759	87.08	0.749
C8	50	0.80	48.34	0.809	78.56	0.785
C9	55	0.80	54.39	0.803	78.90	0.781
C10	60	0.80	63.49	0.783	76.73	0.767
C11	55	0.90	53.69	0.908	68.68	0.896
C12	60	0.90	63.44	0.881	70.22	0.865
C13	45	0.95	40.27	0.982	59.44	0.953
C14	50	1.00	49.50	1.003	59.40	0.991
C15	55	1.00	54.39	1.004	60.36	0.988
C16	60	1.00	63.49	0.979	61.54	0.961

testing, as discussed in section 4.2.3.2. However, the use of wetted clay in series F, versus air-dry clay in series D and E, may have contributed to the difference between results. The tests are grouped based on the wetting procedure used. In all tests, the pressure was incremented 1.0 MPa every five minutes.

Table 5.8 Summary of experimental results for series C.

Test	Measured Initial w (%)	Calculated Initial ρ_c (Mg/m^3)	Measured Final w (%)	Final S_r (%)	p_b (MPa)	t_b (h)
C1	46.89	0.613	111.92	88.75	0.2	0.04
C2	54.60	0.602	114.23	88.50	1.0	0.4
C3	58.15	0.658	108.23	94.16	0.4	0.1
C4	48.34	0.708	93.07	89.31	>8.8	>3.6
C5	54.28	0.703	96.10	91.34	1.0	0.4
C6	60.19	0.699	98.25	92.67	0.6	0.2
C7	58.15	0.759	87.08	91.93	0.6	0.2
C8	48.34	0.809	78.56	90.75	>8.8	>3.6
C9	54.39	0.803	78.90	90.17	2.4	1.0
C10	63.49	0.783	76.73	84.62	>9.0	>3.7
C11	53.69	0.908	68.68	93.95	0.4	0.1
C12	63.44	0.881	70.22	91.83	>7.0	>2.9
C13	40.27	0.982	59.44	91.73	>8.6	>3.5
C14	49.50	1.003	59.40	94.80	>8.6	>3.5
C15	54.39	1.004	60.36	96.48	>8.6	>3.5
C16	63.49	0.979	61.54	94.52	>9.2	>3.8

The first high-pressure specimens (series D) were prepared using air-dry clay and the plugs were wetted at a pressure of 0.2 MPa for 2 d after compaction. Table 5.9 shows the specimen parameters and the experimental results. The measured final w value for each test is the mean of the four results in Table 5.10. The measured final ρ_c is again less than the target value ($\Delta\rho_c = 0.020 \pm 0.006$ Mg/m^3); the target value has been used along with the measured final w in the calculation of the final S_r.

Table 5.9 Summary of experimental results for series D.

Test	Target ρ_c (Mg/m^3)	Measured Initial w (%)	Measured Final w (%)	Measured Final ρ_c (Mg/m^3)	Calculated Final S_r (%)	p_b (MPa)	t_b (h)
D1	0.90	11.64	66.74	0.898	90.10	0.8	0.04
D2a	1.00	10.29	49.58	0.963	78.74	>44.8	>3.7
D2b	1.00	10.25	53.02	0.980	84.21	1.8	0.1[a]
D2c	1.00	10.16	54.18	0.976	86.05	0.8	0.04
D2d	1.00	10.39	54.97	0.992	87.31	>29.8	>2.4
D2e	1.00	10.38	60.95	0.981	96.80	0.8	0.04
D3a	1.05	10.20	48.56	1.041	83.43	39.8	3.3
D3b	1.05	10.96	49.15	1.031	84.45	25.8	2.1
D3c	1.05	10.26	51.68	1.024	88.80	2.8	0.2[a]
D3d	1.05	10.77	52.92	1.023	90.93	1.8	0.1[a]
D3e	1.05	10.91	53.72	1.031	92.30	0.8	0.04
D4a	1.10	11.08	40.30	1.113	74.81	>46.8	>3.9
D4b	1.10	11.25	43.84	1.077	81.38	43.8	3.6
D4c	1.10	10.96	46.47	1.078	86.26	29.8	2.5
D4d	1.10	10.24	49.88	1.074	92.59	1.8	0.1
D4e	1.10	10.66	50.10	1.057	92.98	20.8	1.7
D5a	1.15	10.70	45.96	1.118	92.07	31.8	2.6
D5b	1.15	10.75	NA	NA	NA	34.8	2.9
D5c	1.15	11.10	NA	NA	NA	38.8	3.2
D5d	1.15	10.86	NA	NA	NA	28.8	2.4
D5e	1.15	10.82	NA	NA	NA	44.8	3.7
D6	1.20	11.64	43.73	1.175	94.46	>51.8	>4.3
D7	1.30	11.53	39.13	1.285	98.10	>50.8	>4.2
D8	1.40	11.00	35.22	1.374	102.41	>51.8	>4.3
D9	1.50	NA	NA	NA	NA	>51.8	>4.3

[a]Start of slow breakthrough.

Table 5.10 Final water contents of clay samples (%) for series D.

Test	Gas Inlet (Periphery)	Gas Inlet (Centre)	Gas Inlet (Mean)	Gas Outlet (Periphery)	Gas Outlet (Centre)	Gas Outlet (Mean)	Difference[a]
D1	71.36	62.89	67.12	70.86	61.84	66.35	0.77
D2a	58.42	56.78	57.60	41.44	41.67	41.56	16.04
D2b	54.93	53.29	54.11	52.87	50.97	51.92	2.19
D2c	56.70	53.68	55.19	55.92	50.43	53.18	2.01
D2d	62.28	63.68	62.98	47.99	45.93	46.96	16.02
D2e	62.30	62.59	62.44	60.42	58.48	59.45	2.99
D3a	58.21	46.93	52.57	46.93	42.15	44.54	8.03
D3b	53.40	53.24	53.32	44.64	45.31	44.98	8.34
D3c	53.32	51.88	52.60	50.49	51.02	50.76	1.84
D3d	54.01	53.07	53.54	51.31	53.31	52.31	1.23
D3e	53.04	56.74	54.89	52.49	52.61	52.55	2.34
D4a	47.00	47.81	47.40	34.01	32.37	33.19	14.21
D4b	49.47	49.32	49.40	38.45	38.12	38.28	11.12
D4c	50.61	50.40	50.50	42.17	42.71	42.44	8.06
D4d	49.96	50.58	50.27	50.67	48.31	49.49	0.78
D4e	53.24	52.87	53.06	46.69	47.58	47.14	5.92
D5a	49.72	46.72	48.22	43.99	43.40	43.70	4.52
D6	48.34	47.94	48.14	39.97	38.66	39.32	8.82
D7	42.39	42.38	42.38	36.33	35.41	35.87	6.51
D8	36.71	37.78	37.24	33.30	33.07	33.18	4.06

[a]Difference = Gas Inlet (Mean) - Gas Outlet (Mean)

As discussed in the introduction, dissolved contaminants can move through compacted clays by diffusion. Four plugs (D5b to D5e) were used for diffusion experiments after being ruptured with gas. Hence no final w, ρ_c or S_r values are available for these tests. The diffusion experiments are described in Appendix II.

The reproducibility of the p_b results obtained in the series D tests at $\rho_c \leq 1.10$ Mg/m^3 is poor. For example, at 1.00 Mg/m^3 p_b ranges from 0.8 MPa (the first pressure increment) to >44.8 MPa. To determine why the results were so inconsistent, the tests listed in Table 4.1 were conducted. The conclusion of the tests is that wetting Avonlea bentonite plugs at 0.2 MPa for 2 d does not saturate them. Therefore, small differences in the duration of wetting could affect S_r.

Like series D, the next specimens (series E) were prepared with air-dry clay. Much of the air was then removed from the cell by applying a vacuum, and the plugs were wetted for 2 d at 1.0 MPa. The specimen parameters and test results for series E are in Tables 5.11 and 5.12. The final S_r was calculated from the target ρ_c and final w numbers. The same wetting procedure was used on specimen E6c as used on those specimens which were tested for gas breakthrough, but the plug was extruded, sliced and dried without being tested. This was done to better understand the w results of the specimens on which gas-breakthrough testing was conducted.

The series F tests differed from series D and E in that the clay was wetted before compaction; it was then further wetted towards saturation in the cell for 2 d at 5.0 MPa. Because consistent breakthrough was not obtained in series E at any ρ_c, the ρ_c range for series F was expanded to include 0.60 Mg/m^3 specimens. Tests were conducted on specimens between ρ_c = 0.80 and 1.20 Mg/m^3, even though reproducible breakthrough had not been achieved in series E at $\rho_c \geq 0.70$ Mg/m^3, because the wetting procedure was different in series F. The 0.80 and 1.00 Mg/m^3 tests included specimens with two different

Table 5.11 Summary of experimental results for series E.

Test	Target ρ_c (Mg/m^3)	Measured Initial w (%)	Measured Final w (%)	Measured Final ρ_c (Mg/m^3)	Calculated Final S_r (%)	p_b (MPa)	t_b (h)
E1a	0.70	9.76	88.84	0.679	83.95	>53.8	>4.5
E1b	0.70	9.66	89.41	0.676	84.49	>53.8	>4.5
E2a	0.75	9.66	82.53	0.727	85.70	>52.8	>4.4
E2b	0.75	9.74	82.81	0.728	86.00	>53.8	>4.5
E3a	0.80	10.07	75.87	0.778	86.25	42.8	3.5
E3b	0.80	9.56	76.25	0.780	86.68	>53.8	>4.5
E3c	0.80	10.09	77.24	0.783	87.81	>52.8	>4.4
E4a	0.85	10.32	70.62	0.833	87.61	>53.8	>4.5
E4b	0.85	10.29	72.72	0.810	90.21	>53.8	>4.5
E4c	0.85	10.20	73.57	0.829	91.27	33.8	2.8
E4d	0.85	10.18	73.91	0.830	91.69	>53.8	>4.5
E5a	0.90	10.25	64.78	0.878	87.45	>53.8	>4.5
E5b	0.90	10.09	65.35	0.880	88.22	>52.8	>4.4
E5c	0.90	10.13	65.49	0.878	88.41	>51.8	>4.3
E5d	0.90	10.19	68.28	0.878	92.13	38.8	3.2
E6a	1.00	9.64	58.81	0.972	93.40	>47.8	>4.0
E6b	1.00	9.83	61.38	0.971	97.49	>47.8	>4.0
E6c[a]	1.00	9.52	65.18	0.988	103.52	NA	NA

[a]Gas-breakthrough testing not performed on specimen.

initial w values to determine if this affected p_b. The results of this series of tests are in Tables 5.13 and 5.14. The degree of saturation was calculated using the target ρ_c and final w. Controls, on which gas-breakthrough tests were not conducted, were prepared for each combination of ρ_c and initial w to help interpret the final w data.

Table 5.12 Final water contents of clay samples (%) for series E.

Test	Gas Inlet (Periphery)	Gas Inlet (Centre)	Gas Inlet (Mean)	Gas Outlet (Periphery)	Gas Outlet (Centre)	Gas Outlet (Mean)	Difference[a]
E1a	123.29	101.95	112.62	71.38	58.73	65.06	47.56
E1b	116.13	106.52	111.32	74.59	60.41	67.50	43.82
E2a	110.41	92.08	101.24	69.08	58.54	63.81	37.43
E2b	109.60	94.16	101.88	68.85	58.64	63.74	38.14
E3a	97.73	84.08	90.90	65.90	55.78	60.84	30.06
E3b	102.47	84.34	93.40	64.94	53.25	59.10	34.30
E3c	101.25	90.50	95.88	61.86	55.36	58.61	37.27
E4a	92.82	78.89	85.86	60.23	50.54	55.38	30.48
E4b	95.71	84.32	90.02	59.22	51.64	55.43	34.59
E4c	92.02	79.62	85.82	66.96	55.68	61.32	24.50
E4d	95.38	82.33	88.86	64.10	53.85	58.98	29.88
E5a	82.74	69.29	76.02	58.29	48.78	53.54	22.48
E5b	86.86	68.21	77.54	58.04	48.29	53.16	24.38
E5c	85.13	70.37	77.75	58.55	47.93	53.24	24.51
E5d	87.65	70.62	79.14	63.93	50.91	57.42	21.72
E6a	74.53	70.12	72.32	52.23	48.66	50.44	21.88
E6b	68.29	63.54	65.92	53.76	49.65	51.70	14.22
E6c[b]	69.83	59.23	64.53	70.79	60.86	65.82	-1.29

[a]Difference = Gas Inlet (Mean) - Gas Outlet (Mean)
[b]Gas-breakthrough testing not performed on specimen.

Table 5.13 Summary of experimental results for series F.

Test	Target ρ_c (Mg/m^3)	Measured Initial w (%)	Measured Final w (%)	Measured Final ρ_c (Mg/m^3)	Calculated Final S_r (%)	p_b (MPa)	t_b (h)
F1a	0.60	81.38	120.12	0.563	92.66	11.8	1.0[a]
F1b	0.60	83.80	122.47	0.577	94.48	1.8	0.1[a]
F1c[b]	0.60	82.58	125.28	0.582	96.64	NA	NA
F2a	0.80	56.93	78.17	0.774	88.87	>51.8	>4.3
F2b	0.80	57.70	79.56	0.772	90.45	>50.8	>4.2
F2c[b]	0.80	57.48	88.76	0.782	100.91	NA	NA
F3a	0.80	84.81	76.37	0.783	86.82	>49.8	>4.1
F3b	0.80	85.91	79.68	0.772	90.58	>49.8	>4.1
F3c[b]	0.80	87.20	89.78	0.785	102.07	NA	NA
F4a	1.00	43.74	56.09	0.971	89.08	>51.8	>4.3
F4b	1.00	45.35	57.07	0.985	90.64	>52.8	>4.4
F4c[b]	1.00	44.99	64.56	0.987	102.54	NA	NA
F5a	1.00	56.69	58.49	0.972	92.90	>51.8	>4.3
F5b	1.00	57.21	60.82	0.975	96.60	>51.8	>4.3
F5c[b]	1.00	58.03	65.75	0.982	104.43	NA	NA
F6a	1.20	44.89	44.29	1.184	95.67	>51.8	>4.3
F6b	1.20	45.42	44.86	1.171	96.90	>52.8	>4.4
F6c[b]	1.20	44.60	49.05	1.185	105.95	NA	NA

[a]Start of slow breakthrough.
[b]Gas-breakthrough testing not performed on specimen.

Table 5.14 Final water contents of clay samples (%) for series F.

Test	Gas Inlet (Periphery)	Gas Inlet (Centre)	Gas Inlet (Mean)	Gas Outlet (Periphery)	Gas Outlet (Centre)	Gas Outlet (Mean)	Difference[a]
F1a	130.54	117.83	124.18	127.22	104.87	116.04	8.14
F1b	125.92	112.84	119.38	131.13	119.98	125.56	-6.18
F1c[b]	124.53	116.87	120.70	138.52	121.22	129.87	-9.17
F2a	93.94	90.28	92.11	64.01	64.46	64.24	27.87
F2b	95.05	89.55	92.30	67.84	65.79	66.82	25.48
F2c[b]	90.74	84.31	87.52	91.72	88.28	90.00	-2.48
F3a	90.38	89.32	89.85	63.83	61.97	62.90	26.95
F3b	92.10	91.13	91.62	68.62	66.85	67.74	23.88
F3c[b]	89.24	87.94	88.59	92.67	89.27	90.97	-2.38
F4a	67.50	60.69	64.10	50.19	45.96	48.08	16.02
F4b	68.70	61.64	65.17	52.38	45.55	48.96	16.21
F4c[b]	66.94	59.58	63.26	69.08	62.63	65.86	-2.60
F5a	70.03	67.39	68.71	49.24	47.28	48.26	20.45
F5b	69.20	69.04	69.12	53.31	51.74	52.52	16.60
F5c[b]	66.19	63.63	64.91	68.43	64.75	66.59	-1.68
F6a	49.80	49.32	49.56	40.24	37.78	39.01	10.55
F6b	49.50	49.32	49.41	40.89	39.73	40.31	9.10
F6c[b]	49.45	48.10	48.78	50.14	48.52	49.33	-0.55

[a]Difference = Gas Inlet (Mean) - Gas Outlet (Mean)
[b]Gas-breakthrough testing not performed on specimen.

5.4 Constant High-Pressure Wetted Tests

These experiments (series G) differed from all the other sets of tests in that they were conducted at constant pressure and t_b was measured. The pressure at breakthrough in these tests (p_c) is defined like p_b,

$$p_c = p_i - p_o \,. \qquad [81]$$

The differentiation between p_b and p_c is to signify that p_c is not necessarily the lowest

pressure at which gas breakthrough can be obtained. As in series F, in series G the clay was wetted before compaction into the high-pressure cell, and the plug was further wetted towards saturation in the cell for 2 d at 5.0 MPa. Experiments were run between ρ_c = 0.80 and 1.40 Mg/m^3 at p_c from 0.3 to 19.8 MPa. A typical test result is shown in Figure 5.3 and the data are presented in Table 5.15. The value of S_r was obtained from the target ρ_c and measured final w results. Gas breakthrough was obtained in all of the specimens that were tested, regardless of ρ_c or p_c.

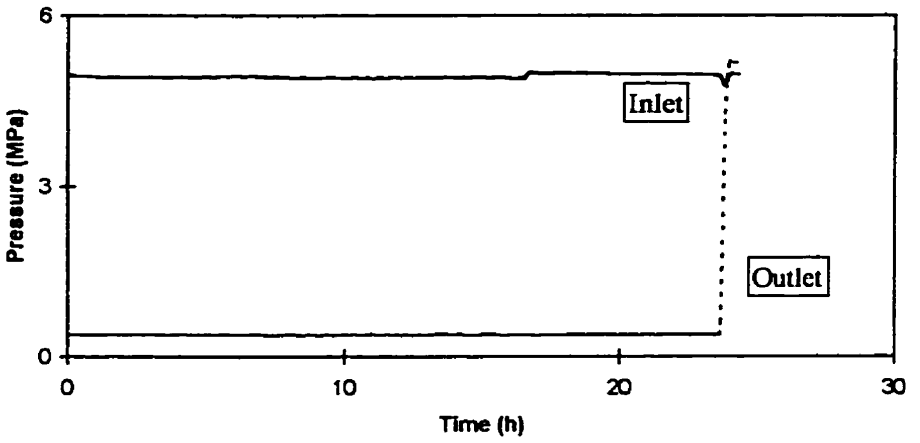

Figure 5.3 Example of the result of a constant-pressure experiment (test G10).

After each test, the clay plug was cut into several slices, perpendicular to the direction of gas movement, and the slices dried to determine the w of each. The ρ_c of each slice is calculated from [12]. The volume of each slice is then determined from [77], assuming w = 0 after drying, and the length of the slice calculated from the volume and surface area. The plug length is obtained by summing the slice lengths. The relative location of the slice

Table 5.15 Summary of experimental results for series G.

Test	Target ρ_c (Mg/m^3)	Measured Initial w (%)	Measured Final w (%)	Measured Final ρ_c (Mg/m^3)	Calculated Final S_r (%)	p_c (MPa)	t_b (h)
G1a	0.80	85.34	75.14	0.776	85.42	4.8	14.0
G1b	0.80	81.59	78.17	0.771	88.87	4.8	10.0
G2a	0.80	84.51	74.09	0.767	84.23	9.8	6.0
G2b	0.80	86.37	80.94	0.768	92.02	9.8	7.8
G2c	0.80	84.25	82.25	0.766	93.51	9.8	5.3
G3	1.00	59.71	63.93	0.988	101.54	0.3	120.5
G4	1.00	59.38	63.41	0.985	100.71	0.8	41.8
G5	1.00	59.28	63.71	0.977	101.19	1.8	16.7
G6	1.00	57.30	63.79	0.978	101.31	2.8	9.2
G7a	1.00	42.29	57.86	0.972	91.90	4.8	9.5
G7b	1.00	60.06	60.56	0.979	96.18	4.8	11.5
G7c	1.00	60.00	67.54	0.878	107.27	4.8	14.5
G8a	1.00	58.57	51.44	0.972	81.70	9.8	10.2
G8b	1.00	58.90	57.05	0.981	90.61	9.8	11.7
G9	1.00	58.50	57.64	0.970	91.55	19.8	12.3
G10	1.20	42.99	47.00	1.181	101.52	4.8	23.7
G11a	1.20	44.51	46.21	1.173	99.81	9.8	12.8
G11b	1.20	44.76	47.06	1.182	101.65	9.8	10.7
G12	1.20	44.43	45.98	1.190	99.32	NA	NA
G13a	1.40	30.29	35.78	1.379	104.04	4.8	58.7
G14a	1.40	29.75	35.01	1.374	101.80	9.8	25.7
G14b	1.40	30.53	37.28	1.365	108.40	9.8	30.7

in the plug is then calculated as the mid-point of the slice, measured from the gas inlet surface, divided by the total plug length.

Some representative plots of ρ_c against relative position will be presented. It is difficult to interpret the results because of the limited data, particularly controls that were not tested

for breakthrough, and therefore this will not be attempted. Many of the plots could be placed in one of three categories. Upward-opening curves, such as shown in Figure 5.4 for test G2a, were obtained. Linear results were also common, such as was obtained for test G7c (Figure 5.5). Lastly, the dry-density profile of several plugs that were tested for gas breakthrough generated a downward-opening curve similar to that of specimen G3 (Figure 5.6). A few of the plots were unlike any of those shown here. Specimen G12 was the only plug sliced without being tested for breakthrough. The resulting plot (Figure 5.7) resembles the one shown in Figure 5.6. This method of plotting w provides more information than is obtained by slicing the plug in two, and dividing each slice into centre and peripheral pieces.

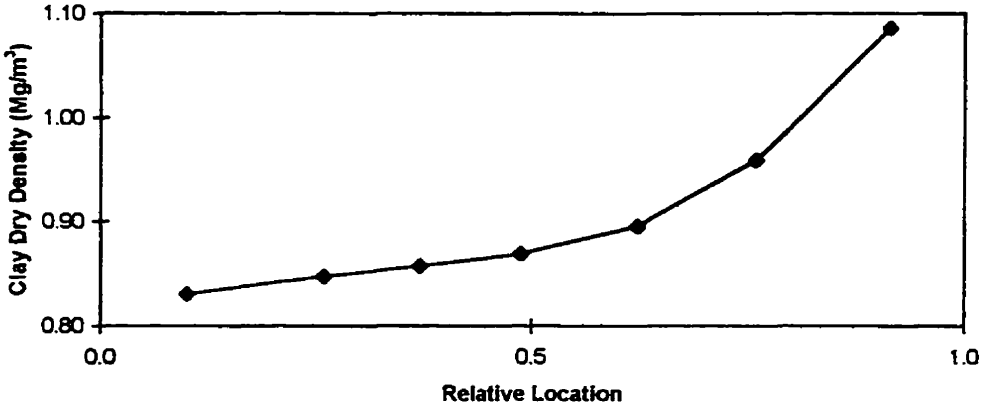

Figure 5.4 Dry density profile for specimen from test G2a.

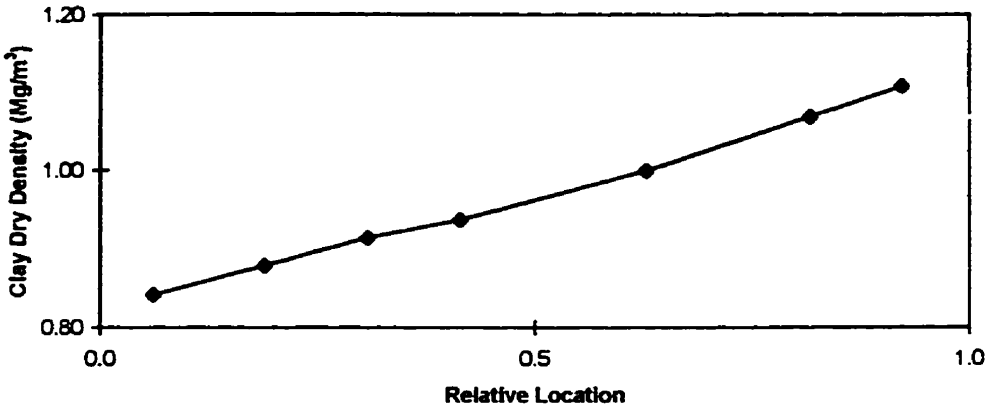

Figure 5.5 Dry density profile for specimen from test G7c.

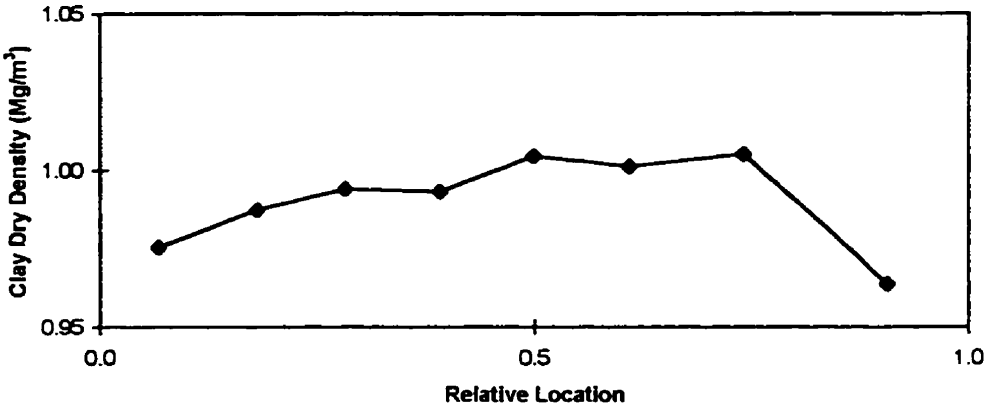

Figure 5.6 Dry density profile for specimen from test G3.

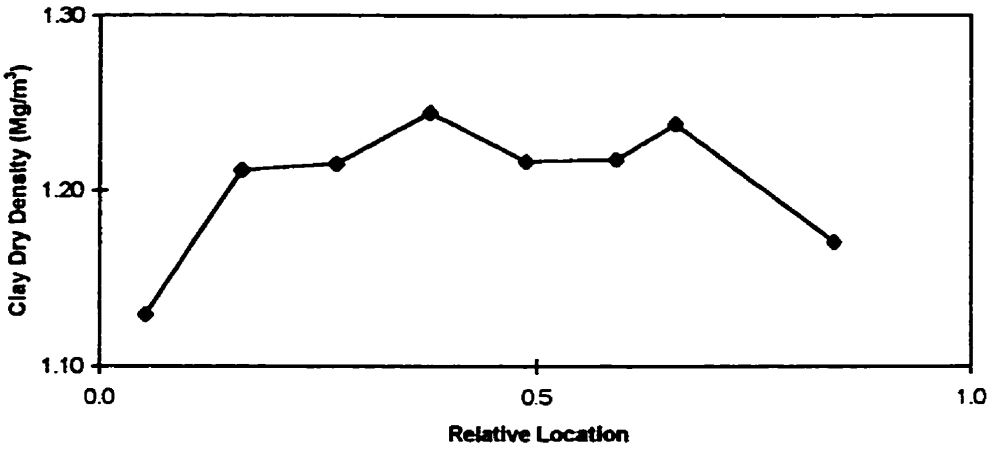

Figure 5.7 Dry density profile for specimen from test G12.

6. DISCUSSION OF GAS-BREAKTHROUGH EXPERIMENTS

6.1 Incremental Low-Pressure Unsaturated Tests[1]

For series A, there is no statistically significant difference between the w results of the peripheral and centre samples on either the inlet ($\Delta w = 0.51 \pm 0.52\%$; that is, -0.01 to 1.03%) or outlet sides ($\Delta w = 0.53 \pm 0.56\%$). Therefore, the mean inlet and outlet w are calculated in Table 5.2. The mean w of the inlet disc is greater than that of the outlet disc ($\Delta w = 1.34 \pm 0.89\%$). Further analysis shows that there is no significant difference if either those specimens with $p_b = 0.2$ MPa or those with $0.4 \leq p_b < 1.0$ MPa are considered. However, for those with $p_b \geq 1.0$ MPa, the difference is $3.13 \pm 1.87\%$. This suggests that the difference in w may be related to p_b, but the correlation of a plot of the two parameters is poor (coefficient of determination (R^2) value of 0.37).

The difference in w across the clay plug cannot easily be attributed to the passage of gas. If the passage of gas is the primary mechanism for water movement, the outlet side of the clay plug should have a higher w than the inlet side. However, the experimental observation is the opposite – the inlet side of the clay plug has a higher w than the outlet side. It is possible that some water is transported by the gas, but a second process must

[1] This section contains information published in Hume et al. (1997).

dominate to produce the observed results.

The observed difference in w across the clay plugs with a $p_b \geq 1.0$ MPa may be explained by the effective stress concept [17]. On the inlet surface of the clay plug, $\sigma = u = p_i$. Therefore the effective stress on the inlet surface (σ'_{in}) is

$$\sigma'_{in} = p_i - p_i = 0 . \qquad [82]$$

Since the areas of both ends of the clay plug are the same, for static equilibrium of the specimen (neglecting the shear force between the specimen and the sleeve) the total stress on the outlet surface must be the same as on the inlet surface (p_i). The value of u at the outlet end is equal to the outlet gas pressure (p_o), and thus the effective stress at the outlet (σ'_{out}) is

$$\sigma'_{out} = p_i - p_o . \qquad [83]$$

Therefore, σ' on the outlet surface is greater than that on the inlet surface by an amount

$$\sigma'_{out} - \sigma'_{in} = (p_i - p_o) - 0 = p_i - p_o = p_b \qquad [84]$$

at the time of breakthrough.

From the concept of effective stress, changes in σ' produce volume strains in clays. Since compression and expansion require water transfer, the low hydraulic conductivities of clays makes these changes time dependent. Since $\sigma' = 0$ at the bottom of the plug (the inlet end) throughout the test, expansion of the specimen is possible in this region. With increased effective stress the outlet side of the specimen will tend to compress, and this tendency will increase with increasing p_b. The combination of compression at the top and

a constant specimen volume means that the bottom of the specimen is able to increase in volume and its water content can rise.

These particular specimens were unsaturated at the start of each test. The compression associated with σ' on the outlet side would cause ρ_c to increase and S_r to approach 100%. As S_r cannot exceed 100%, water would have been forced out of this region of the plug. The water did not move upwards and out of the clay, as this would have resulted in a net loss of water from the plug that was not observed (section 5.1). Therefore, the water forced from the outlet side of the specimen must have moved towards the gas inlet side. As the volume of the plug would tend to decrease as compression occurred on the outlet side, there would be room within the cell for swelling of the specimen as water was forced towards the gas inlet side. (In sections 2.1.5 and 3.2 it was noted that bentonites have a large swelling potential.) Alternatively, as these tests were done on unsaturated specimens, the moving water could have displaced air from the specimen on the gas inlet side, without substantial swelling in this region. Either mechanism, or a combination of the two, could explain why the mean w at the end of the tests was greater on the inlet side than on the outlet side. It is not possible to choose between these two scenarios with the data currently available.

The movement of water from the gas-outlet to the gas-inlet side of the plug is against the gas-pressure gradient. As discussed in section 2.3, gas pressure is only one of several mechanisms for water flow in unsaturated soils. The inlet side is the bottom of the specimen, so water flow in this direction is energetically favoured from a gravitational

perspective. Capillary and osmotic forces also favour water flow into the newly created void spaces near the gas-inlet surface of the clay plug. Energy would be required to overcome the forces of capillarity and osmosis if the displaced water moved upwards and out of the specimen, as neither of these spontaneous processes function in bulk water. The results demonstrate that the combination of gravity, capillarity and osmosis are sufficient to overcome the gas-pressure gradient and control the direction of water movement in this series of experiments.

Table 5.3 shows that p_b for these tests ranges from 0.2 to >9 MPa. Breakthrough pressure increases with S_r provided S_r is above ≈85%, which may imply that this is the value above which there is no continuous air phase through the specimen. The trend of increasing p_b with increasing S_r is evident for the 1.01, 1.04 and 1.08 Mg/m^3 specimens. Test A23 appears to be anomalous and, if it is disregarded, the trend of increasing p_b with increasing S_r is also evident with the 1.11 Mg/m^3 specimens. The trend is not evident at 0.90 Mg/m^3 because all of the specimens have a S_r below the critical value of ≈85%. The data in Table 5.3 appear to show that p_b increases with ρ_c. However, it should be noted that the average S_r is 71% at 0.90 Mg/m^3, 85% at 1.01 Mg/m^3, 90% at 1.04 Mg/m^3 and >90% at 1.08, 1.11 and 1.17 Mg/m^3. From these data it is difficult to make any conclusions about the effect on p_b of ρ_c alone.

For series B, there is no significant difference between the w values of the peripheral and centre pieces on either the inlet ($\Delta w = -0.07 \pm 0.10\%$) or outlet sides ($\Delta w = -0.11 \pm 0.14\%$). This is the same result as in the previous set of experiments. As with series A,

the mean values of w were calculated and are presented in Table 5.5. For this set of experiments, there is no significant difference between the mean inlet and outlet w values ($\Delta w = 0.18 \pm 0.20\%$). If only those specimens with $p_b \geq 1.0$ MPa are considered, the difference in w is still not significant ($\Delta w = 0.40 \pm 0.67\%$). This result is the opposite of that obtained from the series A data. A possible explanation is that, due to the higher average ρ_c of series B compared with series A, the series B specimens exhibited greater resistance to compression at a given σ' (p_b).

Breakthrough pressures for series B range from 0.2 to >9 MPa, as shown in Table 5.6. In Figure 6.1 the averaged results are plotted as p_b against S_r, and Figure 6.2 shows the results with p_b on the z axis and w and ρ_c in the xy plane. It is apparent from the graphs that p_b begins to increase at a S_r value between 80 and 90%. As S_r approaches 100%, p_b increases rapidly. The 'peaks and valleys' appearance of Figure 6.2 is likely because of the limited number of data points; more data would probably produce a smooth surface.

In series B, in all cases where two sets of tests were conducted at one ρ_c, the tests with the higher S_r have the higher mean p_b. This is perhaps best illustrated by the 1.15 Mg/m^3 results where S_r increases from 90.0 to 99.7% and the average p_b increases from 0.8 to >8.8 MPa. This trend is also present in the 1.00, 1.20, 1.30 and 1.40 Mg/m^3 data. The same finding was made in series A.

Breakthrough pressure does not only depend on S_r. The results show that it also depends on ρ_c. For example, at 1.20 Mg/m^3 and $S_r = 97.9\%$, $p_b = 1.4$ MPa. At a higher ρ_c of 1.35

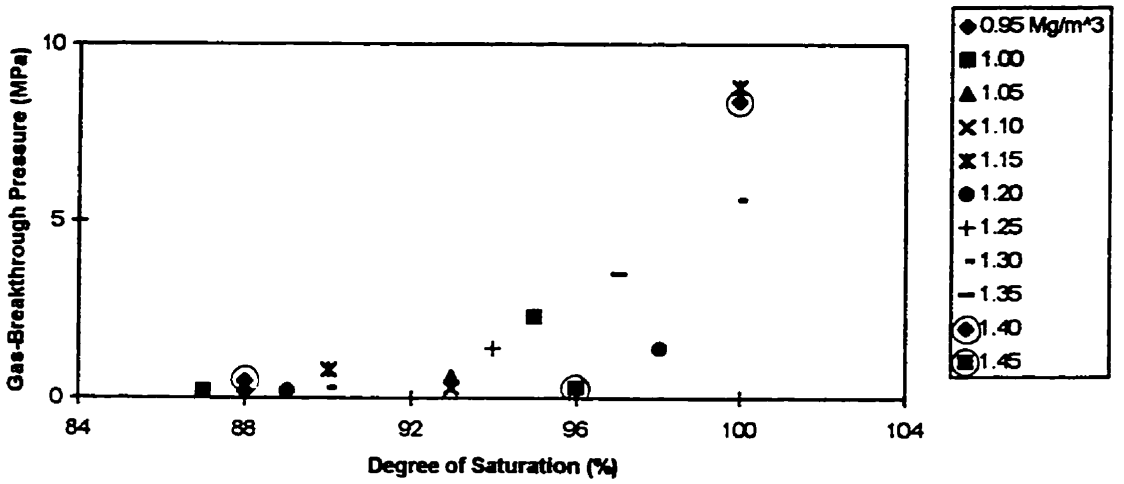

Figure 6.1 Gas-breakthrough pressure as a function of the degree of saturation.

Mg/m^3 and a lower S_r of 97.4%, p_b increases to 3.5 MPa. A similar trend (that is, increasing p_b with increasing ρ_c and decreasing S_r) can be observed in several places in Table 5.6.

The agreement between p_b from the two series of tests is good in most cases, as can be seen by comparing Tables 5.3 and 5.6. An exception is that the data from series B at 1.00 Mg/m^3 and $S_r = 95.7\%$ do not agree with the result of test A12 in Table 5.3. Given that triplicate tests were done in series B, versus only a single test in series A, the series B results are considered more reliable. The results from series B at 1.05, 1.10 and 1.15 Mg/m^3 compare well with the data from series A at 1.04, 1.11 and 1.17 Mg/m^3, at similar S_r.

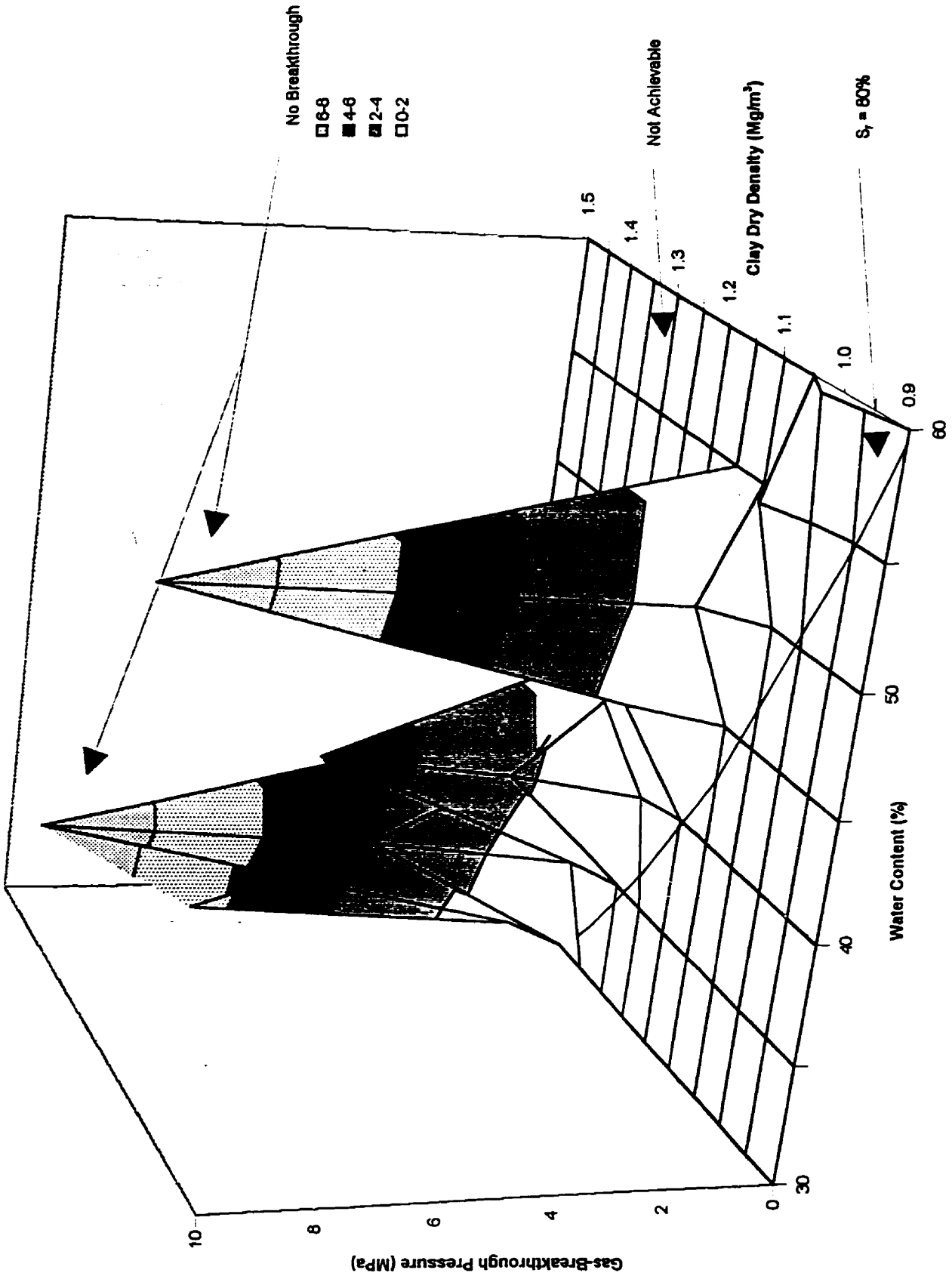

Figure 6.2 Gas breakthrough pressure as a function of clay dry density and water content. (The region beyond and to the right of the peaks is not achievable because it corresponds to a degree of saturation >100%).

6.2 Incremental Low-Pressure Wetted Tests

All of the experiments listed in Table 5.8 have a $S_r < 100\%$; the mean value is 91.59%. The bentonite plugs in this series of tests were wetted for 2 d at 0.2 MPa. Using the high-pressure apparatus, it was demonstrated that plugs wetted under these conditions are not saturated (Table 4.1). Given the similar designs of the low- and high-pressure apparatus, this result is likely applicable to the low-pressure equipment as well. Therefore, the low S_r values are attributed to the plugs being unsaturated before the gas-breakthrough phase of the tests began.

Gas breakthrough was obtained in all of the tests conducted on 0.60 and 0.65 Mg/m^3 specimens. No gas breakthrough occurred on plugs with $\rho_c = 0.95$ or 1.00 Mg/m^3. At intermediate densities, some tests had breakthrough while others did not.

The data in Table 5.8 do not show a relationship between w at the time of plug preparation and p_b. For the 0.6 and 0.9 Mg/m^3 plugs, p_b increases with increasing initial w, whereas the 0.7 Mg/m^3 specimens show the opposite trend. No trend is apparent in the 0.8 Mg/m^3 tests. The conclusion, albeit based on limited data, is that p_b does not depend on the initial w. As well, there is no correlation between p_b and the final S_r. At 0.7 and 0.9 Mg/m^3, p_b increases with decreasing S_r (which is the opposite of the result obtained in the tests conducted on unsaturated specimens) while no trend is apparent in the data obtained on 0.8 Mg/m^3 plugs.

Selecting the largest pore radius from the pore-size range given for 1.2 Mg/m^3 Avonlea bentonite in section 2.2.6 (0.15 μm), the p_b calculated using the pore-radius pressure model [35] is 1.0 MPa. The pore-radius time model predicts a t_b of 0.15 h (mathematical model; [70]) and 0.11 h (computer model; Appendix I.2). The large relative difference between the two time-model predictions is attributed to the use of an incremental (step-wise increase) pressure function in the computer model compared with an approximate linear pressure function in the algebraic model (as discussed in section 2.5.5), combined with the small values of t_b. The most comparable specimens listed in Table 5.8 are those with ρ_c = 1.0 Mg/m^3. Since this ρ_c is less than the 1.2 Mg/m^3 of the specimen used for pore-size analysis, it might be expected that the radius of the pores would be larger than the 0.15 μm used in the calculation and that the measured p_b or t_b would be less than predicted. In the case of the pore-radius time models, a t_b less than predicted might also be expected due to the unsaturated state of the plugs. However, the opposite was observed experimentally – the average p_b and t_b were >8.8 MPa and >3.6 h, respectively, which are both greater than predicted. Therefore, the pore-radius pressure models underestimate p_b and t_b in this set of tests.

The finding that p_b and t_b measured by experiment are greater than calculated implies that the pores in which gas breakthrough occurs are smaller than the radius of the pores used in the calculation. As noted, the radius of the largest pores detected by Hg intrusion porosimetry was used. In using the largest pore radius in the calculation, it is assumed that these pores traverse the plug. This assumption may or may not be true. However

there are no data specifically about the radius of the largest pores that span the length of the specimen.

Table 6.1 contains the results of calculations using the remaining models described in section 2.5 and Appendix I. For all of the specimens which had breakthrough, the two pressure models overestimate p_b. All of the time models overestimate the observed t_b of the specimens in which breakthrough occurred. However, the time models assume that breakthrough occurs when gas pushes water from a pore by a hydraulic-conductivity mechanism. It is reasonable to assume that it would take longer to push the water out of a pore in a saturated plug than in an unsaturated plug. Since the models assume that the plugs are saturated, whereas the specimens used for these tests were unsaturated, the difficulty may be with the experiments rather than the models.

Two other points are noteworthy. First, there is a consistent trend in that the Darcy's-Law time model predicts the longest t_b, followed successively by the hydraulic-radius and Kozeny-Carman models. Similarly, the hydraulic-radius pressure model predicts a greater p_b than does the Kozeny-Carman model. Second, for the parameters used to generate the predictions in Table 6.1, the mathematical and computer time models yield nearly identical results despite the use of a simplified linear equation to describe the gas pressure in the algebraic models.

Table 6.1 Results of model calculations for series C.

Test	Hydraulic-Radius Pressure Model [37] (MPa)	Kozeny-Carman Pressure Model [51] (MPa)	Darcy's-Law Time Model [62] (h)	Darcy's-Law Time Model (App. L1) (h)	Hydraulic-Radius Time Model [73] (h)	Hydraulic-Radius Time Model (App. L3) (h)	Kozeny-Carman Time Model [76] (h)	Kozeny-Carman Time Model (App. L4) (h)
C1	31	23	7.9	7.8	4.9	4.9	3.6	3.6
C2	30	23	7.7	7.7	4.8	4.8	3.6	3.5
C3	34	24	8.5	8.5	5.4	5.4	3.8	3.8
C4	38	26	9.3	9.2	6.0	5.9	4.1	4.0
C5	37	25	9.1	9.1	5.9	5.9	4.0	4.0
C6	37	25	9.1	9.1	5.9	5.8	4.0	4.0
C7	42	27	10.1	10.0	6.6	6.5	4.3	4.3
C8	45	29	11.0	10.9	7.2	7.2	4.6	4.5
C9	45	29	10.9	10.8	7.1	7.1	4.6	4.5
C10	43	28	10.5	10.5	6.9	6.8	4.4	4.4
C11	54	32	12.9	12.9	8.6	8.5	5.0	5.0
C12	51	31	12.3	12.3	8.1	8.1	4.9	4.9
C13	61	34	14.8	14.6	9.6	9.6	5.5	5.4
C14	63	35	15.1	15.0	10.0	9.9	5.6	5.5
C15	63	35	15.1	15.1	10.0	9.9	5.6	5.5
C16	61	34	14.4	14.5	9.6	9.6	5.5	5.4

6.3 Incremental High-Pressure Wetted Tests

For series D, there is no significant difference in w between the peripheral and centre pieces on the inlet side of the plug ($\Delta w = 1.24 \pm 1.57\%$). However, on the outlet side the peripheral pieces have a greater w than the centre pieces ($\Delta w = 1.38 \pm 1.20\%$). The peripheral samples have a higher w on both the inlet and outlet side for series E ($\Delta w = 13.59 \pm 2.37\%$ and $9.72 \pm 1.48\%$, respectively) and series F ($\Delta w = 4.53 \pm 2.94\%$ and $4.75 \pm 4.03\%$, respectively). It is noted that the difference in w between the peripheral and

centre pieces is much greater for series E than series D or F. The w of the peripheral pieces is also greater, relative to the centre pieces, for plug E6c, which was sliced without being tested for gas breakthrough. In the series F plugs that were not tested for gas breakthrough, the peripheral pieces have a higher w than the centre pieces on the inlet side ($\Delta w = 4.44 \pm 3.18\%$) but not on the outlet side ($\Delta w = 5.98 \pm 6.04\%$). There is no obvious explanation for these observations.

The difference in mean w between the inlet and outlet sides is $6.29 \pm 2.32\%$ for series D. The difference is even greater in series E and F ($\Delta w = 30.43 \pm 4.53\%$ and $16.26 \pm 6.25\%$, respectively). Figure 6.3 shows the different textures of the inlet and outlet surfaces of the clay plug at the end of a test. The pitted appearance of the inlet surface is due to wet, low-density clay sticking to the filter paper after it is peeled from the specimen. It was proposed in section 6.1 that the effective stress concept can be used to explain why the inlet side has a greater w than the outlet side, and the concept is also applicable to the series D, E and F results.

Several additional observations support the effective-stress-concept explanation of the phenomenon illustrated in Figure 6.3. Specimen E6c, which was not tested for gas breakthrough, has a small difference in w between the inlet and outlet sides of -1.29% (the inlet side is slightly wetter). Those specimens not tested for gas breakthrough in series F have a statistically insignificant Δw of $-3.14 \pm 3.20\%$. Therefore, water movement is associated with the application of gas pressure. Figure 6.4 shows that at $\rho_c = 1.10$ Mg/m^3 the amount of water movement increases as the maximum applied pressure increases.

Figure 6.3 Photos of the inlet and outlet surfaces (top and bottom pictures, respectively) of a 1.20 Mg/m^3 plug after a high-pressure experiment in which gas breakthrough did not occur (test F6b). The white fibres are filter-paper remnants.

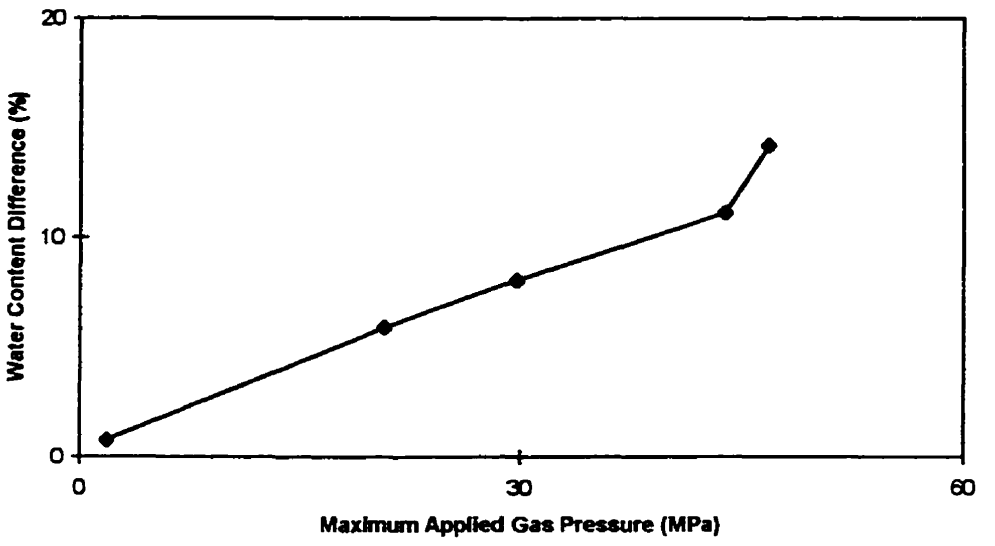

Figure 6.4 Relationship between the difference in water content (inlet minus outlet) and the applied pressure at the end of the test for all of the 1.10 Mg/m^3 series D tests.

This is consistent with the effective stress concept because it was shown earlier that while σ' on the inlet surface is zero throughout the test, σ' on the outlet surface is equal to $p_i - p_o = p_b$; therefore, as the maximum applied pressure increases the driving force for compression increases on the outlet surface. Figure 6.5 is a plot of the mean Δw, for each ρ_c examined, for those series E and F tests that did not have breakthrough. From the effective stress concept, σ' is predicted to be approximately equal in all these tests. Since the clay fabric has a greater resistance to compression as ρ_c increases, Δw decreases with increasing ρ_c. Lastly, a test was conducted on a 0.80 Mg/m^3 specimen with the direction of gas flow reversed; the inlet pressure was increased incrementally to 50.0 MPa but breakthrough did not occur. For the inlet (top) piece of the specimen w = 97.70%, and for the outlet (bottom) portion w = 69.80%. Therefore the side of the plug with the

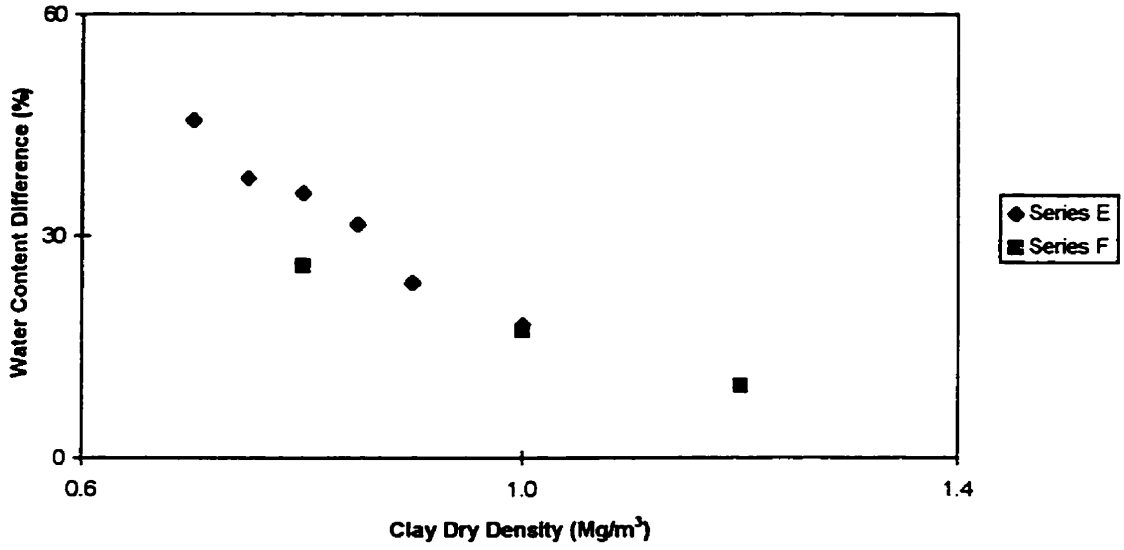

Figure 6.5 Mean difference in water content (inlet minus outlet) for all series E and F tests that did not have gas breakthrough.

greater σ' always has the lower w, regardless whether it is at the top or bottom of the cell. None of these observations contradict the proposed effective-stress-concept explanation.

Using calipers, the length of the plug and attached filter papers was determined after some of the tests. Two 0.80 Mg/m^3 specimens that were not tested for gas breakthrough (tests F2c and F3c) had a mean length of 2.44 cm; four specimens with the same ρ_c (F2a, F2b, F3a and F3b) that were tested to about 50 MPa, without breakthrough, had a mean length of 2.17 cm. Two 1.00 Mg/m^3 specimens that were not tested (F4c and F5c) had a mean length of 2.42 cm whereas three that were tested (F4a, F5a and F5b), but did not have breakthrough, had a mean length of 2.28 cm. The limited data available suggests that applying gas pressure causes the plug length to decrease, thus creating a void between the

bottom of the plug and the cell. Furthermore, the change in plug length increases as ρ_c decreases. If the plug length decreases during an experiment V also decreases, and thus ρ_c must increase. The decrease in V results from a decrease in V_v; if the clay is initially unsaturated, as in series D, air may be forced out of the plug. However, in series E and F the clay was initially saturated and water must be forced from the specimen for V_v to decrease. Given that w_{100} is calculated using the target ρ_c, this may explain why S_r is often <100% after gas pressure has been applied to a plug (Tables 5.11 and 5.13).

In series D, gas breakthrough was obtained for the majority of tests conducted at $\rho_c \leq$ 1.15 Mg/m^3. However, the reproducibility of the p_b results is poor, and at a ρ_c as low as 1.00 Mg/m^3, some specimens did not have breakthrough. There is also a large variation in the final S_r of the plugs. Given the results of the unsaturated tests displayed in Figures 6.1 and 6.2, it might be expected that for a given ρ_c those plugs with a higher S_r would have a higher p_b. However, there is no correlation between S_r and p_b in series D. It is not possible to determine if there is a relationship between w at the time of compaction and p_b, as all of the specimens were prepared with similar material. Therefore, none of the parameters measured in these experiments can be used to predict whether breakthrough will occur.

The wetting procedure used in the series D tests was similar to that in the low-pressure, wetted experiments (series C). The difference was that the series C specimens were wetted prior to compaction, whereas in series D the plugs were prepared with air-dry clay. In both series of tests, the clays were wetted for 2 d at 0.2 MPa following compaction.

The maximum ρ_c at which breakthrough was obtained in the low-pressure tests was 0.90 Mg/m^3; this was increased to 1.15 Mg/m^3 by increasing the pressure limit of the equipment to about 50 MPa. However, breakthrough was still not obtained at the ρ_c of the proposed buffer material ($\approx$1.22 Mg/m^3).

With more vigorous wetting (evacuated and wetted for 2 d at 1.0 MPa (series E) or wetted for 2 d at 5.0 MPa without evacuation (series F)), p_b increased. Occasional breakthrough occurred at $p_b \leq 50$ MPa between 0.80 and 0.90 Mg/m^3 in series E, but most of the specimens did not rupture. No breakthrough occurred in the two tests at 1.00 Mg/m^3 and, somewhat unexpectedly, breakthrough did not occur on either of the two specimens at both $\rho_c = 0.70$ and 0.75 Mg/m^3. In series F no breakthrough was obtained at 0.80, 1.00 or 1.20 Mg/m^3. Breakthrough pressures of 1.8 and 11.8 MPa were measured on 0.60 Mg/m^3 specimens. All of the specimens wetted for 2 d at 1.0 MPa after cell evacuation (series E) or at 5.0 MPa without the removal of air from the cell (series F) have a p_b greater than or equal to that of specimens of comparable ρ_c wetted at 0.2 MPa for 2 d (series D).

No breakthrough was obtained on any of the 0.80 or 1.00 Mg/m^3 specimens in series F, regardless of the initial w. Therefore, no conclusion can be reached about the effect of changes in w at the time of compaction, if any, on p_b for these tests. The series E plugs (which were compacted air dry) had p_b values similar to those of comparable series F plugs (which were wetted before compaction). However the series F data are more

consistent. Therefore, wetting the clay before compacting it and further wetting the plug at 5.0 MPa for 2 d is the best of the three wetting methods used.

Series E and F include several tests in which S_r was measured on specimens that were sliced without being tested for p_b. The data suggest that the wetting procedures used in both series give a $S_r \approx 100\%$. The same result was obtained in the tests described in section 4.2.3.2. Since it was shown in section 4.2.3.2 that wetting for 2 d at 0.2 MPa does not saturate Avonlea bentonite plugs, the series E and F data are considered a more accurate measure of the saturated p_b than are the results of series C and D. Therefore, only the former p_b results will be considered further.

Using the 0.15-μm pore radius measured by Wan (1996) on 1.2 Mg/m^3 clay, the pore-radius pressure model [35] predicts $p_b = 1.0$ MPa and the pore-radius time models predict $t_b = 240$ s (algebraic model; [70]) and $t_b = 120$ s (computer model; appendix I.2). Again the large relative difference between t_b results is attributed to the small values together with the use of different pressure functions in the two models (linear versus incremental). The predicted results are much smaller than the breakthrough values measured at 1.20 Mg/m^3 ($p_b > 52$ MPa and $t_b > 4.4$ h), and therefore the pore-radius models underestimate the values of p_b and t_b. This implies that the pore-radius value used in the calculations was too large.

Table 6.2 shows the results of calculations made with the other models. The predictions of corresponding algebraic and computer time models are very similar. Also noteworthy

Table 6.2 Results of model calculations for series E and F.

ρ_c (Mg/m^3)	Hydraulic-Radius Pressure Model [37] (MPa)	Kozeny-Carman Pressure Model [51] (MPa)	Darcy's-Law Time Model [62] (h)	Darcy's-Law Time Model (App. L1) (h)	Hydraulic-Radius Time Model [73] (h)	Hydraulic-Radius Time Model (App. L3) (h)	Kozeny-Carman Time Model [76] (h)	Kozeny-Carman Time Model (App. L4) (h)
0.60	30	22	3.3	3.3	2.1	2.0	1.5	1.5
0.70	37	25	3.9	3.9	2.5	2.5	1.7	1.7
0.75	41	27	4.3	4.3	2.8	2.8	1.8	1.8
0.80	45	28	4.6	4.6	3.1	3.0	1.9	1.9
0.85	49	30	5.1	5.0	3.3	3.3	2.1	2.0
0.90	53	32	5.5	5.5	3.6	3.6	2.2	2.1
1.00	62	35	6.5	6.4	4.3	4.2	2.4	2.4
1.05	67	37	7.0	7.0	4.6	4.6	2.5	2.5
1.10	73	38	7.6	7.6	5.0	5.0	2.6	2.6
1.15	79	40	8.3	8.2	5.4	5.4	2.7	2.7
1.20	85	41	8.9	8.9	5.8	5.8	2.8	2.8
1.30	98	43	10.5	10.5	6.7	6.7	2.9	2.9
1.40	110	44	12.3	12.3	7.8	7.8	3.0	3.0
1.50	130	42	14.4	14.3	9.1	9.1	2.9	2.8

is that the Kozeny-Carman pressure- and time-model predictions decrease at 1.50 Mg/m^3, which contradicts the general trend of increasing p_b or t_b with increasing ρ_c. At 0.60 Mg/m^3, the pressure models overestimate the p_b measured in series F. At the same ρ_c, the Darcy-law and hydraulic-radius time models overestimate the measured t_b; the Kozeny-Carman time-model predictions are similar to one of the experimental results. Only general observations can be made regarding the remaining theoretical predictions because consistent breakthrough did not occur in the experiments. The hydraulic-radius pressure, Darcy's-law time and hydraulic-radius time models predict that breakthrough should have been observed in some, but not all, of the tests between ρ_c = 0.70 and 1.50 Mg/m^3. The Kozeny-Carman pressure and time models predict that breakthrough should have been detected in all of the series E and F tests.

A form of the Poiseuille equation [39] can be used to calculate the diameter of a capillary through which gas is flowing if the rate of gas passage, capillary length, gas viscosity and pressure differential across the capillary are known. The rate of gas passage in a gas-breakthrough experiment can be obtained using the ideal gas law and the rate of pressure change in the outlet vessel following breakthrough. If it is assumed that breakthrough occurs in only one capillary, and that the capillary length is equal to the plug length, the radius of the pore through which gas is passing can be calculated. However, large differences in the rate of breakthrough were observed for tests of similar ρ_c, resulting in large variations in the calculated pore sizes. As a result, the data cannot be interpreted meaningfully.

In a few tests the maximum gas pressure was applied for longer than the standard time increment, if breakthrough had not occurred after five minutes. Most of the tests did not have breakthrough, as expected if the capillary-rise model of gas breakthrough is correct. However test D2a was an exception, as shown in Figure 6.6. The test was recorded in Table 5.9 as not having breakthrough because none occurred within five minutes of the maximum pressure being applied. However breakthrough did eventually occur, about 0.9 h after the maximum pressure was applied. This suggests that breakthrough may be a time-dependent process. Tests which examined the time dependency of gas breakthrough are described in the next section.

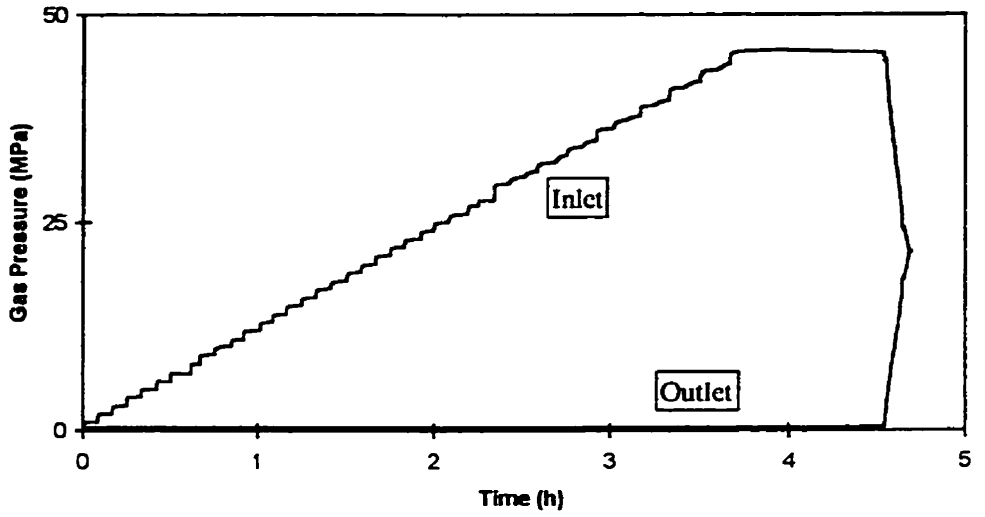

Figure 6.6 Graph of the results of experiment D2a.

6.4 Constant High-Pressure Wetted Tests

Breakthrough was obtained in every constant-pressure test conducted, regardless of ρ_c or p_c, which is a very different result from that obtained in the increasing-pressure tests. For plugs of comparable ρ_c, breakthrough in series G was obtained at p_c values that are often much lower than the p_b values measured in either series E or F. For example, at 1.00 Mg/m^3, breakthrough was obtained at $p_c = 0.3$ MPa in the constant-pressure tests, whereas specimens of comparable ρ_c did not have consistent breakthrough in the increasing-pressure tests ($p_b > 50$ MPa). The breakthrough time in all the constant-pressure tests is longer than the duration of the increasing-pressure tests. For example, $t_b = 120.5$ h at $\rho_c = 1.00$ Mg/m^3 and $p_c = 0.3$ MPa, whereas the longest duration increasing-pressure tests were slightly more than four hours. When compared with the results in

Tables 5.11 and 5.13, the data in Table 5.15 show that gas breakthrough is time dependent. This finding is inconsistent with the capillary-rise models of gas breakthrough, in which p_b is independent of time.

At constant pressure, the time for gas breakthrough tends to increase with increasing ρ_c. This is illustrated in Figure 6.7 where the mean t_b is plotted as a function of ρ_c for all the p_c = 4.8 and 9.8 MPa tests. Figure 6.7 also shows that t_b generally decreases with increasing p_c. The 1.00 Mg/m^3 tests, in which t_b is similar at 4.8 and 9.8 MPa, are unusual. However, the general trend (decreasing t_b with increasing p_c) is observed in the 1.00 Mg/m^3 data at $p_c \leq 2.8$ MPa (Table 5.15). For constant-pressure tests with the same ρ_c and p_c, there is no obvious relationship between t_b and the final S_r (Table 5.15), which is the same observation made for the increasing-pressure wetted tests.

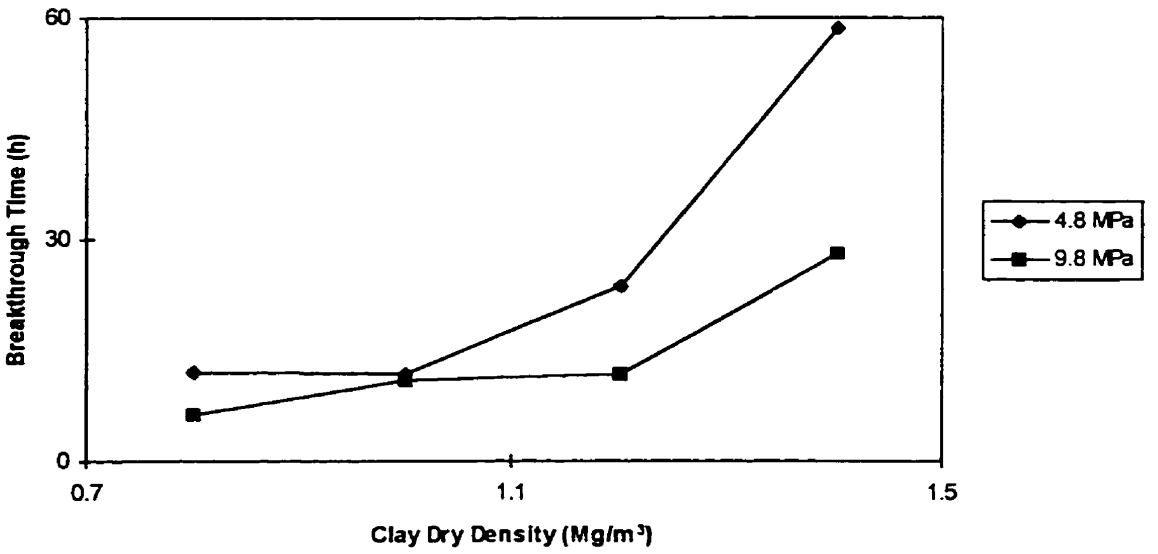

Figure 6.7 Breakthrough times for the constant-pressure tests at several clay dry densities.

Lineham (1989) suggested that gas breakthrough may be a diffusive process. The theory is that gas dissolves in the pore water on the inlet side of the specimen, diffuses through the plug, and comes out of solution on the outlet surface. This suggestion can be examined by comparing the constant-pressure results with theoretical calculated rates of diffusive transport. The Ostwald constant (B) is defined as

$$B = c_l/c_g \,, \qquad [85]$$

where c_l is the concentration of gas in a liquid phase and c_g the concentration in an equilibrium gaseous phase, with both concentrations expressed in the same units. At 10.261 MPa and 25.0°C, Kennan and Pollack (1990) report that B = 0.0276 for Ar. From the ideal gas law, $c_g = 4.0 \times 10^3$ mol/m^3 at 10 MPa and 25°C. If it is assumed that 10 MPa is applied to the inlet surface of a clay plug in a gas-breakthrough test, using [85] and the above Ostwald constant yields $c_l = 110$ mol/m^3 in the inlet-surface liquid.

Fick's first law,

$$dQ/Adt = -D_e(dc)/L \,, \qquad [86]$$

describes steady-state diffusion. In [86], dQ is the quantity diffused in a time increment dt, D_e the steady-state or effective diffusion coefficient and dc the concentration difference across the specimen. Johnson et al. (1994a) report that $D_e = 2.4 \times 10^{-3}$ m^2/year for Ar in buffer ($\rho_c \approx 1.22$ Mg/m^3). If it is assumed that breakthrough is detectable in the high-pressure apparatus when the pressure in the outlet vessel rises by 0.05 MPa, the ideal gas law can be used to calculate that 0.010 mol of Ar must enter the vessel at 25°C for gas breakthrough to be detectable. Solving [86] for dt and replacing the variables with numbers, it is determined that 0.44 years (3.9×10^3 h) must pass for p_o to rise 0.05 MPa.

This time estimate is low because steady-state diffusion has been assumed; the initial (transient) rate of diffusion is less than at steady state. Nevertheless, the observed 11.8 h mean t_b obtained at $\rho_c = 1.20$ Mg/m^3 and $p_c = 9.8$ MPa is more than two orders of magnitude less than the calculated result. Furthermore, if gas breakthrough occurs by diffusion, the rate of gas transport would decrease with time after breakthrough because, assuming p_i is constant, dc decreases as p_o increases. This is clearly not the case in, for example, test G10 (Figure 5.3). Therefore, a diffusion mechanism for gas breakthrough is inconsistent with the experimental results.

In all of the constant-pressure time models derived in sections 2.5.5 through 2.5.8, t_b and p_c are inversely related. In Figure 6.8, the mean t_b for each pressure is plotted against p_c^{-1} for the 1.00 Mg/m^3 tests. The linear relationship that exists between t_b and p_c^{-1} in the range $p_c \leq 2.8$ MPa is consistent with the constant-pressure time models.

There are at least two possible explanations for the non-linear behaviour shown in Figure 6.8 at $p_c > 2.8$ MPa. It has been shown in Figures 5.4 to 5.7 that applying constant gas pressure to clay plugs causes ρ_c to change in some specimens. For ρ_c to change, the clay particles must rearrange, and therefore the pore structure is not constant. As noted in the literature review, the models of gas breakthrough assume a constant pore structure. Alternatively, flow in the pores of the compacted clay may become turbulent at high pressure and, if so, Darcy's law would not be valid. By combining equations [30], [47] and [49], one obtains the following equation for Reynolds number,

$$N_R = 2rk(dP)/(nLg\tau^{0.5}\eta)\,, \qquad [87]$$

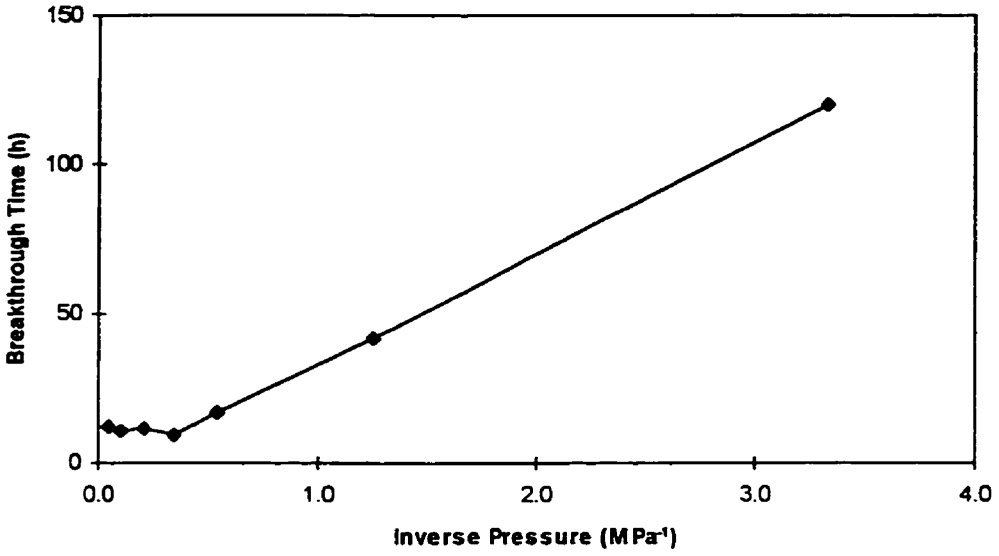

Figure 6.8 Relationship between breakthrough time and inverse pressure for all the 1.00 Mg/m^3 constant-pressure tests.

which contains known variables. The maximum differential pressure used for the tests shown in Figure 6.8 is 19.8 MPa. By substituting this value for dP, the maximum pore radius obtained by Hg intrusion porosimetry for r (0.015 μm as shown in Figure 2.8), values of k, n and τ obtained from [34], [13] and [52], and values for the constants, an N_R of 1.8×10^{-8} is obtained. A smaller value would be obtained at a lower pressure or if a smaller pore radius was substituted. Since this N_R value is much less than one, it is concluded that turbulent flow did not occur in the specimens. Thus the first explanation likely accounts for the non-linearity observed in Figure 6.8 at high pressure.

Given that capillary-rise theory does not explain the observed time dependence of gas breakthrough, it is inappropriate to model the constant-pressure results using the pressure

models. Results of the four constant-pressure time models, for each combination of ρ_c and p_c used, are in Table 6.3. The largest pore radius measured in $\rho_c \approx 1.2$ Mg/m^3 clay (from Figure 2.8) was used in all the pore-radius time model calculations, regardless of the specimen ρ_c. The numeric and algebraic t_b predictions are nearly identical for all of the models. The Darcy's-law time model prediction is close to the observed t_b for the ρ_c = 1.00 Mg/m^3 and p_c = 19.8 MPa test, but for the other tests the model predictions are greater than the observed t_b. The units of the pore-radius time model predictions are seconds, and therefore the theoretical values are all several orders of magnitude less than the observed results. For this model to yield accurate results, a smaller value of the pore radius must be used. The hydraulic-radius time model predictions are fair for tests at $p_c \geq$ 4.8 MPa, but poorer at lower values of p_c.

Table 6.3 Results of model calculations for series G.

ρ_c (Mg/m^3)	p_c (MPa)	Darcy's-Law Time Model [58] (h)	Darcy's-Law Time Model (App. L1) (h)	Pore-Radius Time Model [68] (s)	Pore-Radius Time Model (App. L2) (s)	Hydraulic-Radius Time Model [72] (h)	Hydraulic-Radius Time Model (App. L3) (h)	Kozeny-Carman Time Model [75] (h)	Kozeny-Carman Time Model (App. L4) (h)
0.8	4.8	28	28	20	20	12	12	4.9	4.9
0.8	9.8	14	14	9.7	9.7	5.9	5.8	2.4	2.4
1.0	0.3	850	840	320	320	340	360	120	110
1.0	0.8	320	310	120	120	130	140	43	43
1.0	1.8	140	140	53	53	57	61	19	19
1.0	2.8	91	90	34	34	37	39	12	12
1.0	4.8	53	52	20	20	21	23	7.2	7.1
1.0	9.8	26	26	9.7	9.7	11	11	3.5	3.5
1.0	19.8	13	13	4.8	4.8	5.2	5.5	1.7	1.7
1.2	4.8	96	97	20	20	42	41	9.4	9.4
1.2	9.8	47	47	9.7	9.7	20	20	4.6	4.6
1.4	4.8	190	190	20	20	78	77	11	11
1.4	9.8	94	94	9.7	9.7	38	38	5.5	5.5

The best agreement between theory and experiment is obtained using the Kozeny-Carman time models. The Kozeny-Carman time-model predictions are less than the observed results for tests with $p_c > 2.8$ MPa. However, the agreement is excellent at $p_c \leq 2.8$ MPa. This is also the p_c range in which a linear relationship exists between t_b and p_c^{-1} as shown in Figure 6.8. The experimental and theoretical results in this p_c range are repeated in Table 6.4. As p_c decreases, the agreement between prediction and experiment improves. The equation of the straight line in Figure 6.8 is

$$t_b = (1.2 \times 10^{11} \text{ kg/m·s} \times p_c^{-1}) - (1.6 \times 10^{4} \text{ s}) . \quad [88]$$

The equation of the Kozeny-Carman time model at $\rho_c = 1.00$ Mg/m^3, with all of the algebraic constants converted to numbers is

$$t_b = 1.3 \times 10^{11} \text{ kg/m·s} \times p_c^{-1} . \quad [89]$$

Thus, not only is an advection mechanism for gas breakthrough consistent with the observed inverse relationship between t_b and p_c in the constant-pressure tests at low p_c, but the slope of such a plot is remarkably similar to that predicted by the Kozeny-Carman time model. It is noted that the SI units of the slope in [88] and [89] are kg/m·s, which are also the units of viscosity. The significance of this, if any, remains to be explained.

The constant-pressure results are based on a small number of tests. It is recommended that they be repeated at 1.00 Mg/m^3 and then conducted at other ρ_c. To increase confidence in the Kozeny-Carman time model, it is necessary to show that predictions at other ρ_c agree with experimental results.

Table 6.4 Comparison of experimental and theoretical results for $\rho_c = 1.00$ Mg/m^3 and $p_c \leq 2.8$ MPa.

p_c (MPa)	Experimental t_b (h)	Predicted t_b [75] (h)
0.3	120.5	120
0.8	41.8	43
1.8	16.7	19
2.8	9.2	12

Notwithstanding the preceding discussion, there may be a pressure below which gas will not pass through compacted Avonlea bentonite specimens, regardless of the test duration (a gas-breakthrough pressure (p_b)). That is, an advection mechanism may only apply if $p_c > p_b$. If so, p_b would impose a lower pressure limit to the linear relationship between t_b and p_c^{-1}. This limit, if it exists, was not determined in any of the constant-pressure tests. Given the constant-pressure results, it is also unlikely that p_b was accurately measured in any of the increasing-pressure tests. Furthermore, if a p_b exists, it is lower than predicted by some of the pressure models. The hydraulic-radius and Kozeny-Carman pressure models predict p_b values of 62 and 35 MPa, respectively, for 1.00 Mg/m^3 clay. However, gas breakthrough was obtained in 1.00 Mg/m^3 clay at $p_c = 0.3$ MPa, which is below the p_b predicted by either model. It is not known whether the pore-radius pressure model prediction of $p_b = 1.0$ MPa for 1.20 Mg/m^3 Avonlea bentonite is accurate, because constant-pressure tests were not conducted below $p_c = 4.8$ MPa at this ρ_c.

From an academic perspective, the question of whether p_b exists is intriguing. It has been demonstrated that p_b cannot be accurately predicted by either the hydraulic-radius or Kozeny-Carman pressure models. However, this does not confirm or deny whether p_b exists. The existence of p_b can perhaps be established by conducting constant-pressure tests. The duration of the tests must be long enough to allow water to move out of a clay pore by advection, and thus open a pathway for gas migration. This may be a long time at some ρ_c. For example, Pusch et al. (1987) reported that $p_b = 0.060$ MPa at $\rho_c = 1.00$ Mg/m^3 for MX-80 bentonite (Table 2.3). Assuming the data of Pusch et al. are accurate and that MX-80 and Avonlea bentonites have similar properties, by extrapolating [88] it is calculated that it would take 23 d for gas breakthrough to occur in 1.00 Mg/m^3 Avonlea bentonite at $p_b = 0.060$ MPa. At least one additional test of longer duration would be required to demonstrate that gas does not pass through the clay at a slightly lower p_c.

From the perspective of nuclear waste disposal, it may not be necessary to determine whether p_b exists. Providing that the pressure at which gas passes through the buffer is sufficiently low, no damage will occur to the vault contents. However, for modeling contaminant transport from a disposal vault, it is necessary to know the slope of a plot of t_b against p_c^{-1} for different ρ_c, so that t_b can be predicted for given values of p_c and ρ_c. In addition, the results may be more convincing to regulators if they are obtained using the buffer material proposed for the nuclear waste disposal concept, and the gases and groundwater expected to be present in the vault. Similar experiments also need to be conducted using Lake Agassiz clay or backfill material, or both.

All of the constant-pressure time models predict that t_b is directly related to the square of the plug length. To investigate this hypothesis, constant-pressure tests should be conducted using plugs of different lengths. This may require additional gas-breakthrough cells to be constructed. Confirmation of this proposed relationship would provide increased confidence in the Kozeny-Carman time model.

7. SUMMARY

The approach adopted for the initial gas-breakthrough experiments was similar to that used by several other researchers. As described in the literature, it is often assumed that clay pores are analogous to a bundle of capillary tubes, with respect to gas movement. If so, p_b might equal the pressure required to force gas through water-filled capillaries of the same effective radius.

Increasing-pressure tests were conducted on compacted Avonlea bentonite specimens in an attempt to measure p_b. A pressure differential of 0.2 MPa was applied to the plugs initially, and the differential was increased 0.2 MPa every five minutes to a maximum of about 10 MPa. Tests on unsaturated plugs indicated that p_b is negligible below S_r = 80 to 90%, and that it increases rapidly as S_r nears 100%, in some cases exceeding 10 MPa. Clays wetted before compaction and further wetted at 0.2 MPa for 2 d after compaction were also tested and no breakthrough was obtained at $\rho_c > 0.9$ Mg/m^3. Based on the assumption described above, it was concluded that an apparatus with a higher pressure limit was needed to measure p_b in Avonlea bentonite at $\rho_c > 0.9$ Mg/m^3. Therefore, a test system with an arbitrary pressure limit of 50 MPa was built. An initial pressure differential of 0.8 MPa was used in all the high-pressure tests, and the differential was increased 1.0 MPa every five minutes until the limit of the equipment was reached. Using clay that was compacted in an air-dry state and then wetted in the cell as described for the low-pressure

tests, breakthrough was obtained on compacted Avonlea bentonite specimens at $\rho_c \leq 1.15$ Mg/m^3 with the high-pressure apparatus. However, it was discovered that the wetting procedure was not saturating the plugs. Subsequent series of tests were conducted either on specimens that were compacted using air-dry clay and wetted at 1.0 MPa for 2 d after the gas-breakthrough cell was evacuated, or on plugs that were compacted using wetted clay and then further wetted at 5.0 MPa for 2 d without removing air from the cell. With the high-pressure apparatus, consistent breakthrough could not be obtained at $\rho_c > 0.60$ Mg/m^3 after the wetting procedure was modified.

Tests were also conducted at constant pressure and t_b was measured. All of the Avonlea bentonite specimens tested in this manner had breakthrough (ρ_c = 0.80 to 1.40 Mg/m^3 and p_c = 0.3 to 19.8 MPa). A linear relationship was obtained between t_b and p_c^{-1} at ρ_c = 1.00 Mg/m^3 and p_c = 0.3 to 2.8 MPa. Therefore, it is concluded that gas breakthrough is time dependent in this parameter range. It is also concluded that the capillary theory does not apply to these tests, because mathematical models based on the theory predict that gas breakthrough should be independent of time. However, the results are consistent with models that assume an advection mechanism for gas breakthrough. Furthermore, one model derived assuming an advection mechanism (termed the Kozeny-Carman time model) accurately predicts t_b in the 0.3 to 2.8 MPa range. A non-linear relationship between t_b and p_c^{-1}, at higher values of p_c, may be due to changing clay fabric. The presence of a relationship between t_b and p_c^{-1}, that is consistent with an advection mechanism, neither supports nor refutes the existence of p_b; it only implies that t_b is determined by the time required for water to flow from a clay pore and thus create a path

for gas breakthrough. It is possible that gas breakthrough can only be obtained if $p_c > p_b$. However, from a comparison of the increasing- and constant-pressure results, it is concluded that the former tests are not an accurate measure of p_b. The significance of the increasing-pressure tests is uncertain.

8. CONTRIBUTION TO KNOWLEDGE

Over a pressure range of 2.5 MPa, it has been found that the time required for gas breakthrough is inversely related to the applied pressure for 1.00 Mg/m^3 Avonlea bentonite. This result is consistent with an advection mechanism for gas breakthrough. This finding will facilitate the design of future gas-breakthrough experiments. An understanding of the mechanism of gas breakthrough may help determine if gas migration is a significant contaminant-transport process. If gas migration is a significant contributor to contaminant transport, understanding the mechanism will aid the development of conceptual and mathematical models that include this process.

9. REFERENCES

AECL. 1994. Environmental impact statement on the concept for disposal of Canada's nuclear fuel waste. Atomic Energy of Canada Limited Report, AECL-10711, COG-93-1, Chalk River, ON.

American Society for Testing and Materials. 1992. Annual Book of ASTM Standards, Volume 04.08, Soil and Rock; Dimension Stone; Geosynthetics. American Society for Testing and Materials, Philadelphia, PA.

Atterberg, A. 1911. Lerornas forhallande till vatten, deras plasticitetsgranser och plasticitetsgrader. Kungliga Lantbruksakademiens Handlingar och Tidskrift **50:**132-158.

Barden, L. and Sides, G.R. 1970. Engineering behavior and structure of compacted clay. Journal of the Soil Mechanics and Foundations Division, American Society of Civil Engineers **96:**1171-1200.

Barrow, G.M. 1979. Physical Chemistry, 4th edition. McGraw-Hill Book Company, New York, NY.

Bear, J. 1972. Dynamics of Fluids in Porous Media. American Elsevier Publishing Company, Inc., New York, NY.

Black, D.K. and Lee, K.L. 1973. Saturating laboratory samples by back pressure. Journal of the Soil Mechanics and Foundations Division, American Society of Civil Engineers **99:**75-93.

Carter, D.L., Mortland, M.M. and Kemper, W.D. 1986. Specific surface. Pages 413-423. *in* A. Klute (ed.), Methods of Soil Analysis, Part 1, Physical and Mineralogical Methods, 2nd edition. American Society of Agronomy, Inc., Madison, WI.

Casagrande, A. 1948. Classification and identification of soils. Transactions, American Society of Civil Engineers **113:**901-930.

Chan, T. 1989. An overview of groundwater flow and radionuclide transport modelling in the Canadian Nuclear Fuel Waste Management Program. Pages 39-61. *in* B.E. Buxton (ed.), Proceedings of the Conference on Geostatistical Sensitivity, and Uncertainty Methods for Ground-Water Flow and Radionuclide Transport Modeling, San Francisco, CA. Battelle Press, Columbus, OH.

Christensen, H. and Bjergbakke, E. 1982. Radiolysis of groundwater from HLW stored in copper canisters. Swedish Nuclear Fuel Supply Company Report, SKBF-KBS-TR-82-02, Stockholm, Sweden.

Corey, A.T. 1986. Mechanics of Immiscible Fluids in Porous Media. Water Resources Publications, Littleton, CO.

Cotton, F.A. and Wilkinson, G. 1980. Advanced Inorganic Chemistry, 4th edition. John Wiley & Sons, New York, NY.

Craig, R.F. 1994. Soil Mechanics, 5th edition. Chapman & Hall, London, U.K.

CRC. 1978. R.C. Weast (ed.), CRC Handbook of Chemistry and Physics, 58th edition. CRC Press, Inc., West Palm Beach, FL.

Danielson, R.E. and Sutherland, P.L. 1986. Porosity. Pages 443-461. *in* A. Klute (ed.), Methods of Soil Analysis, Part 1, Physical and Mineralogical Methods, 2nd edition. American Society of Agronomy, Inc., Madison, WI.

Darcy, H. 1856. Les Fontaines Publiques de la Ville de Dijon. Dalmont, Paris, France.

Davies, P.B. 1991. Evaluation of the role of threshold pressure in controlling flow of waste-generated gas into beddded salt at the Waste Isolation Pilot Plant. Sandia National Laboratories Report, SAND90-3246, Albuquerque, NM.

Delage, P. and Graham, J. 1996. Understanding the behaviour of unsaturated soils requires reliable conceptual model. Pages 1223-1256. *in* E.E. Alonso and P. Delage (eds.), Proceedings of the First International Conference on Unsaturated Soils, Paris, France. Balkema, Rotterdam, The Netherlands.

Diamond, S. 1970. Pore size distributions in clays. Clays and Clay Minerals **18:**7-23.

Diamond, S. 1971. Microstructure and pore structure of impact-compacted clays. Clays and Clay Minerals **19:**239-249.

Dixon, D.A. 1995. Towards an understanding of water structure and water movement through dense clays. Doctor of Philosophy Thesis, University of Manitoba, Winnipeg, MB.

Dixon, D.A., Cheung, S.C.H., Gray, M.N. and Davidson, B. 1987. The hydraulic conductivity of dense clay soils. Pages 389-396. *in* Geotechnique in Resource Development, Proceedings of the 40th Canadian Geotechnical Conference, Regina, SK.

Garcia-Benochea, I. and C.W. Lovell. 1981. Correlative measurements of pore size distribution and permeability in soils. Pages 137-150. *in* T.F. Zimmie and C.O. Riggs (eds.), ASTM STP 746, Permeability and Groundwater Contaminant Transport. American Society for Testing and Materials, Philadelphia, PA.

Garcia-Bengochea, I., Lovell, C.W. and Altschaeffl, A.G. 1979. Pore distribution and permeability of silty clays. Journal of the Geotechnical Engineering Division, American Society of Civil Engineers **105:**839-856.

Gascoyne, M. 1992. Fuel waste technology branch memorandum. Pages 58-63. *in* Unpublished Documents Cited in the EIS and Primary References. Atomic Energy of Canada Limited Technical Record, TR-567, COG-92-27, Chalk River, ON.

Gelmich Halayko, K.S. 1998. Gas Flow in Compacted Clays. Master of Science Thesis, University of Manitoba, Winnipeg, MB.

Graham, J., Oswell, J.M. and Gray, M.N. 1992. The effective stress concept in saturated sand-clay buffer. Canadian Geotechnical Journal **29:**1033-1043.

Hillel, D. 1980. Fundamentals of Soil Physics. Academic Press, New York, NY.

Holtz, R.D. and Kovacs, W.D. 1981. An Introduction to Geotechnical Engineering. Prentice Hall, Englewood Cliffs, NJ.

Horseman, S.T. and Harrington, J. 1994. Migration of repository gases in an overconsolidated clay. British Geological Survey Technical Report, WE/94/7, Keyworth, U.K.

Hume, H.B. 1997. High-pressure gas-breakthrough apparatus and a procedure for determining the gas-breakthrough pressure of compacted clay. Atomic Energy of Canada Limited Report, AECL-11827, COG-97-303-I, Chalk River, ON.

Hume, H.B., Gray, M.N. and Graham, J. 1997. Gas breakthrough in unsaturated Avonlea bentonite plugs. Ontario Hydro Report, 06819-REP-01200-0014 R00, Toronto, ON.

Jackson, M.L. 1975. Soil Chemical Analysis - Advanced Course, 2nd edition. Published by the author, Madison, WI.

Johnson, L.H., LeNeveu, D.M., Shoesmith, D.W., Oscarson, D.W., Gray, M.N., Lemire, R.J. and Garisto, N.C. 1994a. The disposal of Canada's nuclear fuel waste: the vault model for postclosure assessment. Atomic Energy of Canada Limited Report, AECL-10714, COG-93-4, Chalk River, ON.

Johnson, L.H., Tait, J.C., Shoesmith, D.W., Crosthwaite, J.L. and Gray, M.N. 1994b. The disposal of Canada's nuclear fuel waste: engineered barriers alternatives. Atomic Energy of Canada Limited Report, AECL-10718, COG-93-8, Chalk River, ON.

Kennan, R.P. and Pollack, G.L. 1990. Pressure dependence of the solubility of nitrogen, argon, krypton, and xenon in water. Journal of Chemical Physics **93**:2724-2735.

Kirkham, T. 1995. Development of test equipment and procedures for determination of the gas-breakthrough pressure of compacted clay materials with preliminary results. Master of Science Thesis, University of Manitoba, Winnipeg, MB.

Kroth, K., Barnert, E., Morlock, G. and Muller, W. 1992. Consequences of gas formation on borehole disposal of ILW packages. Pages 296-308. *in* Gas Generation and Release from Radioactive Waste Repositories. Organization for Economic Cooperation and Development, Nuclear Energy Agency, Paris, France.

Lambe, T.W. and Whitman, R.V. 1979. Soil Mechanics, SI Version. John Wiley & Sons, Inc., New York, NY.

Lineham, T.R. 1989. A laboratory study of gas transport through intact clay samples. NIREX Safety Studies Report, NSS/R155, Didcot, U.K.

Mathers, W.G. 1985. HOTROC, a program for calculating the transient temperature field from an underground nuclear waste disposal vault. Atomic Energy of Canada Limited Technical Record, TR-336, Chalk River, ON.

Mattsson, H. and Olefjord, I. 1984. General corrosion of Ti in hot water and water-saturated bentonite clay. Swedish Nuclear Fuel and Waste Management Co. Report, SKB-KBS-TR-84-19, Stockholm, Sweden.

McBride, M.B. 1994. Environmental Chemistry of Soils. Oxford University Press, New York, NY.

Mitchell, J.K. 1976. Fundamentals of Soil Behavior. John Wiley & Sons, Inc., New York, NY.

Moore, D.M. and Reynolds, R.C. 1989. X-ray diffraction and the Identification and Analysis of Clay Minerals. Oxford University Press, Oxford, U.K.

Oscarson, D.W. and Dixon, D.A. 1989. Elemental, mineralogical and pore-solution compositions of selected Canadian clays. Atomic Energy of Canada Limited Report, AECL-9891, Chalk River, ON.

Oscarson, D.W., Dixon, D.A. and Gray, M.N. 1990. Swelling capacity and permeability of an unprocessed and a processed bentonitic clay. Engineering Geology **28:**281-289.

Oscarson, D.W. and Hume, H.B. 1993. On the smectite-to-illite reaction. Atomic Energy of Canada Limited Report, AECL-10842, COG-93-278, Chalk River, ON.

Oscarson, D.W. and Hume, H.B. 1994. Diffusion of ^{14}C in dense saturated bentonite under steady-state conditions. Transport in Porous Media **14:**73-84.

Oscarson, D.W., Hume, H.B., Sawatsky, N.G. and Cheung, S.C.H. 1992. Diffusion of iodide in compacted bentonite. Soil Science Society of America Journal **56:**1400-1406.

Pacey, J.G. 1956. The Structure of Compacted Soils. S.M. Thesis, Massachusetts Institute of Technology, Cambridge, MA.

Pourbaix, M. 1966. Atlas of Electrochemical Equilibria. Pergamon Press, New York, NY.

Pusch, R. and Forsberg, T. 1983. Gas migration through bentonite clay. Swedish Nuclear Fuel and Waste Management Company Report, SKBF/KBS-TR-83-71, Stockholm, Sweden.

Pusch, R., Hokmark, H. and Borgesson, L. 1987. Outline of models of water and gas flow through smectite clay buffers. Swedish Nuclear Fuel and Waste Management Company Report, SKB-TR-87-10, Stockholm, Sweden.

Pusch, R., Ranhagen, L. and Nilsson, K. 1985. Gas migration through MX-80 bentonite. National Cooperative for the Storage of Radioactive Waste Report, NAGRA-NTB-85-36, Baden, Switzerland.

Quigley, R.M. 1984. Quantitative mineralogy and preliminary pore-water chemistry of candidate buffer and backfill materials for a nuclear fuel waste disposal vault. Atomic Energy of Canada Limited Report, AECL-7827, Chalk River, ON.

Rees, J. H. 1992. An overview of research on gas evolution and migration relevant to the disposal of low and intermediate-level radioactive wastes in clays and fractured hard rocks. Pages 31-40. *in* Gas Generation and Release from Radioactive Waste Repositories. Organization for Economic Cooperation and Development, Nuclear Energy Agency, Paris, France.

Rhoades, J.D. 1982. Cation exchange capacity. Pages 149-157. *in* A.L. Page, R.H. Miller and D.R. Keeney (eds.), Methods of Soil Analysis, Part 2, Chemical and Microbiological Properties. American Society of Agronomy and Soil Science Society of America, Madison, WI.

Richards, B.G. 1974. Behaviour of unsaturated soils. Pages 113-157. *in* I.K. Lee (ed.), Soil Mechanics - New Horizons. Newnes - Butterworths, London, U.K.

Sheppard, M.I., Stroes-Gascoyne, S., Hawkins, J.L., Hamon, C.J. and Motycka, M. 1996. Methane production rates from natural organics of glacial lake clay and granitic groundwater. Atomic Energy of Canada Limited Report, AECL-11510, COG-95-578, Chalk River, ON.

Simmons, G.R. and Baumgartner, P. 1994. The disposal of Canada's nuclear fuel waste: engineering for a disposal facility. Atomic Energy of Canada Limited Report, AECL-10715, COG-93-5, Chalk River, ON.

Sloane, R.L. and Kell, T.F. 1966. The fabric of mechanically compacted kaolin. Clays and Clay Minerals **14:**289-296.

Taylor, D.W. 1948. Fundamentals of Soil Mechanics. John Wiley & Sons, Inc., New York, NY.

Terzaghi, K. 1936. The shearing resistance of saturated soils and the angle between the planes of shear. Pages 54-56. *in* Proceedings of the First International Conference on Soil Mechanics and Foundation Engineering, Cambridge, MA.

Thomas, G.W. 1982. Exchangeable cations. Pages 159-165. *in* A.L. Page, R.H. Miller and D.R. Keeney (eds.), Methods of Soil Analysis, Part 2, Chemical and Microbiological Properties. American Society of Agronomy and Soil Science Society of America, Madison, WI.

Thomas, L.K., Katz, D.L. and Tek, M.R. 1968. Threshold pressure phenomena in porous media. Society of Petroleum Engineers Journal **8:**174-184.

Voinis, S., Gago, J. and Muller, W. 1992. The analytical modeling of gas generation. Pages 111-119. *in* Gas Generation and Release from Radioactive Waste Repositories. Organization for Economic Cooperation and Development, Nuclear Energy Agency, Paris, France.

Volckaert, G., Put, M., Ortiz, L., De Canniere, P., Horseman, S., Harrington, J., Fioravante, V., Impey, M. and Worgan, K. 1993. MEGAS - Modelling and experiments on gas migration in repository host rocks. Pegasus Meeting, Koln, Germany, 1993 June 4-5.

Wan, A.W.L. 1987. Compaction and strength characteristics of sand-clay buffer material formed at swelling pressure - water content equilibrium. Master of Science Thesis, University of Manitoba, Winnipeg, MB.

Wan, A.W.L. 1996. The use of thermocouple psychrometers to measure in situ suctions and water contents in compacted clays. Doctor of Philosophy Thesis, University of Mantioba, Winnipeg, MB.

Wan, A.W.L., Graham, J. and Gray, M.N. 1990. Influence of soil structure on the stress-strain behavior of sand-bentonite mixtures. Geotechnical Testing Journal **13:**179-187.

Whittig, L.D. 1976. X-ray diffraction techniques for mineral identification and mineralogical composition. Pages 671-698. *in* C.A. Black, D.D. Evans, J.L. White, L.E. Ensminger and F.E. Clark (eds.), Methods of Soil Analysis, Physical and Mineralogical Properties, Including Statistics of Measurements and Sampling. American Society of Agronomy, Inc., Madison, WI.

Wonnacott, T.H. and Wonnacott, R.J. 1977. Introductory Statistics, 3rd edition. John Wiley & Sons, New York, NY.

Wyllie, M.R.J. and Spangler, M.B. 1952. Application of electrical resistivity measurements to problems of fluid flow in porous media. Bulletin of the American Association of Petroleum Geologists **36:**359-403.

Yong, R.N., Mohamed, A.M.O. and Warkentin, B.P. 1992. Principles of Contaminant Transport in Soils. American Elsevier Publishing Company, Inc. New York, NY.

Yong, R.N. and Warkentin, B.P. 1975. Developments in Geotechnical Engineering 5, Soil Properties and Behaviour. Elsevier Scientific Publishing Company, Amsterdam, The Netherlands.

10. APPENDICES

I. Numerical Solutions of Time Models

I.1 Darcy's-Law Time Model

```
/* This program performs a numerical integration of the Darcy's-law */
/* time model. It requires the specimen length, the starting */
/* pressure difference, the value of the pressure increment, the */
/* duration of each pressure increment, the specimen porosity and */
/* a calculation time increment. The entered values are converted to SI */
/* units, several variables are initialized and the hydraulic conductivity */
/* is then calculated from [34]. The first loop sets the pressure for the */
/* increment and calculates the end-of-increment time. The second loop */
/* uses [57] to calculate the change in length of water-filled pore (dL) */
/* for a small time increment (dt). The length of water-filled pore */
/* remaining after the time increment, and the total elapsed time after */
/* the time increment, are calculated. If the pore is empty of water, the */
/* program terminates; if the total elapsed time surpasses the calculated */
/* end-of-increment time, program execution continues at the start of the */
/* outer loop with i incremented by one. */

#include "stdio.h"
#include "math.h"

void main(void)
{
        double L, sp, dp, it, n, dt, k, p, eit, rhow, g, t, i, dL;

        printf("\n\n\nIMPORTANT: Enter all values with at least one decimal place.");
        printf("\nDepending on the values chosen for the parameters, very long calculation ");
        printf("\ntimes may result. It is recommended that the calculation time increment ");
        printf("\nbe set equal to the duration of each pressure increment, initially. If ");
        printf("\nthe calculation time is acceptable, the calculation time increment may ");
        printf("\nsubsequently be decreased. To use this program for constant pressure ");
        printf("\ntests, set the pressure increment to 0.0 and the duration of each ");
        printf("\npressure increment to a very large number (e.g. one billion).");

        printf("\n\n\nEnter the specimen length (cm): ");
        scanf("%lf", &L);
        printf("Enter the starting pressure difference (MPa): ");
```

```
        scanf("%lf", &sp);
        printf("Enter the pressure increment (MPa): ");
        scanf("%lf", &dp);
        printf("Enter the duration of each pressure increment (s): ");
        scanf ("%lf", &it);
        printf("Enter the specimen porosity: ");
        scanf("%lf", &n);
        printf("Choose a calculation time increment (s): ");
        scanf("%lf", &dt);

        L = L/100.0;
        sp = sp*1000000.0;
        dp = dp*1000000.0;

        p = 0.0;
        eit = 0.0;
        rhow = 1000.0;
        g = 9.81;
        t = 0.0;

        k = pow(10.0, (4.537*n)-14.597);

        for(i=0.0; ; i++)
        {
                p = sp + (i*dp);
                eit = eit + it;
                for( ; ; )
                {
                        dL = (k*p*dt/(rhow*g*n*L));
                        t = t + dt;
                        L = L - dL;
                        if(L<=0.0) break;
                        if(t>=eit) break;
                }
                if(L<=0.0) break;
        }
        end: printf("\nL = %f cm at t = %f h and P = %f MPa.", L*100.0, t/3600.0, p/1000000.0);
}
```

I.2 Pore-Radius Time Model

```
/* This program performs a numerical integration of the pore-radius */
/* time model. It requires the starting gas pressure difference, */
/* the value of the pressure increment, the largest pore radius, the */
/* specimen length, the duration of each pressure increment and a */
/* calculation time increment. The entered values are converted to SI */
/* units and several variables are initialized. The first loop sets the */
/* pressure for the increment and calculates the end-of-increment time. */
```

```
/* The second loop uses [67] to calculate the change in length of water- */
/* filled pore (dL) for a small time increment (dt). The length of water- */
/* filled pore remaining after the time increment, and the total elapsed */
/* time after the time increment, are calculated. If the pore is empty of */
/* water, the program terminates; if the total elapsed time surpasses the */
/* calculated end-of-increment time, program execution continues at the */
/* start of the outer loop with i incremented by one. */


#include "stdio.h"

void main(void)
{
        double sp, dp, r, L, it, dt, eta, eit, t, i, p, dL;

        printf("\n\n\nIMPORTANT: Enter all values with at least one decimal place.");
        printf("\nDepending on the values chosen for the parameters, very long calculation ");
        printf("\ntimes may result. It is recommended that the calculation time increment ");
        printf("\nbe set equal to the duration of each pressure increment, initially. If ");
        printf("\nthe calculation time is acceptable, the calculation time increment may ");
        printf("\nsubsequently be decreased. To use this program for constant pressure ");
        printf("\ntests, set the pressure increment to 0.0 and the duration of each ");
        printf("\npressure increment to a very large number (e.g. one billion).");

        printf("\n\n\nEnter the starting pressure difference (MPa): ");
        scanf("%lf", &sp);
        printf("Enter the pressure increment (MPa): ");
        scanf("%lf", &dp);
        printf("Enter the maximum pore radius (nm): ");
        scanf("%lf", &r);
        printf("Enter the specimen length (cm): ");
        scanf("%lf", &L);
        printf("Enter the duration of each pressure increment (s): ");
        scanf("%lf", &it);
        printf("Choose a calculation time increment (s): ");
        scanf("%lf", &dt);

        sp = sp*1000000.0;
        dp = dp*1000000.0;
        r = r/1000000000.0;
        L = L/100.0;

        eta = 0.001002;
        eit = 0.0;
        t = 0.0;


        for(i=0.0; ; i++)
        {
                p = sp + (i*dp);
                eit = eit + it;
                for( ; ; )
                {
                        dL = p*r*r*dt/(8*L*eta);
```

```
                    L = L - dL;
                    t = t + dt;
                    if(L<=0.0) break;
                    if(t>=eit) break;
                }
                if(L<=0.0) break;
        }
        printf("L = %f cm at t = %f h and P = %f MPa.", L*100.0, t/3600.0, p/1000000.0);
}
```

I.3 Hydraulic-Radius Time Model

```
/* This program performs a numerical integration of the hydraulic-radius */
/* time model. It requires the starting gas pressure difference, */
/* the value of the pressure increment, the specimen porosity, the */
/* soil specific surface area, the specimen dry density, the specimen */
/* length, the duration of each pressure increment and a calculation time */
/* increment. The entered values are converted to SI units, several */
/* variables are initialized and the hydraulic radius is calculated from */
/* [36]. The first loop sets the pressure for the increment and */
/* calculates the end-of-increment time. The second loop uses [71] to */
/* calculate the change in length of water-filled pore (dL) for a small */
/* time increment (dt). The length of water-filled pore remaining after */
/* the time increment, and the total elapsed time after the time increment, */
/* are calculated. If the pore is empty of water, the program terminates; */
/* if the total elapsed time surpasses the calculated end-of-increment */
/* time, program execution continues at the start of the outer loop with i */
/* incremented by one. */


#include "stdio.h"

void main(void)
{
        double sp, dp, n, Sm, rhoc, L, it, dt, eta, eit, t, rh, i, p, dL;

        printf("\n\n\nIMPORTANT: Enter all values with at least one decimal place.");
        printf("\nDepending on the values chosen for the parameters, very long calculation ");
        printf("\ntimes may result. It is recommended that the calculation time increment ");
        printf("\nbe set equal to the duration of each pressure increment, initially. If ");
        printf("\nthe calculation time is acceptable, the calculation time increment may ");
        printf("\nsubsequently be decreased. To use this program for constant pressure ");
        printf("\ntests, set the pressure increment to 0.0 and the duration of each ");
        printf("\npressure increment to a very large number (e.g. one billion).");

        printf("\n\n\nEnter the starting pressure difference (MPa): ");
        scanf("%lf", &sp);
        printf("Enter the pressure increment (MPa): ");
```

```
        scanf("%lf", &dp);
        printf("Enter the specimen porosity: ");
        scanf("%lf", &n);
        printf("Enter the soil specific surface area (m^2/g): ");
        scanf("%lf", &Sm);
        printf("Enter the specimen dry density (Mg/m^3): ");
        scanf("%lf", &rhoc);
        printf("Enter the specimen length (cm): ");
        scanf("%lf", &L);
        printf("Enter the duration of each pressure increment (s): ");
        scanf("%lf", &it);
        printf("Choose a calculation time increment (s): ");
        scanf("%lf", &dt);

        sp = sp*1000000.0;
        dp = dp*1000000.0;
        Sm = Sm*1000.0;
        rhoc = rhoc*1000.0;
        L = L/100.0;

        eta = 0.001002;
        eit = 0.0;
        t = 0.0;

        rh = n/(Sm*rhoc);

        for(i=0.0; ; i++)
        {
                p = sp + (i*dp);
                eit = eit + it;
                for( ; ; )
                {
                        dL = p*rh*rh*dt/(2*L*eta);
                        L = L - dL;
                        t = t + dt;
                        if(L<=0.0) break;
                        if(t>=eit) break;
                }
                if(L<=0.0) break;
        }
        printf("L = %f cm at t = %f h and P = %f MPa.", L*100.0, t/3600.0, p/1000000.0);
}
```

I.4 Kozeny-Carman Time Model

```
/* This program performs a numerical integration of the Kozeny-Carman */
/* time model. It requires the starting gas pressure difference. */
/* the value of the pressure increment, the specimen porosity, the pore */
```

```
/* shape factor, the specimen length, the specimen dry density, the */
/* duration of each pressure increment and a calculation time increment. */
/* The entered values are converted to SI units, several variables are */
/* initialized and the tortuosity and hydraulic conductivity are calculated */
/* (from [52] and [34]). The first loop sets the pressure for the */
/* increment and calculates the end-of-increment time. The second loop */
/* uses [74] to calculate the change in length of water-filled pore (dL) */
/* for a small time increment (dt). The length of water-filled pore */
/* remaining after the time increment, and the total elapsed time after the */
/* time increment, are calculated. If the pore is empty of water the */
/* program terminates; if the total elapsed time surpasses the calculated */
/* end-of-increment time, program execution continues at the start of the */
/* outer loop with i incremented by one. */


#include "stdio.h"
#include "math.h"

void main(void)
{
        double sp, dp, n, ko, L, rhoc, it, dt, T, k;
        double rhow, g, eit, t, i, p, dL;

        printf("\n\n\nIMPORTANT: Enter all values with at least one decimal place.");
        printf("\nDepending on the values chosen for the parameters, very long calculation ");
        printf("\ntimes may result. It is recommended that the calculation time increment ");
        printf("\nbe set equal to the duration of each pressure increment, initially. If ");
        printf("\nthe calculation time is acceptable, the calculation time increment may ");
        printf("\nsubsequently be decreased. To use this program for constant pressure ");
        printf("\ntests, set the pressure increment to 0.0 and the duration of each ");
        printf("\npressure increment to a very large number (e.g. one billion).");

        printf("\n\n\nEnter the starting pressure difference (MPa): ");
        scanf("%lf", &sp);
        printf("Enter the pressure increment (MPa): ");
        scanf("%lf", &dp);
        printf("Enter the specimen porosity: ");
        scanf("%lf", &n);
        printf("Enter the pore shape factor (2.0 to 3.0): ");
        scanf("%lf", &ko);
        printf("Enter the specimen length (cm): ");
        scanf("%lf", &L);
        printf("Enter the specimen dry density (Mg/m^3): ");
        scanf("%lf", &rhoc);
        printf("Enter the duration of each pressure increment (s): ");
        scanf("%lf", &it);
        printf("Choose a calculation time increment (s): ");
        scanf("%lf", &dt);

        sp = sp*1000000.0;
        dp = dp*1000000.0;
        L = L/100.0;

        rhow = 1000.0;
```

```
        g = 9.81;
        eit = 0.0;
        t = 0.0;

        T = (-0.24*rhoc) + 0.41;
        k = pow(10.0, (4.537*n) - 14.597);

        for(i=0.0; ; i++)
        {
                p = sp + (i*dp);
                eit = eit + it;
                for( ; ; )
                {
                        dL = p*k*ko*dt/(2.0*L*n*rhow*g*T);
                        L = L - dL;
                        t = t + dt;
                        if(L<=0.0) break;
                        if(t>=eit) break;
                }
                if(L<=0.0) break;
        }
        printf("L = %f cm at t = %f h and P = %f MPa.", L*100.0, t/3600.0, p/1000000.0);
}
```

II. Radionuclide Diffusion in Avonlea Bentonite Plugs After Gas Breakthrough

II.1 Introduction

As described in section 1.1, diffusion is expected to be the dominant mechanism for dissolved radionuclide transport through the buffer material. Diffusive transport and gas migration may be coupled processes in a nuclear fuel waste disposal vault. To test one aspect of this possibility, diffusion experiments were conducted on clay plugs that had previously been used for gas-breakthrough testing.

II.2 Procedure

Clay plugs with a target ρ_c of 1.15 Mg/m^3 were prepared in the high-pressure gas-breakthrough apparatus using air-dry clay. After compaction, they were wetted for 2 d at a pressure of 0.2 MPa. Gas breakthrough experiments were then performed on the plugs. The back pressure was 0.2 MPa and the inlet pressure was set at 1.0 MPa for the first five minutes. The inlet pressure was then incremented 1.0 MPa, and it was increased 1.0 MPa every five minutes until gas breakthrough occurred. Controls were prepared similarly but they were not subjected to gas breakthrough. After the gas-breakthrough tests, or following wetting in the case of the controls, the clay plugs were extruded from the gas-breakthrough cell.

An illustration of the diffusion cell that was used for the experiments is in Figure II.1 and a detailed description is in Hume (1993). The gas-breakthrough specimens were too large to fit into the sample rings used in the diffusion cells. Therefore, a piece of tubing sharpened on one end was used to punch 4.12-cm-diameter pieces of clay from the gas-breakthrough specimens. The plugs were punched parallel to the direction of gas flow in the gas-breakthrough tests. These plugs were wedged into the diffusion-cell sample rings so that the direction of diffusion would be parallel to the direction of gas migration, and the ends were shaved until the specimens were the same length as the rings. The rings containing the clay specimens were placed into diffusion cells. Synthetic groundwater solution (Hume 1993) was passed over both ends of the clay plugs for 7 to 10 d before the diffusion testing was started.

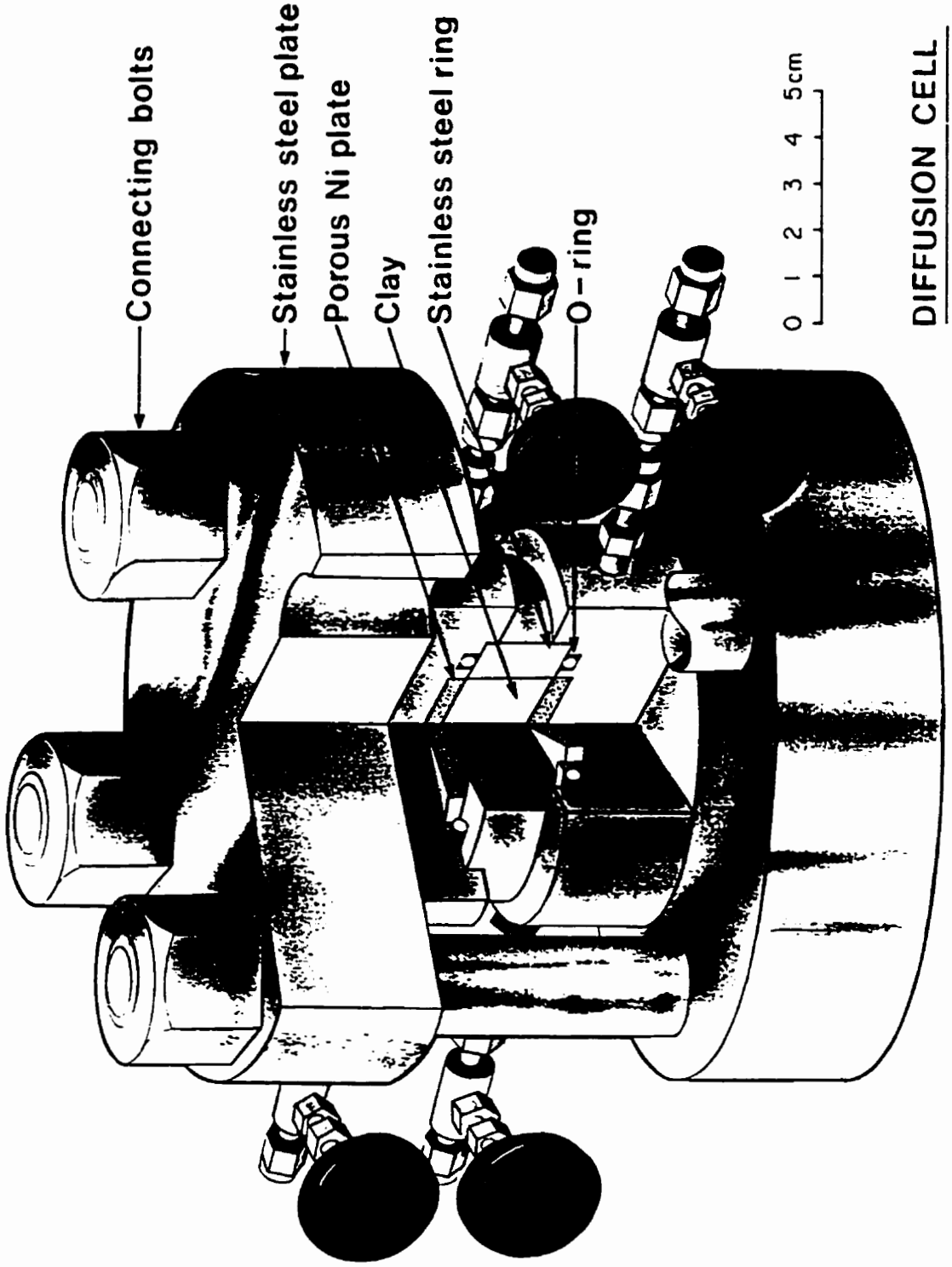

Figure II.1 Schematic of the diffusion cell.

For the diffusion experiments, a solution containing the radionuclide I-125 (1.8×10^{-10} mol/L on the start date of the experiments) was passed over one end of the clay plugs. Because the half life of I-125 is only 60 d, stable I^- was added to the tracer solution (1.0×10^{-8} mol/L) to maintain a relatively constant I^- concentration. Synthetic groundwater that did not contain I^- was passed across the opposite ends of the clay plugs to collect diffused tracer. At regular intervals the volume in each collection bottle was measured. A sample of each collection bottle solution, of known volume, was analyzed for I-125 and the total amount of diffused I^- in each collection bottle calculated.

II.3 Results

Table II.1 contains the results of the gas-breakthrough experiments. Breakthrough occurred in all the samples that were exposed to gas, at pressures between 28.8 and 44.8 MPa.

Table II.1 Results of gas-breakthrough tests.

Test	p_b (MPa)
D5b	34.8
D5c	38.8
D5d	28.8
D5e	44.8
D5f	Control
D5g	Control
D5h	Control

The form of Fick's first law that is applicable to the diffusion experiments described here, once steady state is achieved, is

$$dQ/Adt = -D_e(dc/L), \qquad [II.1]$$

where dQ is the quantity diffused in a time increment dt, A the cross-sectional area of the clay plug, D_e the steady-state or effective diffusion coefficient, dc the concentration difference across the specimen and L the plug length. Since dc and L are known, the slope of a plot of Q/A against t is all that is needed to calculate D_e. Figure II.2 shows an example of the results obtained in a diffusion experiment plotted as described. The diffusion data are tabulated in Table II.2. Diffusion coefficients are not reported for tests D5b and D5h because steady state had not been achieved when the experiments were stopped.

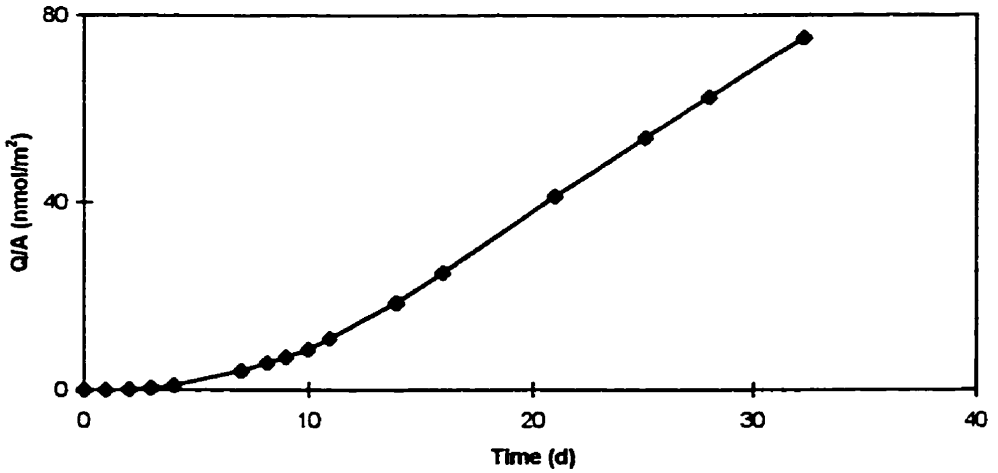

Figure II.2 Results of experiment D5c.

Table II.2 Diffusion results.

Test	Plug Type	ρ_c (Mg/m^3)	D_e ($\mu m^2/s$)
D5b	Gas Broken	NA[a]	NA[a]
D5c	Gas Broken	1.20	46
D5d	Gas Broken	1.10	15
D5e	Gas Broken	1.13	25
D5f	Control	1.04	21
D5g	Control	1.06	22
D5h	Control	1.07	NA[a]

[a]NA = Not Available

II.4 Discussion

The mean ρ_c of the three ruptured samples is 1.14 Mg/m^3 and the mean D_e value is 29 $\mu m^2/s$. The mean ρ_c of the two blanks, on which results were obtained, is 1.05 Mg/m^3 and the mean D_e value is 22 $\mu m^2/s$. Oscarson et al. (1996) report that single D_e results can vary by a factor of four in this type of experiment; therefore the difference between the two averages is not large.

Oscarson et al. (1992) obtained the I^- diffusion results in Table II.3. The mean ρ_c of the specimens is 1.09 Mg/m^3 and the mean D_e value is 30 $\mu m^2/s$. This result is essentially the same as the 29 $\mu m^2/s$ obtained on gas ruptured specimens in the current work.

In Oscarson et al. (1996), the results of diffusion experiments performed on plugs that were manually slotted, wetted and then tested are reported. The rates of Cs^+ and I^-

Table II.3 I^- diffusion in Avonlea bentonite[a].

ρ_c (Mg/m^3)	D_e ($\mu m^2/s$)
1.08	46
1.11	27
1.09	18

[a]From Oscarson et al. (1992).

diffusion did not differ between the defected plugs and controls of comparable ρ_c that were not defected. This finding is consistent with the current results.

II.5 Conclusion

Provided the specimens are allowed to absorb water and swell between tests, the passage of gas through Avonlea bentonite clay does not effect the subsequent rate of I^- diffusion.

II.6 References

Hume, H.B. 1993. Procedures and apparatus for measuring diffusion and distribution coefficients in compacted clays. Atomic Energy of Canada Limited Report, AECL-10981, COG-93-447, Chalk River, ON.

Oscarson, D.W., Dixon, D.A. and Hume, H.B. 1996. Mass transport through defected bentonite plugs. Applied Clay Science **11:**127-142.

Oscarson, D.W., Hume, H.B., Sawatsky, N.G. and Cheung, S.C.H. 1992. Diffusion of iodide in compacted bentonite. Soil Science Society of America Journal **56:**1400-1406.

IMAGE EVALUATION
TEST TARGET (QA-3)

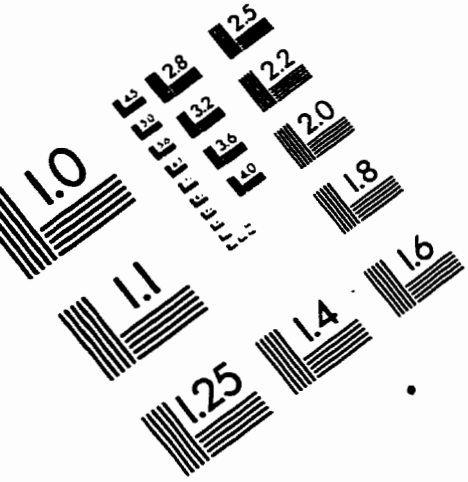

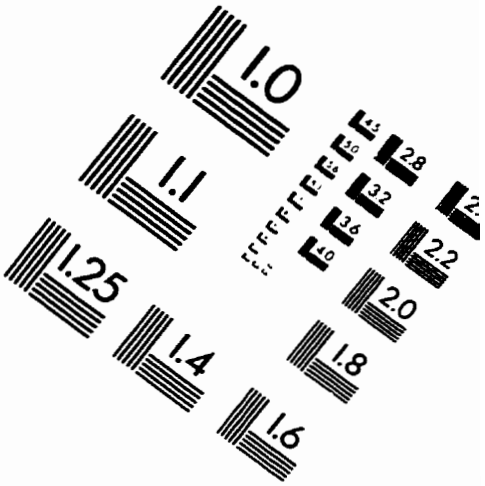

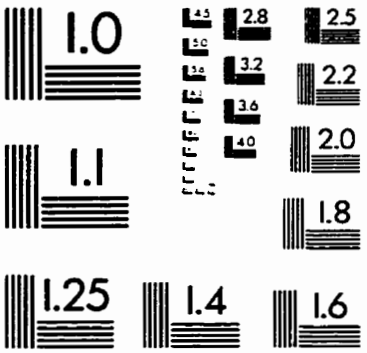

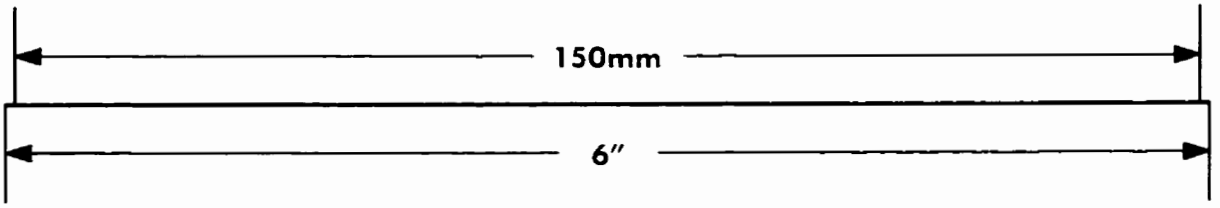

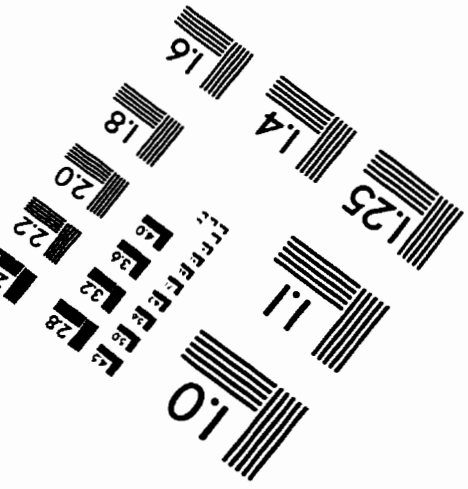

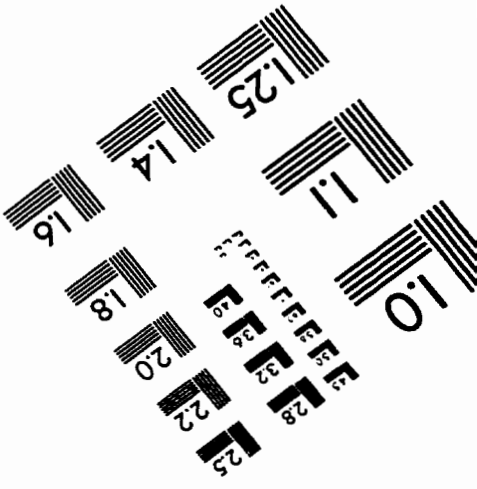

APPLIED IMAGE, Inc
1653 East Main Street
Rochester, NY 14609 USA
Phone: 716/482-0300
Fax: 716/288-5989

© 1993, Applied Image, Inc., All Rights Reserved